

**RADIATION PRESSURE ACCELERATION OF  
IONS IN BULK TARGETS BY ULTRA-INTENSE  
LASER PULSES**

By  
**Ujjwal Sinha**

**INSTITUTE FOR PLASMA RESEARCH, GANDHINAGAR**

A thesis submitted to the  
Board of Studies in Physical Sciences

In partial fulfillment of the requirements

For the Degree of

**DOCTOR OF PHILOSOPHY**

*of*

**HOMI BHABHA NATIONAL INSTITUTE**



February 2013



# Homi Bhabha National Institute

Programme: Ph.D.

Board of Studies in PHYSICAL Sciences

1. Name of the Constituent Institution:

INSTITUTE FOR PLASMA RESEARCH

2. Name of the Student: UJJWAL SINHA

3. Enrolment Number: PHYS 06200704014

4. Date of Enrolment in HBNI: SEPTEMBER 3, 2007

5. Date of Submission of Thesis: FEBRUARY 5, 2013

6. Title of the Thesis: RADIATION PRESSURE ACCELERATION OF IONS IN BULK TARGETS BY ULTRA-INTENSE LASER PULSES

7. Composition of the Doctoral Committee:

Sr No	Composition	Designation in HBNI	Name
a.	Chairman	SENIOR PROFESSOR	PROF. ABHIJIT SEN
b.	Convener (Guide)	SENIOR PROFESSOR	PROF. PREDHIMAN KRISHAN KAW
c.	Co-Guide, if any		
d.	Member	PROFESSOR	PROF. AMITA DAS
e.	Member	ASSOCIATE PROFESSOR	DR. SUDIP SENGUPTA
f.	The Technology Adviser, if any	Invitee	

8. Number of Doctoral Committee Meetings held with respective dates: FIVE

10/11/2008 , 27/01/2010 , 18/01/2011 , 06/02/2012 , 29/08/2012

9. Name and Organization of the Examiner 1: PROF. G. RAVINDRA KUMAR, TIFR MUMBAI

Recommendations of the Examiner 1 (Thesis Evaluation) (i) accepted, (ii) accepted after revisions, or (iii) rejected:

10. Name and Organization of the Examiner 2: PROF. VICTOR MALKA, LOA, ENSTA, PARIS

Recommendations of the Examiner 2 (Thesis Evaluation) (i) accepted, (ii) accepted after revisions, or (iii) rejected:

Name & Signature of Dean-Academic, CI: Dr. S. MUKHERJEE

## Recommendations of the Viva Voce Board

1. Date of Viva Voce Examination: 05/7/2013

2. Recommendations for the award of the Ph.D. degree: Recommended / Not Recommended  
(If Recommended, give summary of main findings and overall quality of thesis)  
(If Not Recommended, give reasons for not recommending and guidelines to be communicated by Convener of the Doctoral committee to the student for further work)

This is a high quality thesis on a very contemporary and challenging problem in intense laser-matter interactions. The production of ion beams at  $10^2 - 10^3$  MeV energies using ultrashort and high intensity laser pulses is a ~~new~~ new paradigm that encompasses many areas of science and technology. This thesis presents several interesting features on the optimization of ion energies under different target and laser conditions. Analytical models, backed by simulations have brought out features not revealed in previous studies.

Ujwal made a very thorough and impressive presentation and answered all the questions confidently and satisfactorily. His command on the thesis topic was evident in the viva voce. Award of the Ph.D. degree is recommended.

In case Not Recommended, another date will be fixed by the Dean-Academic, CI, which shall not be earlier than a month after and not later than six months from the date of first viva.

Date:

Name and Signature of the Viva Voce Board (Doctoral Committee and External Examiner):

PROF. G. RAVINDRA KUMAR

G. Ravindra Kumar

PROF. ABHIJIT SEN

Abhijit

PROF. PREDHIMAN K. KAW

Prediman

PROF. AMITA DAS

Amita Das.

DR. SUDIP SENGUPTA

Sudip

# Homi Bhabha National Institute

## Recommendations of the Viva Voce Board

As members of the Viva Voce Board, we recommend that the dissertation prepared by **Ujjwal Sinha** entitled "**Radiation Pressure Acceleration of Ions in Bulk Targets by Ultra-Intense Laser Pulses**" may be accepted as fulfilling the dissertation requirement for the Degree of Doctor of Philosophy.

  
----- Date : 5/07/2013  
Chairman : Prof. Abhijit Sen

  
----- Date : 5/07/2013  
Convener : Prof. Predhiman K Kaw

  
----- Date : 5/07/2013  
Member : Prof. Amita Das

  
----- Date : 5/07/2013  
Member : Dr. Sudip Sengupta

Final approval and acceptance of this dissertation is contingent upon the candidate's submission of the final copies of the dissertation to HBNI.

I hereby certify that I have read this dissertation prepared under my direction and recommend that it may be accepted as fulfilling the dissertation requirement.

  
----- Date : 5/07/2013  
Guide : Prof. Predhiman K Kaw

## STATEMENT BY AUTHOR

This dissertation has been submitted in partial fulfillment of requirements for an advanced degree at Homi Bhabha National Institute (HBNI) and is deposited in the library to be made available to borrowers under rules of the HBNI.

Brief quotations from this dissertation are allowable without special permission, provided that accurate acknowledgement of source is made. Requests for permission for extended quotation from or reproduction of this manuscript in whole or in part may be granted by the competent authority of HBNI when in his or her judgement the proposed use of the material is in the interests of scholarship. In all other instances, however, the permission must be obtained from the author.



Ujjwal Sinha

## DECLARATION

I, hereby declare that the investigation presented in the thesis has been carried out by me. The work is original and the work has not been submitted earlier as a whole or in part for a degree/diploma at this or any other Institution or University.



Ujjwal Sinha

To my dear wife Subham  
and  
lovely son Reyansh

Why do we fall?

So we might learn to pick ourselves up.

-Batman Begins(2005)

## ACKNOWLEDGEMENTS

Foremost, I would like to express my sincere gratitude to my advisor Prof. Predhiman K Kaw. His continuous support and guidance had been inspiring. His enthusiasm and friendly nature has made this journey possible. I really appreciate his tolerance for listening and answering to even the most kiddish question during the days of my work. I am also thankful to him for providing me enough independence during this work and teaching me the methodology of research.

I am also very grateful to Dr. Sudip Sengupta, who helped me a lot during the initial days of my Ph.D. His lectures on the Green's Function is something which I will never forget. It was only after his lectures that I have been able to solve problems in this area with utmost ease. Besides this, I have always admired his extremely rigorous way of solving problems and tried hard to incorporate this quality in me.

I would also like to acknowledge Prof. Abhijit Sen, who supervised me on the project on wakefield acceleration during my course work. It was he who first introduced me to the area of plasma based particle acceleration. His guidance and discussions made the basis of my Ph.D work.

I am grateful to Prof Abhijit Sen, Prof. Amita Das and Dr. Sudip Sengupta for being my doctoral committee members. Their comments during my reviews had been quite helpful in improving this work.

I would like to thank Dr. P Chattopadhyay, Dr. S Sengupta, Dr. D Raju, Dr. M Warriar, Dr. R Srinivasan, Dr. Indranil Bandopadhyay, Dr. R Ganesh, Dr. N Ramsubramaniam, Dr. Joydeep Ghosh, Dr. Raj Singh, Prof. Raghvendra Singh, Dr. Devendra Sharma, Dr. R Goswami, Dr. S Mukherji, Prof. A Das and Prof. R Jha for their endurance while teaching us during the first year course.

Thanks to the library, computer and administrative staff Mr. Saroj Das, Mr. Shra-  
van Kumar, Ms. Smita Parmar, Mrs. Arundhati Das, Mrs. Pragya Pathak, Mrs.  
Sutapa Ranjan, Mr. Shailendra Trivedi, Mr. Arvind Singh, Mr. Hemant Joshi,  
Mr. Gaurav Garg, Mr. Govind Lokhande, Mr. M Sourabhan, Mr. M. H. Vartak,  
Mr. H. K. Sharma, Mr. H. C. Khanduri, Mr. Hitesh Mehta, Mr. Dinesh Nair, Mr.  
Silel Shah, Ms. Shirin Bhesania and Mr. H. Chamunde for their help. I would  
like to make a special mention of the note in Mr. Chamunde's office saying "This  
too shall pass away" which always brought a smile on my face every time I left my

cabin irrespective of how the day had been.

I enjoyed the friendly hostel life at IPR. Greetings and best wishes to my dear Pintu da, Ritu di, Manash Paul, Rajneesh Yadav, Anand Srivastava, Suraj Sinha, Bhaskar Chaudhary, Anurag Mishra, Vikrant Saxena, Kishore Karatiparambil, Padduvatti N. Maya, Subhas, Sanjay Mishra, Swati Baruah, Ajai, Jugal Chaudhury, Satyanand Kar, Sharad Yadav, Shekhar T. Goud, Sunita Negi, Kshitish Barada, Gurudatt Gaur, Deepak Sangwan, Vikram Narang, Prabal Singh Verma, Ashwin Joy, Rameswar Singh, Sita Sundar, Sushil, Sanat, Pravesh, Partha, Nishant, Sayak, Manjit, Soumen, Aditya, Iliyas, Vikram Singh Dharodi, Rana, Veda, Sandeep, Zuber, Rupendra, Mangilal, Bibhu, Varaprasad, Harish, Sameer, Neeraj, Deepa, Akanksha, Vidhi, Dushyant, Anup, Arghya, Bhumika, Debraj, Modhuchandran, Narayan, Amit, Rajnarayan, Ratan, Sonu, Surabhi and Umesh.

My batch mates Kshitish Barada, Gurudatt Gaur, Deepak Sangwan, Vikram Narang, Prabal Singh Verma, Ashwin Joy, Sita Sundar, Sanjib Muhuri, Mohd. Tayyab, Arabind Yadav and Linthish P. deserve special thanks for always being supportive for me.

I would like to make a special mention of Vikram Narang and Ashwin Joy with whom I had an unending list of topics to discuss on. The Ph.D journey has been fun with them. Also Kshitish has been very helpful at times when I needed him.

I take this opportunity to thank my teachers during my MSc at Indian Institute of Technology, Delhi for motivating me to pursue higher studies.

My heartfelt gratitude to my parents and brother Prashant for their goodwill and support all through my life. I would like to mention my father whose continuous support and faith in me to pursue a research career had never let me deviate from my inherent interest.

In the end I would like to mention my dear wife Subham for her patience and who always stood beside me during the toughest times as well as rejoiced even the smallest achievement of mine. She has been with me since the beginning of my Ph.D journey and had never let me feel anything was impossible. Her constant support and strength was what made me rise even after numerous failures. She has also been a good teacher. Her extraordinary skills to manage the most complicated situations is something I am still trying to learn. It would not be exaggerating to say that she has had the greatest influence in shaping my scientific outlook.

**Ujjwal Sinha**

## LIST OF PUBLICATIONS

### Thesis:

- [1] **Ujjwal Sinha** and Predhiman Kaw, "Ponderomotive Ion Acceleration in dense magnetized laser irradiated thick target plasmas", *Physics of Plasmas* **19**, 033102(2012)
- [2] **Ujjwal Sinha**, "Self Consistent model for ponderomotive ion acceleration of laser irradiated two species dense target plasmas", *Physics of Plasmas* **19**, 043104(2012)
- [3] **Ujjwal Sinha**, "Multistage Ion Acceleration in Finite Overdense Target with a Relativistic Laser Pulse", *Physics of Plasmas* **20**, 073116(2013)
- [4] **Ujjwal Sinha** and Predhiman Kaw, "Analytical model for axial magnetic field generation by interaction of radially inhomogeneous laser pulse with a solid target", (to be submitted)

## Abstract

The present thesis examines some important issues regarding acceleration of plasma ions to high energies by ultra-intense circularly polarized (CP) lasers in the Hole Boring (HB) mode of Radiation Pressure Acceleration (RPA). A major part of the study is devoted to the analysis of the accelerating structure (laser piston) under the influence of a longitudinal magnetic field as well as for a plasma target composed of multiple ion species. The laser piston is a charge separation layer created due to the ponderomotive force of the incident laser. This induced charge separation field is responsible for accelerating the plasma ions. Under the influence of a static magnetic field, the polarization state (i.e left or right circulation) plays an important role in this process. It has been found that right circularly polarized (RCP) lasers are more efficient as the net ponderomotive force on plasma electrons is enhanced in this case due to resonance between their quiver motion in laser field and cyclotron motion due to applied magnetic field. Further a residual ion space charge behind the laser piston is discovered. It is found that this space charge undergoes coulomb explosion under its own field and do not contribute to the accelerated ion beam. However when an energetic test ion is incident in the direction opposite to the incident laser, this coulomb exploding region reflects it with a velocity higher than the incident velocity, thus amplifying the kinetic energy of the test ion.

Further acceleration of ions using ultra-intense laser irradiated on an overdense target plasma composed of two ion species has been described using a self consistent approach. The analytical model for the steady state described here gives a complete description of the charge separation zone, i.e., ion space charge and electron sheath, created due to ponderomotive force of the laser. It successfully explains the jump in electrostatic potential or field in the laser piston responsible for a major part of the acceleration. The information about the structure of laser piston obtained from the analytical model is used for the stability analysis of the process. It has been found that the stability of the laser piston depends on the target composition. The reflection of incoming test ion from the coulomb exploding region of the ion space charge has been described in context of the charge on the incident beam species.

Extending the theory of ion acceleration to two dimensions (i.e. radial and axial

with azimuthal symmetry), it was found that a radial intensity variation in the incident circularly polarized (CP) laser introduced radial electron density inhomogeneity in the electron sheath formed due to ponderomotive pressure. This density inhomogeneity drives an azimuthal current. Besides this the circular motion of the plasma electrons under the influence of the CP laser field induces a magnetic dipole moment. This dipole moment when summed over all the plasma electrons give rise to a net magnetization. The azimuthal and magnetization current together generates a quasi-static axial magnetic field in the mega-gauss regime. Finally the multi-stage process of ion acceleration is studied in the relativistic regime. A fully relativistic calculation for the second stage ion velocity is presented and is validated using 1D3V particle in cell (PIC) simulations. Also a comparative study between non-relativistic and relativistic case is done and it is found that at high piston velocities the relativistic results differ a lot from the non-relativistic ones.

# Contents

List of Figures . . . . .	ii
<b>1 Introduction</b>	<b>1</b>
1.1 Overview and Motivation . . . . .	1
1.2 Laser pulse interaction with overdense plasmas . . . . .	5
1.3 Ion acceleration in solid targets . . . . .	8
1.3.1 Target Normal Sheath Acceleration (TNSA) . . . . .	8
1.3.2 Radiation Pressure Acceleration (RPA) . . . . .	9
1.4 Organization of the thesis . . . . .	12
1.4.1 Chapter 2: Ponderomotive Ion Acceleration in dense magnetized laser-irradiated thick target plasmas . . . . .	13
1.4.2 Chapter 3: Self consistent model for ponderomotive ion acceleration of laser irradiated two species dense target plasmas	14
1.4.3 Chapter 4: Analytical model for axial magnetic field generation by interaction of radially inhomogeneous laser pulse with solid target . . . . .	15
1.4.4 Chapter 5: Relativistic theory for multistage ion acceleration	16
1.4.5 Chapter 6: Conclusions and Future direction . . . . .	16
<b>2 Ponderomotive Ion Acceleration in dense magnetized laser-irradiated thick target plasmas</b>	<b>26</b>
2.1 Introduction . . . . .	26
2.2 Theoretical model for laser piston . . . . .	28
2.2.1 Laser piston velocity in HB RPA . . . . .	28
2.2.2 Structure of the laser piston . . . . .	29
2.3 Conclusions . . . . .	44
<b>3 Self consistent model for ponderomotive ion acceleration of laser irradiated two species dense target plasmas</b>	<b>52</b>
3.1 Introduction . . . . .	52
3.2 Acceleration process with two ion species . . . . .	54
3.3 Ion space charge for a two species target . . . . .	55
3.3.1 Mixed species ion sheath . . . . .	55

3.3.2	Heavier species ion sheath . . . . .	58
3.3.3	Coulomb exploding ion space charge region . . . . .	59
3.4	Electron sheath for a two ion species target . . . . .	64
3.5	Stability analysis of Laser Piston . . . . .	68
3.6	Velocity amplification of an incoming test ion . . . . .	71
3.7	Conclusions . . . . .	75
<b>4</b>	<b>Analytical model for axial magnetic field generation by interaction of radially inhomogeneous laser pulse with solid target</b>	<b>80</b>
4.1	Introduction . . . . .	80
4.2	Laser fields in the electron sheath . . . . .	82
4.3	Magnetic field generation . . . . .	89
4.4	Conclusions . . . . .	92
<b>5</b>	<b>Relativistic Theory for Multistage Ion Acceleration</b>	<b>96</b>
5.1	Introduction . . . . .	96
5.2	Non Relativistic theory of HB-RPA . . . . .	97
5.2.1	First acceleration process . . . . .	97
5.2.2	Second acceleration process . . . . .	98
5.3	Relativistic theory of HB-RPA . . . . .	99
5.3.1	First Acceleration Process . . . . .	99
5.3.2	Second Acceleration Process . . . . .	100
5.4	Comparison with PIC simulations . . . . .	101
5.5	Conclusions . . . . .	105
<b>6</b>	<b>Conclusion and Future Direction</b>	<b>113</b>
6.1	Conclusions . . . . .	113
6.2	Future Directions . . . . .	118

# List of Figures

2.1	Schematic diagram (not to scale), representing the process of interaction of an ultraintense circularly polarized laser with a thick overdense plasma target. The region $[-z_i, -\delta]$ represents the ion space charge region undergoing coulomb explosion, $[-\delta, 0]$ represents the ion sheath, in which the ions present undergo direct radiation pressure acceleration. The region $[0, z_{es}]$ represent the electron sheath formed due to laser ponderomotive force and beyond $z_{es}$ is the region of undisturbed plasma. . . . .	31
2.2	Dimensionless amplitude of evanescent laser field profiles inside the electron sheath for equilibrium plasma density $n_0/n_c = 10$ , $\beta_f = 0.05$ and $\Omega_c = 0.5$ for left and right circularly polarized lasers together with the profile in the absence of magnetic field. . . . .	36
2.3	Dimensionless incident laser amplitudes required for different $\beta_f$ for the case of left and right circularly polarized light and $B_s = 0$ . The initial plasma density $n_0/n_c = 10$ and $\Omega_c = 0.5$ . . . . .	38
2.4	Dimensionless incident laser amplitudes required for different $\beta_f$ for the case of left and right circularly polarized light and $B_s = 0$ . The initial plasma density $n_0/n_c = 10$ and $\Omega_c = 0.5$ . . . . .	38
2.5	Induced longitudinal electric field at different times for $n_0/n_c = 10$ , $\beta_f = 0.05$ , $\Omega_c = 0.5$ and $\alpha = +1$ . $\lambda$ is the laser wavelength. . . . .	41
2.6	Trajectories of incoming test ion with different velocities with in the ion space charge region undergoing coulomb explosion together with that of the laser piston. The laser piston moves ahead with a constant velocity because of which the test ion has to traverse a longer distance to enter the piston region upon reflection. . . . .	43
2.7	Velocity profile of test ion incident with different initial velocities with in the ion space charge region with time. The graphs are plotted upto the time at which the reflected ion re-enter the laser piston. . . . .	43

2.8	Maximum velocity magnitude the incoming test ion can have for different $\beta_f$ keeping initial ion density constant. $n_0/n_c = 10, \mu = 1/2000, \Omega_c = 0.5$ and $Z = 1$ . . . . .	45
2.9	Reflected ion velocities for different $ v_{bmax} $ . $n_0/n_c = 10, \mu = 1/2000, \Omega_c = 0.5$ and $Z = 1$ . . . . .	45
3.1	Charge separation layer maintained by the radiation pressure of the incident laser. The blue curve represent heavy ions, red represent light ions and black curve refers to electrons. The region $[0, z_{es}]$ represents the electron sheath. The region $[-\delta_l, 0]$ is an ion sheath comprising of both the light and heavy ion species. $[-\delta_h, -\delta_l]$ comprises primarily of the heavy ion species and in the region $[-z_i, -\delta_h]$ the ions are undergoing coulomb explosion. $z > z_{es}$ is the region of undisturbed plasma. . . . .	56
3.2	Density profiles of the ion species in the laser piston for $n_0/n_c = 10$ and $\beta_f = 0.2$ . The green curves represent heavier ions ( $C^{6+}$ ) and blue curves represent lighter ions ( $H^+$ ). (a) shows the ion sheaths for density ratio $n_{h0}/n_{l0} = 1$ , (b) is for $n_{h0}/n_{l0} = 3/7$ and (c) for $n_{h0}/n_{l0} = 1/9$ . $\lambda$ here is the laser wavelength. . . . .	60
3.3	Velocity profiles of the ion species in the laser piston in the piston frame for $n_0/n_c = 10$ and $\beta_f = 0.2$ . The green curves represent heavier ions ( $C^{6+}$ ) and blue curves represent lighter ions ( $H^+$ ). (a) shows the local ion velocities with in the piston for density ratio $n_{h0}/n_{l0} = 1$ , (b) is for $n_{h0}/n_{l0} = 3/7$ and (c) for $n_{h0}/n_{l0} = 1/9$ . . . . .	62
3.4	Electrostatic potential within the laser piston for $n_0/n_c = 10$ and $\beta_f = 0.2$ for different ratios of ion species. . . . .	63
3.5	Time evolution of the number density of both the ion species normalized to their equilibrium densities. Blue curves represent carbon ions and green curves represent hydrogen. (a) shows the time evolution for $C^+$ and $H^+$ , whereas (b) is for $C^{6+}$ and $H^+$ . . . . .	63
3.6	Spatial profile of longitudinal electric field $E_z$ for $n_0/n_c = 10$ and $n_{h0}/n_{l0} = 1$ with $\beta_f = 0.2$ at different times. . . . .	67
3.7	Time evolution of the laser piston of a composite target with $n_0/n_c = 10$ and $n_{h0}/n_{l0} = 1$ with the incident laser amplitude $a_0 = 50$ . . . . .	70

3.8 Cusp formation time with incident laser intensity for different target compositions keeping  $n_0/n_c = 10$ . . . . . 71

3.9 Trajectories of test ions comprising of  $C^+$  and  $C^{6+}$  with incident velocity  $v_b = -0.15c$ .  $n_0/n_c = 10$  and  $n_{h0}/n_{l0} = 1$ . Red curve is for  $C^{6+}$  and green for  $C^+$ . The blue line represent the laser piston moving with velocity  $v_f = 0.2c$ . . . . . 72

3.10 Maximum permissible incident velocities for test ion comprising of  $C^+$  and  $C^{6+}$ .  $n_{h0}/n_{l0} = 1$  and  $n_0/n_c = 10$ . . . . . 74

3.11 Reflected ion velocities corresponding to maximum permissible incident velocity for  $C^+$  and  $C^{6+}$ .  $n_{h0}/n_{l0} = 1$  and  $n_0/n_c = 10$ . . . . . 74

4.1 Density profiles of the electrons in the sheath at different times for  $n_0/n_c = 2$  and  $a_0 = 2$  for a gaussian laser pulse and homogeneous overdense plasma at different radial locations. The red curves represent electron density at  $r/\sigma = 0$ , green curves represent electron density at  $r/\sigma = 0.25$  and blue curves represent electron density at  $r/\sigma = 0.5$ .  $\Delta(r_0)$  is the electron displacement at  $t/\tau = 0$  at a given  $r$ . 87

4.2 Evanescent laser field profiles in the electron sheath at different times for  $n_0/n_c = 2$  and  $a_0 = 2$  for a gaussian laser pulse and homogeneous overdense plasma at different radial locations. The red curves represent evanescent field at  $r/\sigma = 0$ , green curves represent the field at  $r/\sigma = 0.25$  and blue curves at  $r/\sigma = 0.5$ .  $\Delta(r_0)$  is the electron displacement at  $t/\tau = 0$  at a given  $r$ . . . . . 88

4.3 Normalized axial magnetic field profiles in the electron sheath at different times for  $n_0/n_c = 2$  and  $a_0 = 2$  for a gaussian laser pulse and homogeneous overdense plasma at different radial locations. The red curves represent axial magnetic field at  $r/\sigma = 0$ , green curves the field at  $r/\sigma = 0.25$  and blue curves at  $r/\sigma = 0.5$ .  $\Delta(r_0)$  is the electron displacement at  $t/\tau = 0$  at a given  $r$ . . . . . 91

5.1 Spatial density profile of ions at different times for  $n_i = 10n_c$  and  $a_0 = 20$ . In (a) the ion density at time  $-11\tau$  is shown i.e. when the face of the laser pulse is at the extreme left of the simulation domain and the ions are undisturbed. (b) shows the ion density profile at  $31\tau$ . We can notice here that the tail of the plasma is at  $15\lambda$  hence indicating that all the ions have passed through the accelerating field generated by the double layer by this time. (c) and (d) shows ion densities at  $50\tau$  and  $70\tau$  respectively, from which we can see that the ions have been further displaced leading to a indication of multistage acceleration process. . . . . 103

5.2 Figures (a), (c) and (e) shows the longitudinal electric field at times  $31\tau, 50\tau$  and  $70\tau$  respectively for  $n_i = 10n_c$  and  $a_0 = 20$ . (b), (d) and (f) shows the longitudinal velocity spectrum at similar times. We see that at  $31\tau$  the ions peak at a velocity  $0.248c$ . At  $47\tau$  we can see a second peak emerging at  $0.41c$  to which almost all the ions get dumped at  $70\tau$ . . . . . 104

5.3 Spatial density profile of ions at different times for  $n_i = 10n_c$  and  $a_0 = 30$ . In (a) the ion density at time  $-11\tau$  is shown i.e. when the face of the laser pulse is at the extreme left of the simulation domain and the ions are undisturbed. (b) shows the ion density profile at  $23\tau$ . We can notice here that the tail of the plasma is at  $15\lambda$  hence indicating that all the ions have passed through the accelerating field generated by the double layer by this time. (c) and (d) shows ion densities at  $35\tau$  and  $45\tau$  respectively, from which we can see that the ions have been further displaced leading to a indication of multistage acceleration process. . . . . 106

5.4 Figures (a), (c) and (e) shows the longitudinal electric field at times  $23\tau, 35\tau$  and  $45\tau$  respectively for  $n_i = 10n_c$  and  $a_0 = 30$ . (b), (d) and (f) shows the longitudinal velocity spectrum at similar times. We see that at  $23\tau$  the ions peak at a velocity  $0.348c$ . At  $45\tau$  we can see a second peak at a velocity of  $0.524c$ . . . . . 107

5.5 Plots of 1<sup>st</sup> and 2<sup>ND</sup> stage ion velocity of accelerated ions for  $a_0 = 20$ . The analytical results are represented by solid lines and the dots and circles represent first and second stage velocities respectively. The broken lines are the non-relativistic results. . . . . 108

5.6 Plots of 1<sup>st</sup> and 2<sup>ND</sup> stage ion kinetic energy of accelerated ions for  $a_0 = 20$ . The analytical results are represented by solid lines and the dots and circles represent first and second stage velocities respectively. The broken lines are the non-relativistic results. . . . . 108

5.7 Plots of 1<sup>st</sup> and 2<sup>nd</sup> stage ion velocity of accelerated ions for  $a_0 = 30$ . The analytical results are represented by solid lines and the dots and circles represent first and second stage velocities respectively. The broken lines are the non-relativistic results. . . . . 110

5.8 Plots of 1<sup>st</sup> and 2<sup>nd</sup> stage ion kinetic energy of accelerated ions for  $a_0 = 30$ . The analytical results are represented by solid lines and the dots and circles represent first and second stage velocities respectively. The broken lines are the non-relativistic results. . . . . 110

# 1

## Introduction

### 1.1 Overview and Motivation

For the last 100 years, physicists have used particle accelerators to explore atomic and sub-atomic structure, material science, structural biology, nuclear medicine, fusion research, food sterilization, transmutation of nuclear waste, cancer treatment and find answers to some of nature's profound questions.

Twentieth century witnessed an explosion in development of particle accelerators that can provide mono-energetic, ultra-intense particle beams that can go upto energies in TeV. These devices are either linear or circular and use radio frequency (RF) voltages across materials to accelerate particles. By increasing the RF voltages applied, the acceleration gradient could be increased. However, such devices are limited by the surface breakdown voltages which are of the order of MV/m. Due to this, there is an upper limit to the voltage that can be applied. Thus, if one has to increase the energy of accelerated beams, the size of the accelerator has to be increased. Energetic particle beams have wide variety of uses depending on their kinetic energies. Particle beams of energy ranging from a few hundred MeVs to a few GeVs have uses in particle therapy for oncological processes, generation of X-rays, building light sources, condensed matter physics, ion implantation, industrial processing and bio medical research. For particle physics, the beam velocities required are close to that of light and hence very large accelerators are required. Accelerators like LHC and Tevatron have diameter in kilometers [1]. Because of their large size, they are very expensive. Using current technology, generating ion beams of energy 200 to 300 MeV (required for cancer therapy) would cost around

\$200M, thus making such treatments beyond the reach of common people.

Need of the hour is therefore devising mechanisms to accelerate charged particles to high energies at a small distance. One of the mechanisms may be directly exposing charged particles to high electric fields in vacuum as there is no surface breakdown limit here. Ultra-intense lasers are a source of very high electric fields. Present day lasers are capable of intensities of the order of  $10^{22}W/cm^2$ [2]. This has been possible because of the chirped pulse amplification (CPA) technique developed by Mourou et.al.[3, 4]. As laser field constitute of oscillating electric ( $\mathbf{E}$ ) and magnetic ( $\mathbf{B}$ ) fields, the equation of motion of electrons in these fields can be written as,

$$\frac{d\mathbf{p}}{dt} = -e[\mathbf{E} + \mathbf{v} \times \mathbf{B}] \quad (1.1)$$

Here  $\mathbf{p}$  is the electron momentum. Electron motion in laser fields is referred to as quiver motion, and is defined as,

$$\frac{p_{osc}}{m_e c} = \frac{\gamma v_{osc}}{c} = \frac{eE_0}{m_e \omega c} = \sqrt{\frac{I \lambda_\mu^2}{1.3 \times 10^{18}}} \quad (1.2)$$

Here  $p_{osc}(v_{osc})$  is the transverse quiver momentum (velocity) of an electron in the laser field with an electric field amplitude  $E_0$ ,  $I$  is the laser intensity (in  $W/cm^2$ ),  $\lambda_\mu$  is the laser wavelength in microns and  $\gamma$  is the relativistic factor. Defining a dimensionless laser amplitude as  $a = eE_0/m_e \omega c$  the relativistic factor can be written such that  $\gamma = \sqrt{1 + \alpha a^2}$  with  $\alpha = 1$  for circularly polarized light and  $1/2$  for linear polarization. The energy associated with this momentum can easily reach MeV levels for electrons in the presence of lasers with intensities  $10^{19}W/cm^2$ . It is compelling that with the availability of high intensity lasers, electrons alone can be accelerated to very high energies in vacuum. However, electromagnetic energy cannot be easily dumped as kinetic energy in a particle. It is because an electron in a plane infinite EM field in the absence of any external fields in vacuum with no boundaries surrenders its energy back to the wave. This effect is known as Lawson-Woodward (LW) theorem[5, 6]. So in order to accelerate electrons in vacuum by an EM pulse the LW theorem needs to be violated. One of the ways to do this is by tightly focussing a laser beam[7, 8, 9, 10, 11, 12, 13]. A finite focal spot size will cause an electron to drift away from the beam axis, converting

its quiver energy to forward directed kinetic energy in the process. The energy gain from this essentially adiabatic process is almost equal to the ponderomotive energy  $\Delta u \approx 0.25m_e c^2 a^2$ . Thus, the electron simply slides down the ponderomotive potential without picking up any longitudinal component. Another method is by tailoring a laser beam profile in such a way that it creates ponderomotive potential well. One way by which this can be done is by superposing higher order light modes in such a way that there is an intensity minimum at the radial position  $r = 0$ [14].

We observed here that to accelerate charged particles by EM pulses in vacuum, the entire emphasis was to devise ways to violate the LW theorem. If we shift our attention from vacuum to plasma (a quasineutral gas of charged i.e. electrons and ions and neutral particles), we observe that all the assumptions of the LW theorem are violated[15]. Under the influence of an inhomogeneous EM field a charged particle drifts towards the weak field region. This drift is because of a nonlinear force called the ‘‘Ponderomotive force’’ arising due to the  $\mathbf{v} \times \mathbf{B}$  part of the Lorentz force. For a plasma of density  $n_0$ , the ponderomotive force exerted on the plasma species of mass  $m$  is given by [16]

$$\mathbf{F}_p = -\frac{\omega_p^2}{\gamma\omega^2} \nabla \left\langle \frac{\epsilon_0 \mathbf{E}^2}{2} \right\rangle \quad (1.3)$$

where  $\omega_p = (4\pi n_0 e^2/m)^{1/2}$  and  $\omega$  is the laser frequency. Electrons being much lighter than ions respond quickly to externally applied electric and magnetic fields generating local concentrations of positive and negative charge which give rise to self consistent electric fields. A particle injected into such a plasma would be accelerated by this charge separation field. As the magnitude of the ponderomotive force directly depends on the incident laser amplitude we observe that a plasma has an interesting property to efficiently convert transverse field of an electromagnetic wave to a longitudinal field of a plasma wave or other high gradient plasma structures like shock and sheath fields. The electrostatic field ( $E_s$ ) in these structures is proportional to the square root of the plasma density  $n_0$ . Hence for a plasma density of  $10^{18} \text{cm}^{-3}$  the electrostatic field gradient turns close to  $1 \text{GeV/cm}$ [17]. To analyze the interaction of EM waves in a plasma, we first look at the wave equation

governing the EM field which is given as,

$$\nabla^2 \mathbf{E} + \epsilon \mathbf{E} = 0 \quad (1.4)$$

where  $\epsilon = (1 - \omega_{pe}^2/\omega^2)$  is the plasma dielectric constant[16]. From Eq. 1.4 it is clear that there exists two class of solutions depending on the sign of  $\epsilon$ . When  $\epsilon$  is positive i.e.  $\omega_{pe}/\omega < 1$  (underdense plasma), we have propagating solutions. On the other hand, when  $\epsilon < 0$  i.e.  $\omega_{pe}/\omega > 1$  (overdense plasma) we have decaying solutions.

When the laser pulse interacting with the plasma is relativistically intense, strong nonlinear effects come to play. For such high intensities the quiver velocity of electrons become comparable to the velocity of light and the effect of relativistic mass variation becomes important. The electrons oscillating in the laser field gets heavier due to relativistic effects as  $m_{eff} = \gamma m_e$  where  $\gamma = 1/\sqrt{1 - v_{osc}^2/c^2}$  is the relativistic factor and  $v_{osc}$  is the quiver velocity of the electron. As a result of this relativistic increase in the electron mass the effective plasma frequency reduces to  $\omega_{peff} = \omega_p/\sqrt{\gamma}$  [18] and can even go below the frequency of the incident pulse. Consequently, the propagation of such intense pulses is allowed even in overdense region of the plasma . For such cases reflection will take place only when the local electron plasma frequency  $\omega_{peff}$  is greater than the laser frequency  $\omega$ . It should be noted that in such case the laser fields are evanescent at the surface with in the thickness of the order of skin depth. As the field intensity gain a spatial dependence, interaction with electrons become highly nonlinear.

An underdense plasma allows a laser pulse to normally pass through it. The coupling of electromagnetic wave energy into such plasma leads to generation of longitudinal plasma waves[19, 20]. A finite laser pulse injected into a plasma would generate an electrostatic wake behind the pulse via ponderomotive force. The group velocity of the pulse travelling inside the plasma is close to that of light. Once the light pulse has passed the space charge produced by this displacement pulls the electron back and a plasma oscillation is set up. The wake which propagates with velocity close to  $c$ , can trap electrons. The trapped electrons can gain a large amount of energy under the influence of the longitudinal field of the wake. This mechanism was first formulated by Tajima and Dawson in 1979[21]. The energy gained by the trapped electrons depended on the amplitude of the wake

generated. High amplitude wake could produce high energy electrons. However as the laser pulse move very fast, the plasma ions because of their high mass did not have enough time to respond to these wakefields. As a result this mechanism was limited to studying electron acceleration.

Overdense plasmas on the other hand reflect incident laser light due to the formation of electrons sheath on the plasma surface as a result of ponderomotive force. This induces an electrostatic charge separation field. If the pulse length is long enough, the plasma ions get sufficient time to respond to this field. This phenomenon is exploited to accelerate ions. The next section describes in detail the interaction of laser pulses with overdense plasma and how such interactions can give rise to energetic ions.

## 1.2 Laser pulse interaction with overdense plasmas

Laser interaction with underdense plasmas can be described as a reactive response of the matter to the light passing through it. In other words, one either considers how the properties of the pulse changes as it propagates, or either tries to find out what leaves behind assuming the material ahead of the pulse to be undisturbed. For overdense plasmas the picture is radically different. A overdense target (like metal) will initially reflect the laser pulse like a mirror.

Coupling the laser energy to the target material in overdense plasmas still remain one of the hottest issues in this field. This is because more than one physical picture is possible depending on whether the material is treated like a conductor or a sandwich of cold solid plus a hot, thin or extended layer of plasma in the region of the laser's focal spot. There is no single model which can adequately describe all the main pieces of absorption physics, mass and energy transport and so on.

Departures from the common wisdom which prevailed for nanosecond interactions [22] were predicted towards the end of the 1980's by a number of authors anticipating the first experiments with sub-picosecond lasers [23, 24, 25, 26]. They pointed out several ways in which the traditional laser plasma physics would not apply to short pulse lasers.

The first thing to be noted in interaction with solid targets is the field ionization over the first few laser cycles rapidly creates a surface plasma layer with a density

many times the critical density  $n_c$ . This is the density at which the plasma becomes opaque for an electromagnetic wave with frequency  $\omega$ , and is defined such that

$$\omega^2 = \frac{4\pi e^2 n_c}{m_e} \quad (1.5)$$

In practical units, this translates to

$$n_c \approx 1.1 \times 10^{21} \left( \frac{\lambda}{\mu m} \right)^{-2} cm^{-3} \quad (1.6)$$

Another aspect is the short pulse duration, which means that there is not enough time for a substantial region of coronal plasma to form in front of the target during the interaction. Just as in long pulse inertial confinement fusion (ICF) interactions, this underdense region is created by ablation. The plasma pressure created during heating causes matter to blow off at roughly the sound speed:

$$c_s = \left( \frac{Z k_B T_e}{m_i} \right)^{1/2} \approx 3.1 \times 10^7 \left( \frac{T_e}{keV} \right)^{1/2} \left( \frac{Z}{A} \right)^{1/2} cms^{-1} \quad (1.7)$$

where  $k_B$  is the Boltzmann constant,  $T_e$  the electron temperature and  $m_i$  the ion mass. Assuming the plasma expands isothermally[22], the density profile will assume an exponentially decreasing form with a well defined scale length “L” given in angstrom ( $A^0$ ) by the formula

$$L = c_s \tau_L \approx 3 \left( \frac{T_e}{KeV} \right)^{1/2} \left( \frac{Z}{A} \right)^{1/2} \tau_{fs} A^0 \quad (1.8)$$

Finally, because of a steep density gradient, the laser pulse interacts directly with the solid density plasma which has just formed and the laser energy can be deposited at much higher intensities than in nanosecond interactions. The initial situation we are faced with then, is an intense EM wave impinging on a highly overdense mirror like wall of plasma. In the absence of absorption, the electromagnetic field will form a standing wave pattern in front of the target, augmented by an evanescent component penetrating into the overdense region to a characteristic skin depth  $l_s = c/\omega_p$ . In the evanescent region, the laser intensity is non-uniform giving rise to nonlinear effects. The nonlinear force exerted in this region is the

ponderomotive force. When the laser pulse is linearly polarized, this force is

$$\mathbf{F}_p = \mathbf{f}_p(1 + \cos(2\omega t)) \quad (1.9)$$

where  $\mathbf{f}_p = -m_e c^2 / 2\gamma \nabla a^2$ . The ponderomotive force in this case is composed of a dc component and an oscillatory component that oscillates the electrons within the skin depth with a frequency of twice the laser frequency. If the magnitude of the force is large enough, all the electrons at the boundary will oscillate in this field in the direction of  $\mathbf{k}$  vector of the laser. The phases of some electrons in this field may be such that they gain energy from this oscillation, i.e. the electrons are given a non-adiabatic kick into the overdense plasma. The fraction of electrons that escape depends on the strength of the oscillating force. This gives rise to the  $\mathbf{J} \times \mathbf{B}$ [27] heating of the plasma. On the other hand, for a circularly polarized laser the oscillatory component is zero when averaged over one laser cycle. Hence, there is no such heating. It is because of this reason that a circularly polarized laser can lead to steady shock structures in an overdense plasma[28].

It has been shown in [29, 30, 31, 31, 32, 33, 34] that there are two different cases when it comes to interaction of a circularly polarized laser beam with a plasma of density  $n_0$ : (i) When  $n_0 < 1.5n_c$  and (ii)  $n_0 > 1.5n_c$ , which are also confirmed by computer simulations[35, 36]. In fact, at  $n_0 < 1.5n_c$ , it was shown by Marburger and Trooper[29] that in a stationary regime there is a continuous family of solutions for the everywhere positive electron density distribution. This means that the penetration deep into the plasma occurs in a “classical” way, through lowering the effective plasma frequency due to both relativistic and ponderomotive nonlinearities. Modelling the self induced transparency (SIT) effect using PIC simulations and the fluid approach showed quantitatively close results, indicating that kinetic effects are not important for this case, at least for incident intensities not much exceeding the threshold of penetration. The situation changes drastically at densities  $n_0 > 1.5n_c$ , when the relativistic EM wave can considerably reduce the electron density in the region of its front until electron cavitation takes place. This electron cavitation acts as a “wall” making the plasma opaque to the propagation. Thus, for laser penetration into a rather thick overdense plasma, a travelling plane wave approach cannot be applied because in real situations this regime cannot be achieved, although, due to the relativistic increase of the electron mass and

the associated decrease of the effective plasma frequency, the nonlinear refractive index may become positive. The nonlinear ponderomotive force generated in the laser plasma interaction leads to a compression of the electron density profile that counteracts the increased penetration due to relativistic nonlinearity and plays a crucial role in the description of the interaction between an overdense plasma and high intensity laser radiation[37, 38].

### 1.3 Ion acceleration in solid targets

The direct interaction of protons and heavier ions with laser light at presently achievable intensities is by far not strong enough to accelerate these particles to MeV energies. Similar to the relativistic threshold for electrons  $I_e \lambda^2 = 1.37 \times 10^{18} [W \mu m^2 / cm^2]$ , one can derive the intensity when the kinetic energy of an oscillating proton in the laser field is equal to its rest energy[39],

$$I_p \lambda^2 = \left( \frac{m_p}{m_e} \right)^2 \approx 5 \times 10^{24} [W \mu m^2 / cm^2] \quad (1.10)$$

This intensity is far beyond the present laser technology. However, the plasma electrons can mediate the forces of laser fields on ions by generation of strong and quasi-static electric fields arising from local charge separations. These fields can be of the same magnitude as the fast oscillating laser fields, but they vary on a time scale comparable to the laser pulse duration giving the ions a significantly longer time to be accelerated. In this section we describe three mechanisms of laser ion acceleration: (i) Target Normal Sheath Acceleration (TNSA), (ii) Radiation pressure acceleration (RPA) and (iii) Ion acceleration in clusters.

#### 1.3.1 Target Normal Sheath Acceleration (TNSA)

In this mechanism foils, several microns thick are irradiated with ultra-intense laser pulses. On reaching a plasma vacuum interface, the plasma electrons stream out into vacuum, while the plasma ions are relatively immobile due to their higher mass. Because of negative charge escaping into vacuum a large positive charge is induced at the plasma vacuum interface. The positive potential electrostatically

traps most of the relativistic electrons, drawing them back to the interface. As long as there is a source of fast electrons, i.e. over the laser pulse duration, a capacitor plate like charge separation is formed with electric fields of the order of  $10^{12}\text{V/m}$  generated at the interface. Light ions at the plasma vacuum surface are most readily accelerated in the field, reaching energies of tens of megavolts over an acceleration length of few tens of microns, over picosecond time scales. As the ions gain energy, the sheath field drops and the fast ions and electrons propagate ballistically as a quasi-neutral beam. This mechanism was first devised by Snavely and Wilks[40] in short-pulse experiments using the NOVA-Petawatt laser at the Lawrence Livermore National Laboratory where the emission of protons to both rear surfaces of a wedge -shaped target was observed. The basic theory describing this mechanism has been further developed in[41, 42, 43, 44, 45].

### 1.3.2 Radiation Pressure Acceleration (RPA)

Radiation pressure acceleration (RPA) of ions occur in two regimes depending on the thickness of the plasma target on which the laser is normally incident. (i) Light Sail regime and (ii) Hole Boring regime. Both these mechanisms are described separately below.

#### *Light Sail regime of RPA*

When a high-irradiance laser pulse with sufficiently large focal spot interacts with a thin foil, it can push forward the electrons due to the radiation pressure; ideally, all electrons are involved. The ions respond slowly, and a large charge separation field builds up and efficiently accelerates the main body of the irradiated target area, i.e. the ions. If this charge separation field is strong enough to accelerate ions quickly to relativistic velocity, the distance between the electrons and ions remains relatively small, and instabilities do not have time to develop [46]. Note that this scenario in the optimum condition borders with the Coulomb explosion mechanism described above. At the second stage, the ions and electrons moving together represent a relativistic mirror co-moving with the laser pulse, as in the “light sail”paradigm. Even if at the early stage the foil is partly transparent to the laser due to relativistic effects, at a later time, when the foil velocity approaches  $c$ ,

it becomes highly reflective due to the laser frequency downshift in the co-moving frame. Further, due to the double Doppler effect, the frequency of the reflected light becomes  $\omega_r \approx \omega_0/4\gamma^2$ , where  $\gamma \gg 1$  is the relativistic gamma-factor of the accelerated foil, and the reflected light energy significantly decreases; almost all of the laser pulse energy is transferred to the foil. At the final acceleration phase, the ions moving with nearly the same velocity as electrons take most of this energy due to their much larger mass. This acceleration mechanism has much in common with Veksler's collective acceleration[47, 48].

The equation of motion of the moving foil was derived in [46, 49, 50]. Tripathi et al. [50] also calculated the critical thickness  $\Delta$  of the foil required for this process. The critical thickness was given as

$$\Delta = \frac{a_0 n_c \lambda_L}{\pi n_0} \quad (1.11)$$

where  $a_0$  is the dimensionless laser amplitude,  $\lambda_L$  is the laser wavelength,  $n_0$  is the initial plasma density and  $n_c$  is the critical density. It was found that the reflectivity, calculated using the sliding mirror approximation ([51, 52, 53, 54, 55]), of the thin foil increases with the velocity of the foil and tends to 1 as the foil velocity approaches  $c$ .

In order to implement this idealized scenario, however, several conditions should be met. First, in order to repel all electrons, which corresponds to the maximum achievable acceleration, the laser electric field should be of the order of the maximum charge-separation field, which corresponds to the target thickness given by Eq. 1.11 [50, 54]. Second, the ions must be quickly accelerated up to relativistic velocity to suppress the development of instabilities. 1D and 2D PIC simulations suggest that the intensity requirement to achieve high velocities can be substantially relaxed by using circular polarization, which induces much less electron heating [56, 57, 58, 59, 60, 61, 62, 63] and target structuring [62]. Third, the focal spot size must be relatively large to keep the quasi-1D dynamics; for this reason, a super-Gaussian or flat-top pulse is advantageous compared with a Gaussian one [57, 58, 59, 64]. Fourth, for large ion energies the Rayleigh length should be at least of the order of the acceleration length; other possibilities include several focused laser pulses[65, 66]. Another elegant way is to employ a cocoon formed by the plasma to confine the laser pulse, which can in this case propagate

without divergence much longer than the Rayleigh length[46, 67]. Fifth, the pulse duration should be sufficiently short, such that the instabilities do not destroy the foil, but sufficiently long, such that the very efficient final acceleration phase is achieved.

### *Hole Boring regime of RPA*

If an overdense target is relatively thick, it cannot be treated as a thin foil, as in the “light sail”RPA acceleration regime. However, the plasma is still pushed forward by the radiation pressure, the so-called hole boring process[68]. This gives rise to another kind of radiation pressure acceleration mechanism, hole boring acceleration or collisionless shock acceleration [69, 70, 71, 72, 73, 74]. Ion acceleration attributed to collisionless shocks has been reported by Henig et. al.[75] (protons up to 8 MeV using 0.6 J, 45 fs, 20TW laser irradiating overdense micro-sphere targets) and Wei et. al.[76] (helium up to 13 MeV using 180 J, 0.5-0.7 ps, 0.25PW laser irradiating an underdense gas jet target).

In a simple 1D quasi-stationary model of hole boring acceleration [77], the laser pulse piles up the electrons, forming a thin electron spike in front of the pulse; an electron free area appears behind the spike. It is assumed that the laser pulse is totally reflected from the electron spike. The ions left behind are pulled by the arising charge separation field, thus forming the second ion spike. In the boosted frame moving with the hole boring velocity, the unperturbed plasma ions impinging on these moving spikes are accelerated (“reflected”) by the electric field existing between the spikes; at the turning point, the ion velocity changes sign, and at zero velocity the ion density tends to infinity. Analogously, the electron spike also has a sharp rear edge. Thus, an electrostatic shock propagating into a plasma is formed (hence there is another name for this acceleration mechanism, collisionless electrostatic shock acceleration (CESA)). In contrast to the electrostatic collisionless shocks in low-density plasmas, in the case of high-density, low-temperature i.e. small thermal velocity and large ( $\gg 1$ ) Mach number plasmas, the unperturbed plasma electrons and ions can be nearly totally reflected by the laser ponderomotive pressure and the longitudinal charge separation electric field between the two spikes. For this reason, a circularly polarized laser pulse normally incident to the target is advantageous for this mechanism, as in this case the plasma is heated less

effectively [54, 72, 73].

Unlike the “light sail” case, hole boring has a quasi-stationary velocity, because the radiation pressure is balanced by the momentum change of the continuously reflecting particles of the unperturbed plasma, mostly ions due to their larger mass. The 1D model of hole boring predicts a mono-energetic ion spectrum. This is indeed confirmed in the 1D PIC simulations. However, even for constant-intensity pulses, as  $a_0$  increases, the finite acceleration time, which is in contrast to the instantaneous ion reflection assumed in the model, causes periodical oscillations of the hole boring velocity and periodical overtaking of the electron spike by the ion spike, which in turn results in broad ion spectra [77, 78].

It is seen that the ions obtained in hole boring mode of acceleration has lower peak energies and wide energy distribution than that obtained by light sail. However, the problems with making ultra-thin targets and less sensitivity of thick targets towards laser prepulse and spatial intensity variation makes hole boring mode an attractive choice for high intensity laser ion acceleration.

There are a number of issues with hole boring and light sail modes of ion acceleration. These are the effect of longitudinal magnetic field that induces cyclotron motion [79, 80], transverse instabilities [59, 81, 82, 83], effect of multiple ion species and laser spot profile [59, 57, 73, 84]. These issues are important to understand the mechanism of ion acceleration in realistic conditions and hence needs to be investigated thoroughly. In the context of scope mentioned above, this thesis is related to study of issues related to ponderomotive ion acceleration in bulk targets like effect of axial static magnetic field, transverse instabilities, presence of multiple ion species, axial magnetic field generation because of transverse inhomogeneity of laser and multi-stage acceleration as a result of long pulse length.

## 1.4 Organization of the thesis

This thesis is mainly devoted to analytical and computational investigation of ion acceleration by relativistic laser pulses in overdense plasma targets having thickness of a few laser wavelengths. Analytical theories have been developed to describe the ion acceleration process for plasma targets composed to single and multiple species together with effects of externally applied fields. 1D3V particle in cell simulations

have been carried out to further study and validate the theories. The thesis consists of six chapters including the present one. The brief contents of the next five chapters are presented below.

### 1.4.1 Chapter 2: Ponderomotive Ion Acceleration in dense magnetized laser-irradiated thick target plasmas

Application of static longitudinal magnetic field induces cyclotron motion in the electron sheath formed due to ponderomotive force of the laser. The magnetic fields which are observed in experiments with laser irradiated solid targets[85, 86, 87], can play an important role in laser driven ion acceleration. Wilks et.al.[68] and Sudan[88] studied the interaction of an ultra-intense laser with an overdense target and predicted magnetic fields upto 1GG. Cai et. al.[89] studied the role of electron cavitation in the generation of strong quasi-static magnetic field in the interaction of ultra-intense laser pulse with overdense plasmas. Haines[90] proposed a mechanism for generation of an axial magnetic field through the deposition of spin of the photons during the absorption of circularly polarized light of finite radius in an underdense plasma. The time dependent magnetic field thus generated has a magnitude proportional to the transverse gradient of the absorbed intensity but inversely proportional to the electron density.

Plasma electrons under the influence of the electric field of a circularly polarized laser produce circular motion. Same kind of motion is also exhibited by electrons in an axial magnetic field. We find that the electron motion under the field of a right circularly polarized (RCP) laser is in the same direction of the cyclotron motion. This gives rise to a resonance state that leads to an enhanced ponderomotive force. On the other hand for left circularly polarized (LCP) light, the oscillatory and cyclotron motion are in opposite direction leading to a reduction in the ponderomotive force exerted. Thus, we find that for a given laser intensity, the ponderomotive forces exerted by RCP and LCP light differs. As a result of this the extent upto which the electrons are pushed inside the plasma also varies and gives rise to different charge separation leading to varying electrostatic fields. As it is this induced electrostatic field that accelerates plasma ions, RCP and LCP lasers give ion beams of different energies for a given intensity and plasma density.

It has been seen in sec.1.3.2 that the accelerated ions originate from a thin ion sheath lying close to the electron sheath. Behind this ion sheath lies a region of residual ions that do not take part in the direct acceleration process. In this chapter, we find that this region undergoes coulomb explosion and its density decreases uniformly with time. It has also been found that the electrostatic field within this region can reflect incoming ions and the reflected velocity is found to be greater than the incident velocity. As a result, this region acts as a velocity amplifier for incoming ions.

### 1.4.2 Chapter 3: Self consistent model for ponderomotive ion acceleration of laser irradiated two species dense target plasmas

It has been observed in previous theories that the ion energy obtained in HB-RPA increases with laser intensity and decreases with plasma density for a plasma target composed of single ion species [73, 78]. As the energy obtained by the ions are a result of net momentum transfer from the laser pulse to the plasma ions, it can be expected that if the target plasma is doped with lighter ions then the total light momentum will be distributed proportionally to both the species. The laser piston in this case moves at a constant velocity determined by the mass and proportion of both the ion species. For a given laser intensity and plasma number density, the piston velocity is higher for lighter mass ions than the heavier species. However, in case of a composite target the piston velocity will be intermediate between the two cases. As a result both the species will move with the same velocity and the kinetic energy of heavier species will be higher than that obtained in the single species target [74, 91]. A self consistent analytical theory has been formulated to describe this process. From the theory it is clear that in such processes the laser piston is composed of three layers instead of two as in case of single ion species. The structure of the laser piston gave information about the thickness and mass of the accelerating region.

The accelerating structure (laser piston) seems analogous to a heavy fluid suspended over a light fluid (laser radiation pressure in this case) under the influence of an electrostatic force (analogous to gravity). Such a system is susceptible to Rayleigh-Taylor (RT) instability. Using the analytical model described in this

chapter we determine the growth rate of RT instability and its dependence on the ratio of number density of both the species in the target.

### 1.4.3 Chapter 4: Analytical model for axial magnetic field generation by interaction of radially inhomogeneous laser pulse with solid target

Recent remarkable progress in the development of intense ( $I\lambda^2 > 10^{18} \text{W}\mu\text{m}^2/\text{cm}^2$ ) short pulse ( $< 1\text{ps}$ ) lasers has stimulated worldwide interest in relativistic intense laser plasma interaction[92]. In this interaction, the generation of huge quasi-static magnetic fields is one of the most significant phenomena which has considerable influences on the whole nonlinear plasma dynamics. The study of this problem has wide applications in fast ignition scheme[93] for inertial confinement fusion, particle acceleration[94], and laboratory astrophysics[95]. The experiments[96, 97] report that magnetic fields about tens of mega-Gauss (MG), including the axial component  $B_z$  and the azimuthal one  $B_\theta$ , are generated in underdense plasma. It should be noted that in case of interaction of a circularly polarized wave with matter, the axial magnetic field is inherently generated due to inverse Faraday effect (IFE) if the transverse effects are taken into account [90, 98, 99, 100].

Although much effort has been devoted to quasi-static axial magnetic field generation in plasmas using circularly polarized lasers, a self consistent fluid theory incorporating both azimuthal and magnetization currents determined solely from laser and plasma parameters do not exist. In this chapter the hole boring radiation pressure acceleration model is further extended to two dimensions with transverse inhomogeneity in laser intensity profile. A two dimensional analytical fluid treatment has been done for the interaction process and it was found that such laser pulses produce transverse electron density inhomogeneity which produce non-zero azimuthal currents. Also the circular motion of electrons under the influence of laser fields produces magnetization current. Thus the azimuthal and magnetization currents together produce an axial magnetic field extending to a few hundred megagauss. Using azimuthal symmetry, electron density profile of the sheath is determined self consistently as a function of radial (r) and axial coordinates (z). The density inhomogeneity introduced gives rise to azimuthal current as well as a

magnetization is induced due to the circular motion of sheath electrons under the influence of the laser field. An algebraic expression for this magnetic field obtained self consistently from laser and plasma parameter has been given.

#### 1.4.4 Chapter 5: Relativistic theory for multistage ion acceleration

In the HB-RPA regime, it has been found that when the initial target is cold, the flat-top laser pulse acts as a steady piston and drives a flow of ions in the front surface into the target, which is similar to ions reflecting off an electrostatic shock front. The electrostatic field induced by the charge separation at the front surface of the target is steady enough to accelerate ions in multiple stages. That is, after the whole ion plasma is accelerated to a quasi-monoenergetic state, another acceleration process begins for the continuing steady state.

A non relativistic theory has been given in [73] and has been verified using particle in cell (PIC) simulations. However, further from PIC simulations it can be seen that at very high laser intensities, such that the piston velocity turns relativistic, this theory is no more valid. In this chapter a fully relativistic analytical theory has been devised for multistage acceleration process. Further 1D3V PIC simulations for such systems have been performed using LPIC++[101]. The simulation results are found to closely match with the analytical prediction, thus validating our proposed theory. Also a comparative study of the relativistic and non-relativistic theories have been done and a significant difference in both the cases has been noted.

#### 1.4.5 Chapter 6: Conclusions and Future direction

In this chapter we briefly summarize the results of the whole thesis. We then provide a glimpse of the possible future research that can be carried out in continuation of the work described here.

# Bibliography

- [1] <http://www.cern.ch>; <http://www.fnal.gov>
- [2] V. Yanovsky, V. Chvykov, G. Kalinchenko, P. Rousseau, T. Planchon, T. Mat-suoka, A. Maksimchuk, J. Nees, G. Cheriaux, G. Mourou and K. Krushelnick, *Opt. Express* **16**, 2109 (2008).
- [3] G. Mourou and D. Umstadter, *Phys. Fluids B* **4**, 2315 (1992).
- [4] G. Mourou, C.P.J. Barty and M.D. Perry, *Phys. Today* **51**, 22 (1998).
- [5] P.M. Woodward, *J. Inst. Electr. Eng.* **93**, 1554 (1947).
- [6] J.D. Lawson, *IEEE Trans. Nuc. Sci.* **26**, 4217 (1979).
- [7] Salamin, Yousef I. and Keitel, Christoph H., *Phys. Rev. Lett.* **88**, 095005 (2002); <http://link.aps.org/doi/10.1103/PhysRevLett.88.095005>.
- [8] Salamin, Yousef I. and Mocken, Guido R. and Keitel, Christoph H., *Phys. Rev. ST Accel. Beams* **10**, 101301 (2002).
- [9] Han Xu and Wei Yu and Peixiang Lu and V. K. Senecha and Feng He and Baifei Shen and Liejia Qian and Ruxin Li and Zhizhan Xu, *Phys. Plasmas* **12**, 013105 (2005).
- [10] He, Feng and Yu, Wei and Lu, Peixiang and Xu, Han and Qian, Liejia and Shen, Baifei and Yuan, Xiao and Li, Ruxin and Xu, Zhizhan, *Phys. Rev. E* **68**, 046407 (2003).
- [11] Vikram Sagar and Sudip Sengupta and Predhiman Kaw, *Phys. Plasmas* **19**, 113117 (2012).
- [12] Wang, P. X., Ho, Y. K., Yuan, X. Q., Kong, Q., Cao, N., Sessler, A. M., Esarey, E. and Nishida, Y., *Appl. Phys. Lett.* **78**, 2253 (2001).
- [13] Kong, Q. and Ho, Y. K. and Wang, J. X. and Wang, P. X. and Feng, L. and Yuan, Z. S., *Phys. Rev. E* **61**, 1981 (2000).
- [14] Stupakov, G. V. and Zolotarev, M. S., *Phys. Rev. Lett.* **86**, 5274 (2001).

- [15] Paul Gibbon, Short Pulse Laser Interactions with Matter, Imperial College Press (2005).
- [16] Francis F. Chen, Plasma Physics and Controlled Fusion, Vol. 1 second edition, pp. 305-307.
- [17] W.P. Leemans, B. Nagler, A.J. Gonsalves, Cs Toth, K. Nakamura, C.G.R. Geddes, E. Esarey, C.B. Schroeder and S.M. Hooker, Nature Physics **2**, 696 (2006).
- [18] Predhiman Kaw and John Dawson, Physics of Fluids **13**, 472 (1970).
- [19] A. I. Akheizer and R. V. Polovin, Sov. Phys. JETP **3**, 696 (1956).
- [20] John M. Dawson, Phys. Rev. **113**, 383-387 (1959).
- [21] T. Tajima and J.M. Dawson, Physical Review Letters **43**, 267 (1979).
- [22] Kruer, William L., and John M. Dawson. "The physics of laser plasma interactions." Physics Today **42** (1989): 69.
- [23] Gamaliy E G and Tikhonchuk V T (1988), JETP Lett. **48**, 453-5.
- [24] More, R. M., Z. Zinamon, K. H. Warren, R. Falcone, and M. Murnane. "Heating of solids with ultra-short laser pulses." Le Journal de Physique Colloques **49**, no. C7 (1988): 7-7.
- [25] Mulser P, Pfalzner S and Cornolti F (1989) Laser Interaction with Matter ed G Velarde et al (Singapore: World Scientific) pp 142-5.
- [26] Milchberg, H. M., and Richard R. Freeman. "Light absorption in ultrashort scale length plasmas." JOSA B **6**, no. 7 (1989): 1351-1355.
- [27] Wilks, Scott C., and William L. Kruer. "Absorption of ultrashort, ultra-intense laser light by solids and overdense plasmas." IEEE Journal of Quantum Electronics **33**, no. 11 (1997): 1954-1968.
- [28] Lichters, Roland, J. Meyer-ter-Vehn, and A. Pukhov. "Short-pulse laser harmonics from oscillating plasma surfaces driven at relativistic intensity." Physics of Plasmas **3**, no. 9 (1996): 3425-3437.

- [29] JH Marburger and RF Trooper, Phys. Rev. Lett. **35**, 1001 (1975).
- [30] CS Lai, Phys. Rev. Lett. **36**, 966 (1976).
- [31] F. S. Felber and J. H. Marburger, Phys. Rev. Lett. **36**, 1176 (1976).
- [32] A. Kim, F. Cattani, D. Anderson, and M. Lisak, JETP Lett. **72**, 241 (2000).
- [33] A. V. Korzhimanov, V. I. Eremin, A. V. Kim, and M. R. Tushentsov, JETP **105**, 675 (2007).
- [34] B. Shen and Z. Xu, Phys. Rev. E **64**, 056406 (2001).
- [35] M. Tushentsov, A. Kim, F. Cattani, D. Anderson, and M. Lisak, Phys. Rev. Lett. **87**, 275002 (2001).
- [36] V. I. Berezhiani, D. P. Garuchava, S. V. Mikeladze, K. I. Sigua, N. L. Tsintsadze, S. M. Mahajan, Y. Kishimoto, and K. Nishikawa, Phys. Plasmas **12**, 062308 (2005).
- [37] F. Cattani, A. Kim, D. Anderson, and M. Lisak, Phys. Rev. E **62**, 1234 (2000).
- [38] Eremin, V. I., A. V. Korzhimanov, and A. V. Kim. "Relativistic self-induced transparency effect during ultraintense laser interaction with overdense plasmas: Why it occurs and its use for ultrashort electron bunch generation." Physics of Plasmas **17**, no. 4 (2010): 043102-043102.
- [39] Pukhov, Alexander. "Strong field interaction of laser radiation." Reports on progress in Physics **66**, no. 1 (2002): 47.
- [40] R. A. Snavely, M. H. Key, S. P. Hatchett, T. E. Cowan, M. Roth, T. W. Phillips, M.A. Stoyer, E. A. Henry, T. C. Sangster, M. S. Singh, S. C. Wilks, A. J. Mackinnon, A. Offenberger, D. M. Penning, K. Yasuike, A. B. Langdon, B. F. Lasinski, J. Johnson, M. D. Perry, and E. M. Campbell, Intense high-energy proton beams from petawatt-laser irradiation of solids, Physical Review Letters **85**, 2945 (2000).
- [41] S. C. Wilks, A. B. Langdon, T. E. Cowan, M. Roth, M. Singh, S. Hatchett, M. H.Key, D. Pennington, A. MacKinnon, and R. A. Snavely, Energetic proton

- generation in ultra-intense laser-solid interactions, *Physics of Plasmas* **8**, 542 (2001).
- [42] P. Mora, *Phys. Rev. Lett.* **90**, 185002 (2003).
- [43] V. Yu. Bychenkov, V. N. Novikov, D. Batani, V. T. Tikonchuk and S. G. Bochkarev, *Phys. Plasmas* **11**, 3242 (2004).
- [44] Y. Sentoku, T. E. Cowan, A. Kemp and H. Ruhl, *Phys. Plasmas* **10**, 2009 (2003).
- [45] A. J. Kemp and H. Ruhl, *Phys. Plasmas* **12**, 033105 (2005).
- [46] T. Esirkepov, M. Borghesi, S. V. Bulanov, G. Mourou and T. Tajima, *Phys. Rev. Lett.* **92**, 175003 (2004).
- [47] Veksler V I (1956), Coherent principle of acceleration of charged particles Proc. CERN Symp. of High Energy Accelerators and Pion Physics (Geneva, Switzerland) vol **1**, p 80.
- [48] Veksler V I (1957), *Atomnaya Energiya* **2**, 427.
- [49] Bulanov S V, Esirkepov T Zh, Koga J and Tajima T (2004), Interaction of electromagnetic waves with plasma in the radiation-dominated regime *Plasma Phys. Rep.* **30**, 196-213.
- [50] V. K. Tripathi, C. S. Liu, X. Shao, B. Eliasson and R. Z. Sagdeev, *Plasma Phys. Controlled Fusion* **51**, 024014 (2009).
- [51] Vshivkov V A, Naumova N M, Pegoraro F and Bulanov S V (1998), Nonlinear electrodynamics of the interaction of ultra-intense laser pulses with a thin foil *Phys. Plasmas* **5**, 2727-2741.
- [52] Pirozhkov A S, Bulanov S V, Esirkepov T Zh, Mori M, Sagisaka A and Daido H (2006), Generation of high-energy attosecond pulses by the relativistic-irradiance short laser pulse interacting with a thin foil *Phys. Lett. A* **349**, 256-263.

- [53] Pirozhkov A S, Bulanov S V, Esirkepov T Zh, Mori M, Sagisaka A and Daido H, (2006) Attosecond pulse generation in the relativistic regime of the laser–foil interaction: the sliding mirror model *Phys. Plasmas* **13**, 013107.
- [54] Macchi A, Veghini S and Pegoraro F (2009), “Light sail” acceleration reexamined *Phys. Rev. Lett.* **103** 085003.
- [55] Macchi A, Veghini S, Liseykina T V and Pegoraro F (2010), Radiation pressure acceleration of ultrathin foils *New J. Phys.* **12**, 045013.
- [56] Liseykina T V and Macchi A (2007), Features of ion acceleration by circularly polarized laser pulses, *Appl. Phys. Lett.* **91**, 171502.
- [57] Klimo O, Psikal J, Limpouch J and Tikhonchuk V T (2008), Monoenergetic ion beams from ultrathin foils irradiated by ultrahigh-contrast circularly polarized laser pulses, *Phys. Rev. ST Accel. Beams* **11**, 031301.
- [58] Liseykina T V, Borghesi M, Macchi A and Tuveri S (2008), Radiation pressure acceleration by ultraintense laser pulses *Plasma Phys. Control. Fusion* **50**, 124033.
- [59] Robinson A P L, Zepf M, Kar S, Evans R G and Bellei C (2008), Radiation pressure acceleration of thin foils with circularly polarized laser pulses, *New J. Phys.* **10**, 013021.
- [60] Rykovanov S G, Schreiber J, Meyer-ter-Vehn J, Bellei C, Henig A, Wu H C and Geissler M (2008), Ion acceleration with ultra-thin foils using elliptically polarized laser pulses, *New J. Phys.* **10**, 113005.
- [61] X. Q. Yan, C. Lin, Z. M. Sheng, Z. Y. Guo, B. C. Liu, Y. R. Lu, J. X. Fang and J. E. Chen, *Phys. Rev. Lett.* **100**, 135003 (2008).
- [62] Chen M, Pukhov A, Yu T P and Sheng Z M (2009), Enhanced collimated GeV monoenergetic ion acceleration from a shaped foil target irradiated by a circularly polarized laser pulse, *Phys. Rev. Lett.* **103**, 024801.
- [63] Macchi A, Liseykina T V, Tuveri S and Veghini S (2009), Theory and simulation of ion acceleration with circularly polarized laser pulses, *C. R. Physique* **10**, 207–215.

- [64] Bulanov S S et. al. (2008), Accelerating monoenergetic protons from ultrathin foils by flat-top laser pulses in the directed-Coulomb-explosion regime, *Phys. Rev. E* **78**, 026412.
- [65] McLeod J H (1954), The Axicon: a new type of optical element, *J. Opt. Soc. Am.* **44**, 592-7.
- [66] Bunkin F V, Korobkin V V, Kurinyi Y A, Polonskii L Y and Pyatnitskii L N (1983), Laser spark with a continuous channel in air, *Sov. J. Quantum Electron.* **13**, 254-5.
- [67] Bulanov S V, Esirkepov T, Migliozi P, Pegoraro F, Tajima T and Terranova F (2005), Neutrino oscillation studies with laser-driven beam dump facilities *Nucl. Instrum. Methods, Phys. Res. A* **540**, 25-41.
- [68] Wilks S C, Kruer W L, Tabak M and Langdon A B (1992), Absorption of ultra-intense laser-pulses, *Phys. Rev. Lett.* **69**, 1383-6.
- [69] Denavit J (1992), Absorption of high-intensity subpicosecond lasers on solid density targets, *Phys. Rev. Lett.* **69**, 3052-5.
- [70] Zhidkov A, Uesaka M, Sasaki A and Daido H (2002), Ion acceleration in a solitary wave by an intense picosecond laser pulse, *Phys.Rev. Lett.* **89**, 215002.
- [71] Silva L O, Mati M, Davies R, Fonseca R A, Ren C, Tsung F S and Mori W B (2004), Proton shock acceleration in laser-plasma interaction, *Phys. Rev. Lett.* **92**, 015002.
- [72] Macchi A, Cattani F, Liseykina T V and Cornolti F (2005), Laser acceleration of ion bunches at the front surface of overdense plasmas, *Phys. Rev. Lett.* **94**, 165003.
- [73] Zhang X, Shen B, Li X, Jin Z and Wang F (2007), Multistaged acceleration of ions by circularly polarized laser pulse: monoenergetic ion beam generation, *Phys. Plasmas* **14**, 073101.
- [74] Zhang X, Shen B, Li X, Jin Z, Wang F and Wen M (2007), Efficient GeV ion generation by ultraintense circularly polarized laser pulse, *Phys. Plasmas* **14**, 123108.

- [75] Henig A et. al. (2009), Laser-driven shock acceleration of ion beams from spherical mass-limited targets, *Phys. Rev. Lett.* **102**, 095002.
- [76] Wei M S et. al. (2004), Ion acceleration by collisionless shocks in high-intensity-laser-underdense-plasma interaction, *Phys. Rev. Lett.* **93**, 155003.
- [77] Schlegel T, Naumova N, Tikhonchuk V T, Labaune C, Sokolov I V and Mourou G (2009), Relativistic laser piston model: ponderomotive ion acceleration in dense plasmas using ultraintense laser pulses, *Phys. Plasmas* **16**, 083103.
- [78] A. P. L. Robinson, P. Gibbon, M. Zepf, S. Kar, R. G. Evans and C. Bellei, *Plasma Phys. Controlled Fusion* **51**, 024004 (2009).
- [79] S. Anamika, C. S. Liu and V. K. Tripathi, *Phys. Plasmas* **17**, 013101 (2010).
- [80] U. Sinha and P. Kaw, *Phys. Plasmas* **19**, 033102 (2012).
- [81] F. Pegoraro and S. V. Bulanov, *Phys. Rev. Lett.* **99**, 065002 (2007).
- [82] K. Adusumilli, D. Goyal, and V. K. Tripathi, *Phys. Plasmas* **19**, 013102 (2012), DOI:10.1063/1.3671957.
- [83] U. Sinha, *Phys. Plasmas* **19**, 043104 (2012).
- [84] Zhang, Xiaomei, Baifei Shen, Liangliang Ji, Fengchao Wang, Zhangying Jin, Xuemei Li, Meng Wen, and John R. Cary. "Ion acceleration with mixed solid targets interacting with circularly polarized lasers." *Physical Review Special Topics-Accelerators and Beams* **12**, no. 2 (2009): 021301.
- [85] M. Borghesi, A. J. MacKinnon, A. R. Bell, R. Gaillard, and O. Willi, *Phys. Rev. Lett.* **81**, 112 (1998).
- [86] U. Wagner, M. Tatarakis, A. Gopal, F. N. Beg, E. L. Clark, A. E. Dangor, R. G. Evans, M. G. Haines, S. P. D. Mangles, P. A. Norreys, M. S. Wei, M. Zepf, and K. Krushelnick, *Phys. Rev. E* **70**, 026401 (2004).
- [87] M. Tatarakis, A. Gopal, I. Watts, F. N. Beg, A. E. Dangor, K. Krushelnick, U. Wagner, P. A. Norreys, E. L. Clark, M. Zepf, and R. Evans, *Phys. Plasmas* **9**, 2244 (2002).

- [88] Sudan, R. N. "Mechanism for the generation of  $10^9$  G magnetic fields in the interaction of ultraintense short laser pulse with an overdense plasma target", *Physical review letters* **70**, no. 20 (1993): 3075-3078.
- [89] H. Cai, W. Yu, S. Zhu, and C. Zhou, *Phys. Rev. E* **76**, 036403 (2007).
- [90] M. G. Haines, *Phys. Rev. Lett.* **87**, 135005 (2001).
- [91] Robinson, A. P. L., D. H. Kwon, and K. Lancaster. "Hole-boring radiation pressure acceleration with two ion species." *Plasma Physics and Controlled Fusion* **51**, no. 9 (2009): 095006.
- [92] Borisov, A. B., A. V. Borovskiy, V. V. Korobkin, A. M. Prokhorov, O. B. Shiryaev, X. M. Shi, T. S. Luk et al. "Observation of relativistic and charge-displacement self-channeling of intense subpicosecond ultraviolet (248 nm) radiation in plasmas." *Physical review letters* **68**, no. 15 (1992): 2309-2312.
- [93] Tabak, Max, James Hammer, Michael E. Glinsky, William L. Kruer, Scott C. Wilks, John Woodworth, E. Michael Campbell, Michael D. Perry, and Rodney J. Mason. "Ignition and high gain with ultrapowerful lasers." *Physics of Plasmas* **1** (1994): 1626.
- [94] Qiao, Bin, X. T. He, Shao-ping Zhu, and C. Y. Zheng. "Electron acceleration in combined intense laser fields and self-consistent quasistatic fields in plasma." *Physics of plasmas* **12** (2005): 083102.
- [95] Ripin, B. H., C. K. Manka, T. A. Peyser, E. A. McLean, J. A. Stamper, A. N. Mostovych, J. Grun, K. Kearney, J. R. Crawford, and J. D. Huba. "Laboratory laser-produced astrophysical-like plasmas." *Laser and Particle Beams* **8**, no. 1-2 (1990): 183-190.
- [96] Najmudin, Z., M. Tatarakis, A. Pukhov, E. L. Clark, R. J. Clarke, A. E. Dangor, J. Faure et al. "Measurements of the inverse faraday effect from relativistic laser interactions with an underdense plasma." *Physical Review Letters* **87**, no. 21 (2001): 215004.
- [97] Fuchs, J., G. Malka, J. C. Adam, F. Amiranoff, S. D. Baton, N. Blanchot, A. Heron et al. "Dynamics of subpicosecond relativistic laser pulse self-channeling

- in an underdense preformed plasma." *Physical review letters* 80, no. 8 (1998): 1658-1661.
- [98] Sheng, Z. M., and J. Meyer-ter-Vehn. "Inverse Faraday effect and propagation of circularly polarized intense laser beams in plasmas." *Physical Review E* **54**, no. 2 (1996): 1833.
- [99] Karpman, V. I., and A. G. Shagalov. "The ponderomotive force of a high-frequency electromagnetic field in a cold magnetized plasma." *Journal of Plasma Physics* **27** (1982): 215-224.
- [100] Hertel, Riccardo. "Theory of the inverse Faraday effect in metals." *Journal of magnetism and magnetic materials* **303**, no. 1 (2006): L1-L4.
- [101] R. Lichters, R. E. W. Pfund, and J. Meyer-Ter-Vehn, LPIC++: A parallel one-dimensional relativistic electromagnetic particle-in-cell-code for simulating laser-plasma-interactions, Report MPQ 225, Max-Planck-Institut for Quantenoptik, Garching, Germany, 1997, the code is available at <http://www.lichters.net/download.html>.

# 2

## Ponderomotive Ion Acceleration in dense magnetized laser-irradiated thick target plasmas

### 2.1 Introduction

Ponderomotive force of intense electromagnetic pulse is considered for many years as a promising way to accelerate matter upto relativistic velocities [1, 2]. For non relativistic intensities, the absorption of laser energy results in an increase in plasma temperature and therefore the ablation pressure quickly dominates the radiation effects. The situation changes considerably at extremely high intensities. It has been demonstrated theoretically and experimentally [3, 4] that ions can be accelerated to high energies by the electric field of the electron cloud expelled by the radiation pressure of ultra-intense lasers.

Recently there has been an increasing interest in the area of laser induced ion acceleration. Using the chirped pulse amplification (CPA) technique [5, 6] present day lasers are capable of producing intensities of the order of  $10^{22}W/cm^2$  [7] which makes this area feasible for experimental studies. Its application covers a broad spectrum extending from medical applications to inertial fusion [8, 9, 10, 11, 12, 13]. An intense laser pulse can accelerate ions up to energies of the order of GeV within micrometers with a very small energy spread [14, 15].

As mentioned in the previous chapter several mechanisms like target normal sheath acceleration (TNSA) [16, 17, 18, 19, 20], radiation pressure acceleration (RPA)[2,

[3, 13, 15, 21, 22, 23, 24, 25, 26, 27, 28, 29] and laser interaction with clusters [30, 31, 32, 33, 34] are employed for accelerating ions to sufficiently high energies. The mechanism we deal with in this chapter is the Hole-Boring radiation pressure acceleration (HB-RPA)[2, 3, 13, 15, 21, 22, 23, 24, 25]. In this mechanism of radiation pressure acceleration the laser pushes the plasma electrons via ponderomotive force inside the plasma so as to create an electron compression region or an electron sheath in front of it leaving behind almost a pure ion space charge. This charge separation induces a longitudinal electric field which pulls the electron sheath back. This electrostatic force increases as the electrons are pushed further inside by the laser. The position at which the ponderomotive force is equal to the electrostatic force of charge separation is the equilibrium position. Under the influence of the electrostatic field, the plasma ions are dragged in the laser propagation direction. This causes the electron sheath to move inside the plasma. The electron sheath and the ion space charge together form a double layer. As the intrinsic electric field of this double layer is responsible for ion acceleration, this double layer acts as a “laser piston”. Such ion acceleration process has been studied under several parameters like initial plasma temperature with ions as neutralizing background [35], laser polarization [15, 36], target thickness [3], pulse amplitude [22] and initial plasma density [24]. The polarization of incident laser (linear or circular) plays an important role in this mechanism. Linearly polarized (LP) lasers lead to  $\mathbf{J} \times \mathbf{B}$  heating because of the oscillatory nature of the ponderomotive force which in turn destroys the laser piston. On the other hand for a circularly polarized (CP) laser the oscillatory component goes to zero when averaged over one laser cycle. Hence CP lasers are ideal for this acceleration process. It has also been observed in thick targets that if the pulse is long enough then the acceleration process is repeated leading to a multistage acceleration [37]. Nonlinear penetration of an electromagnetic wave in an overdense plasma plays a significant role in this process [38]. This area has been studied with self consistent electron density modification due to incoming electromagnetic wave with ions acting as a uniform neutralizing background [39, 40, 41]. Such studies are valid only when the longitudinal electric field produced is so small that the time scale at which the ions respond to it is very large as compared to the interaction time with the incoming pulse. At relativistic intensities, the ions quickly respond to the electrostatic field generated inside the plasma leading to their density modification. This phenomenon has been discussed

in [26], where they have described the structure of laser piston comprising of electron and ion sheath. However, the ion space charge region present behind the ion sheath of the laser piston has been neglected. It is seen that for a finite spot size CP laser, axial magnetic field is inherently generated due to inverse faraday effect (IFE)[42, 43, 44]. Further, transverse density inhomogeneities introduced by the laser pulse or the shape of plasma target leads to azimuthal currents and in turn a longitudinal magnetic field[45]. This magnetic field is oriented along the propagation direction and induces cyclotron motion in the plasma electrons. Thus the plasma electrons exhibit two kinds of motion: (i) Quiver motion in the laser fields and (ii) Cyclotron motion due to magnetic field.

In this chapter, we present a detailed analysis of the quasi stationary regime of ion acceleration in the laser piston in the presence of an external static axial magnetic field by applying analytical methods (the magnetic field here is assumed to be self generated or externally applied). In the analytical model we describe the internal structure of the laser piston as well as explore the region of residual ions left behind. The longitudinal magnetic field changes the plasma dielectric constant due to cyclotron effects which in turn enhances or reduces the ponderomotive force exerted by the laser depending on whether the laser is left or right circularly polarized. The residual ion space charge present behind the laser piston undergoes coulomb explosion and their dynamics has been explored for the first time. In figuring out the usage of this region, we have found that it has got the ability to enhance the kinetic energy of incoming ion beams and hence can act as energy amplifiers.

## 2.2 Theoretical model for laser piston

### 2.2.1 Laser piston velocity in HB RPA

We consider a 1D situation where a beam of light of constant intensity  $I$  is normally incident on a plasma of uniform density and one ion species. Assuming that the plasma is effectively collisionless and the light beam is perfectly reflected at the plasma surface, the steady state of this system can be found by examining the momentum balance in the instantaneous rest frame (IRF). Let the velocity of the plasma surface in the lab frame be  $v_f$ . The light intensity in the IRF is not equal

to the light intensity in the lab frame. In fact, it can be shown that

$$\frac{I^{IRF}}{I} = \frac{1 - v_f/c}{1 + v_f/c} \quad (2.1)$$

The plasma that is at rest in the lab frame now approaches the plasma surface at  $v_f$  in the IRF. In order to conserve the particle number there must therefore be a beam of plasma propagating at  $+v_f$  away from the plasma surface. The momentum balance in the IRF is therefore given by,

$$\frac{2I}{c} \frac{1 - \beta_f}{1 + \beta_f} = 2\gamma_f^2 m_i n_i v_f^2 \quad (2.2)$$

where  $\beta_f = v_f/c$ ,  $\gamma_f$  is the relativistic factor,  $m_i$  is the ion mass and  $n_i$  is the initial ion density. Rearranging the above equation we arrive at a quadratic equation in  $\beta_f$ , which when solved for its roots gives,

$$\beta_f = \frac{\sqrt{\Xi}}{1 + \sqrt{\Xi}} \quad (2.3)$$

where  $\Xi = I/m_i n_i c^3$ , and the ion energy can be given by,

$$E = m_i c^2 \frac{2\Xi}{1 + 2\sqrt{\Xi}} \quad (2.4)$$

The parameter  $\epsilon$  defines the piston velocity such that  $\beta_f$  is dependent both on incident laser intensity and plasma mass density. The piston velocity and ion energy are decreasing function of the plasma density and increasing function of laser intensity. However, an interesting fact is that the ion energy does not depend on the ion charge. Therefore, the ponderomotive mechanism is well suited for the acceleration of heavy ions independently on their charge. The important conditions for an efficient ponderomotive ion acceleration are a reflection of the laser pulse from the electron density peak and suppression of the energy transfer to electrons.

### 2.2.2 Structure of the laser piston

When a circularly polarized laser pulse falls normally on an overdense plasma, it pushes the electrons via ponderomotive force creating a charge separation region.

To visualize this process, a schematic diagram is presented in Fig. 2.1. The entire target plasma can be divided in four regions. First, an ion charge region undergoing coulomb explosion  $[-z_i, -\delta]$ , second, an ion sheath  $[-\delta, 0]$ , third, the electron sheath region  $[0, z_{es}]$  and fourth, the undisturbed plasma  $[z > z_{es}]$ . In the region  $[0, z_{es}]$ , electrons pile up as a sheath in front of the laser to reflect it. Within this sheath the laser field is evanescent. The dynamics of this sheath in the absence of any external magnetic field has been presented in [26]. In the region between  $0 < z < z_{es}$  there is an overlap of plasma electrons moving toward the piston and reflected from it. For ions this region of overlap extends from  $z = -\delta$  to  $z = z_{es}$ . Assuming the structure to be quasistationary, we have the unperturbed ions with velocity  $-v_f$ , arriving to the piston from the undisturbed region. These ions are decelerated passing from  $z = z_{es}$  to  $z = -\delta$ . They reverse their motion at  $z = -\delta$  and are then accelerated in the region  $[-\delta, z_{es}]$ . These two steps correspond to ion acceleration. A similar scenario takes place in the region of electron sheath. We discuss the laser piston by dividing it into two regions of electron and ion sheath. We further explore the evolution of residual ions in the rear of the ion sheath i.e. the region  $z < -\delta$ .

### A. Electron sheath in an overdense magnetized plasma

We first investigate the structure of the electron sheath layer  $[0, z_{es}]$  and the laser intensity profile within under the influence of a static axial magnetic field  $B_s$ . The laser fields are evanescent in the electron sheath. The incident and reflected circularly polarized laser pulse in the electron depletion region ( $z < 0$ ) is given as [46],

$$\begin{aligned}\vec{E}_i &= (\hat{x} + i\alpha\hat{y})E_0 \exp[-i(\omega t - kz)] \\ \vec{E}_r &= (\hat{x} + i\alpha\hat{y})RE_0 \exp[-i(\omega t + kz)]\end{aligned}\tag{2.5}$$

where  $E_0$  is the electric field amplitude,  $R$  is the reflection coefficient and  $\alpha$  equal to +1 or -1, corresponding to right and left circularly polarized light respectively.

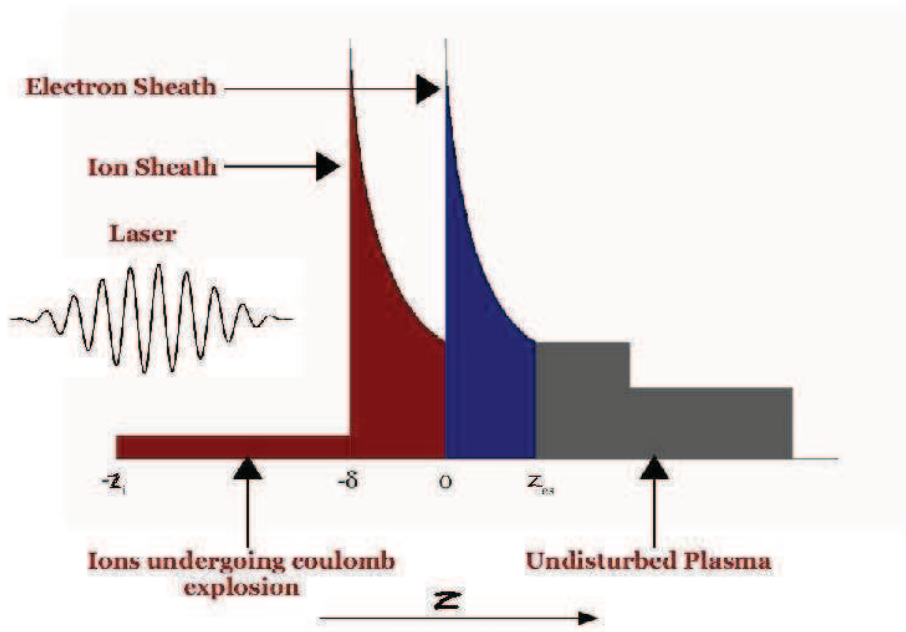


Figure 2.1: Schematic diagram (not to scale), representing the process of interaction of an ultraintense circularly polarized laser with a thick overdense plasma target. The region  $[-z_i, -\delta]$  represents the ion space charge region undergoing coulomb explosion,  $[-\delta, 0]$  represents the ion sheath, in which the ions present undergo direct radiation pressure acceleration. The region  $[0, z_{es}]$  represent the electron sheath formed due to laser ponderomotive force and beyond  $z_{es}$  is the region of undisturbed plasma.

The evanescent laser fields inside the electron sheath is given by,

$$\vec{E}_T = (\hat{x} + i\alpha\hat{y})E_T(z)\exp[-i(\omega t)], \quad \vec{B}_T = \frac{c}{i\omega}\nabla \times \vec{E}_T \quad (2.6)$$

The momentum equation for electrons under the influence of evanescent laser fields and static longitudinal magnetic field can be written as,

$$\frac{d\vec{p}}{dt} = -e\vec{E}_T - \frac{e}{c}(\vec{v} \times \vec{B}_T) - \frac{e}{c}(\vec{v} \times \vec{B}_s) \quad (2.7)$$

Considering transverse components of Eq.2.7, we obtain the expression for quiver velocity of the electrons as,

$$\vec{v}_\perp = (\hat{x} + i\alpha\hat{y})\frac{a_T\omega c}{i(\gamma_e\omega - \alpha\omega_c)}\exp[-i\omega t] \quad (2.8)$$

where  $\omega_c = eB_s/m_e c$  and  $a_T = eE_T/m_e\omega c$  is the dimensionless evanescent laser amplitude. Besides the transverse quiver velocity the electrons also acquire a longitudinal velocity because of an induced longitudinal electric field  $E_z$ . The relativistic factor  $\gamma_e = (1 + p_\parallel^2/m_e^2c^2 + p_\perp^2/m_e^2c^2)^{1/2}$  where  $p_\parallel = \gamma_e m_e v_{ez}$  and  $p_\perp = \gamma_e m_e v_\perp$  are the longitudinal and transverse components of electron momentum. Substituting for  $v_\perp$  from Eq.2.8, the expression for the longitudinal electron velocity takes the form,

$$\beta_{ez} = \frac{\sqrt{(\gamma_e^2 - 1)(\gamma_e - \alpha\Omega_c)^2 - a_T^2\gamma_e^2}}{\gamma_e(\gamma_e - \alpha\Omega_c)} \quad (2.9)$$

where  $\beta_{ez} = v_{ez}/c$  and  $\Omega_c = \omega_c/\omega$ . In the frame of the double layer, the electrons in the undisturbed plasma appears to come towards the electron layer and the ones with in the electron sheath get pushed away towards the undisturbed region via ponderomotive force. Thus, in this frame, the electron sheath comprises of two electron streams with opposite directed velocities. Following conservation of particle flux, the electron continuity equation gives the electron density with in the sheath as,

$$n_e = 2Zn_0\gamma_f\frac{\beta_f}{\beta_{ez}} \quad (2.10)$$

where  $\beta_f = v_f/c$  with  $v_f$  as the piston velocity,  $Z$  is the ion charge,  $n_0$  is the equilibrium ion density and  $\gamma_f$  is the relativistic factor corresponding to  $v_f$ . As the continuity equation describes the transport of a conserved quantity (like energy,

momentum, mass, charge etc.) the total momentum of all the electrons present at a given cross section of the electron sheath must remain constant. As the electron velocity is maximum at  $z = z_{es}$  and decreases monotonically as  $z$  decreases reaching a minimum ( $\approx 0$ ) at  $z = 0$ , to conserve momentum the number of electrons monotonically increases as we move from  $z = z_{es}$  to  $z = 0$ . This electron sheath also contains plasma ions. The induced electrostatic field acts on both electrons and ions within the sheath. Hence the ion density becomes  $n_i = 2n_0\gamma_f\frac{\beta_f}{\beta_{iz}}$  with  $\beta_{iz} = v_{iz}/c$  where  $v_{iz}$  is the local longitudinal ion velocity. The Poisson's equation with modified electron and ion densities given by their equations of continuity can be written as,

$$\frac{d^2\phi}{dz^2} = 8\pi eZn_0\gamma_f\beta_f\left(\frac{1}{\beta_{ez}} - \frac{1}{\beta_{iz}}\right) \quad (2.11)$$

where  $\phi = m_e c^2 / e(\gamma_e - 1)$  is the ponderomotive potential. Using this expression for the potential and electron velocity from Eq.2.9, we can derive the equation governing the electron relativistic factor to be given as,

$$\frac{d^2\gamma_e}{dz^2} = 2\frac{\omega_{pe0}^2}{c^2}\gamma_f\beta_f\left(\frac{\gamma_e(\gamma_e - \alpha\Omega_c)}{\sqrt{(\gamma_e^2 - 1)(\gamma_e - \alpha\Omega_c)^2 - a_T^2\gamma_e^2}} - \frac{\gamma_i}{\sqrt{\gamma_i^2 - 1}}\right) \quad (2.12)$$

where  $\omega_{pe0} = (4\pi n_{e0}e^2/m_e)^{1/2}$  is the electron plasma frequency and  $n_{e0} = Zn_0$  is the electron density. From Eq.2.12 we discover that the evolution of electron relativistic factor  $\gamma_e$  also depends on the evanescent laser field and the ion relativistic factor  $\gamma_i$ . In the sheath region, as the ions and electrons are moving under same electrostatic field, the relation between their relativistic factors can be seen as in [26],

$$\gamma_i(z) = \gamma_f - \mu(\gamma_e(z) - \gamma_f) \quad (2.13)$$

$\mu = m_e/m_i$  (the electron to ion mass ratio). For  $a_T$ , one has to account for the wave equation governing the evanescent laser field given by,

$$\frac{d^2a_T}{dz^2} = \frac{\omega^2}{c^2}\left(\frac{\omega_{pe}^2/\omega^2}{\gamma_e - \alpha\Omega_c} - \frac{1 - \beta_f}{1 + \beta_f}\right)a_T \quad (2.14)$$

where  $\omega_{pe}$  corresponds to the local plasma frequency at a given  $z$  within the electron sheath. Substituting for electron density from the equation of continuity

and  $\beta_{ez}$  from Eq.2.9, Eq.2.14 takes the form,

$$\frac{d^2 a_T}{dz^2} = 2 \frac{\omega_{pe0}^2}{c^2} \gamma_f \beta_f \frac{a_T \gamma_e}{\sqrt{(\gamma_e^2 - 1)(\gamma_e - \alpha \Omega_c)^2 - a_T^2 \gamma_e^2}} - \frac{\omega^2}{c^2} \frac{1 - \beta_f}{1 + \beta_f} a_T \quad (2.15)$$

Equations 2.12, 2.13 and 2.15 together corresponds to the evolution of the electron relativistic factor  $\gamma_e$  as well as the evanescent laser field  $a_T$ . The coupled set of equations (8) and (11) are solved backwards from  $z \gg c/\omega_{pe0}$ , taking  $\gamma_e = \gamma_f + \delta\gamma$  and  $\delta\gamma, a_T(z) \ll 1$ . Upon integrating Eqs. 2.12 and 2.15 by multiplying them with their first derivatives under the limits discussed, we arrive at the initial conditions as,

$$\left. \frac{da_T}{dz} \right|_{z \gg c/\omega_{pe0}} = - \left[ 2 \frac{\omega_{pe0}^2}{c^2} \frac{\gamma_f}{\gamma_f - \alpha \Omega_c} - \frac{\omega^2}{c^2} \frac{1 - \beta_f}{1 + \beta_f} \right]^{1/2} a_T \quad (2.16)$$

$$\left. \frac{d\delta\gamma}{dz} \right|_{z \gg c/\omega_{pe0}} = - \left[ \frac{\omega_{pe0}^2}{c^2} \frac{\gamma_f}{\beta_f^2 (\gamma_f - \alpha \Omega_c)^2} \left[ - \frac{\delta\gamma^2}{\gamma_f^2} + a_T^4 \right] \right]^{1/2} \quad (2.17)$$

For a given  $B_s$  and  $\beta_f$  we obtain the initial value of the first derivative of the evanescent field from Eq. 2.16. In Eq. 2.17 as we do not have any free constants,  $\delta\gamma$  can be taken as the same order of magnitude as  $a_T^2$ , as in [26]. Using these initial conditions, we can numerically integrate the coupled set of Eqs. 2.12 and 2.15 for a given magnetic field and  $\beta_f$ . The equations are integrated until the condition,

$$\left. \frac{d\gamma_e}{dz} \right|_{z=0} = -2 \sqrt{\frac{1}{Z\mu} \frac{\omega_{pe0}}{c}} \sqrt{\gamma_f \beta_f [\gamma_i^2(0) - 1]}^{1/4} \quad (2.18)$$

obtained from the continuity of longitudinal electric field is satisfied. Taking this position as  $z = 0$ , the incident amplitude of laser field is can be obtained by the boundary condition,

$$\left( \left. \frac{da_T}{dz} \right) \right|_{z=0}^2 + \frac{\omega^2}{c^2} \frac{1 - \beta_f}{1 + \beta_f} a_T^2(0) = 4 \frac{\omega^2}{c^2} \frac{1 - \beta_f}{1 + \beta_f} a_0^2 \quad (2.19)$$

where  $a_0$  is the dimensionless laser vector potential in the laboratory frame. Here we study the process of ion acceleration for both left and right circularly polarized light i.e.  $\alpha = -1$  and  $+1$  respectively. For the laser field in the sheath to be evanescent the permittivity of the plasma  $\epsilon = (1 - \omega_{peff}^2/\omega^2)$ , where  $\omega_{peff} = \omega_{pe}/\sqrt{\gamma_e - \alpha \Omega_c}$  and  $\omega_{pe}$  is the local electron plasma frequency, has to be negative.

In case of left circularly polarized (LCP) laser for an overdense plasma we can choose any value of  $\Omega_c$  or  $B_s$  as  $\alpha = -1$  in this case. However, the laser intensity required to achieve a given  $\beta_f$  in this case is higher than that without magnetic field. For example in case of  $\beta_f = 0.05$ ,  $Z = 1$ ,  $\mu = 1/2000$  and  $\Omega_c = 0.5$ ,  $a_0 = 8.2$  for a plasma with density  $n_0/n_c = 10$ , where  $n_c = m_e\omega^2/4\pi e^2$  is the critical plasma density. Whereas the required amplitude in the absence of magnetic field would have been  $a_0 = 7.5$ . With increase in magnetic field the required incident laser intensity also increases for LCP. Next we consider right circularly polarized (RCP) laser light. Here we have a restriction on the choice of  $\Omega_c$  as  $\alpha = +1$  and the permittivity has to be kept negative for the laser field to be evanescent. For the same parameters discussed above, the required incident laser pulse amplitude is  $a_0 = 6.7$ , which corresponds to nearly 80% of the intensity required without magnetic field. In Fig. 2.2, the normalized evanescent field  $a_T$  has been plotted for both LCP, RCP and  $B_s = 0$ . For RCP lasers (*i.e.*  $\alpha = +1$ )  $\omega_{peff}$  increases with application of magnetic field, because in this case the direction of rotation of electrons due to electric field of the laser pulse is the same as that induced due to externally applied magnetic field. As a result, the skin depth  $c/\omega_{peff}$  decreases because of which the transmitted laser field in the electron sheath decreases for a fixed laser intensity. As the laser field falls to zero at a shorter distance in the electron sheath, the ponderomotive force increases with magnetic field for RCP. For LCP (*i.e.*  $\alpha = -1$ ), the effect is reversed as the electron gyrations induced by the laser and magnetic field are opposite, hence  $\omega_{peff}$  decreases with magnetic field. This phenomena can be collectively referred to as cyclotron effects. It is tempting to believe that for  $\Omega_c > 0.5$  we may achieve the same  $\beta_f$  for even lower  $a_0$ , but in this case we observe that the electron density at the ion-electron interface reaches infinity, or the electron wave breaks much before the longitudinal electric field is balanced. This is an unstable double layer and not suitable for ion acceleration. Hence, we can conclude that for RCP there is an upper limit of  $\Omega_c$  for a required  $\beta_f$ . We have observed that for higher  $\beta_f$  the upper limit of  $\Omega_c$  increases but slowly. For  $\beta_f = 0.124$  the maximum  $\Omega_c = 0.62$  which makes the required intensity go down to 88% of that with  $B_s = 0$ . Fig. 2.3 shows the required laser amplitudes for LCP, RCP and  $B_s = 0$  for different  $\beta_f$ . It is clear that using an RCP laser with a longitudinal magnetic field is advantageous over LCP as a desired ion velocity can be achieved with relatively smaller incident intensity. Influence of magnetic field

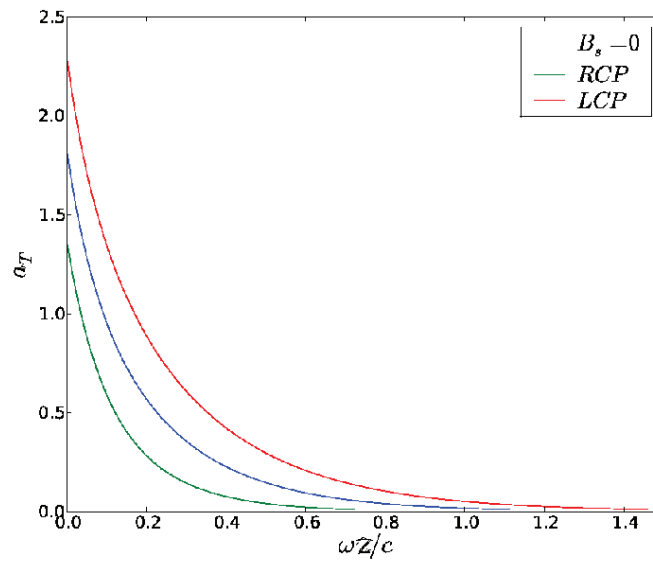


Figure 2.2: Dimensionless amplitude of evanescent laser field profiles inside the electron sheath for equilibrium plasma density  $n_0/n_c = 10$ ,  $\beta_f = 0.05$  and  $\Omega_c = 0.5$  for left and right circularly polarized lasers together with the profile in the absence of magnetic field.

on thin foil has been reported in [46], where the optimum foil thickness is found to be sensitive to laser polarization (for LCP lasers it is less than that for RCP). It was found that LCP lasers are more efficient than RCP ones as they have to propel a comparatively lighter target. However, in the hole boring mode of ion acceleration, presented here, target plasma thickness is not a critical parameter. Unlike [46] the ion velocity is not time dependent and we have a steady state. As the ponderomotive force is enhanced for RCP lasers due to cyclotron effects, RCP lasers exert a greater force than LCP leading to higher ion velocity at comparatively lower intensities which is converse of what is presented in [46]. Fig. 2.4 shows the ratio of incident intensity for RCP to that required with  $B_s = 0$  for different  $\beta_f$ . It can be seen that as  $\beta_f$  increases the required intensity for RCP lasers approach close to that for  $B_s = 0$ . From this we can say that applying a longitudinal magnetic field is more advantageous for lower  $\beta_f$ . However, the corresponding lower  $\beta_f$ s represent ion beams of energies sufficient for processes like fission of  $Ra^{226}$  [47] and transmutation of  $N^{14}$  [48]. Besides this, they can act as source beams for energy amplification process described in the next section.

## B. Structure of the ion space charge region

In this section we first recollect the model for ion sheath proposed in [26]. Here, the ion charge separation layer extends with in a small region say  $[-\delta, 0]$ . The electrostatic field in this region is the one that is responsible for acceleration of ions. In the frame of the piston, the ion sheath comprises of incoming and reflected ions. From the conservation of ion particle flux the ion density here is given in terms of the ion velocity as,

$$n_i = 2n_0\gamma_f \frac{\beta_f}{\beta_{iz}} \quad (2.20)$$

The ion energy conservation with ion kinetic energy  $E_i(z) = m_i c^2(\gamma_i - 1)$  at a given  $z$  gives,  $E_i + Ze\phi(z) = m_i c^2(\gamma_f - 1)$ . This gives the value of the potential jump in this layer as,  $\phi(-\delta) = m_i c^2 / Ze(\gamma_f - 1)$ , needed to stop and reflect the ions. The electric field in this region is given as  $E_z(z) = -d\phi(z)/dz$ . The equation governing the ion relativistic factor  $\gamma_i = 1/\sqrt{1 - v_i^2/c^2}$  in the frame of the laser piston moving with velocity  $v_f$  is derived from the ion equation of continuity and

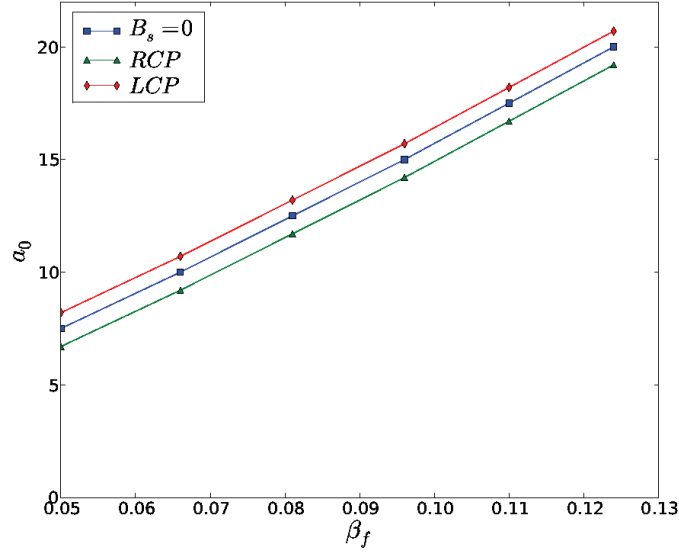


Figure 2.3: Dimensionless incident laser amplitudes required for different  $\beta_f$  for the case of left and right circularly polarized light and  $B_s = 0$ . The initial plasma density  $n_0/n_c = 10$  and  $\Omega_c = 0.5$ .

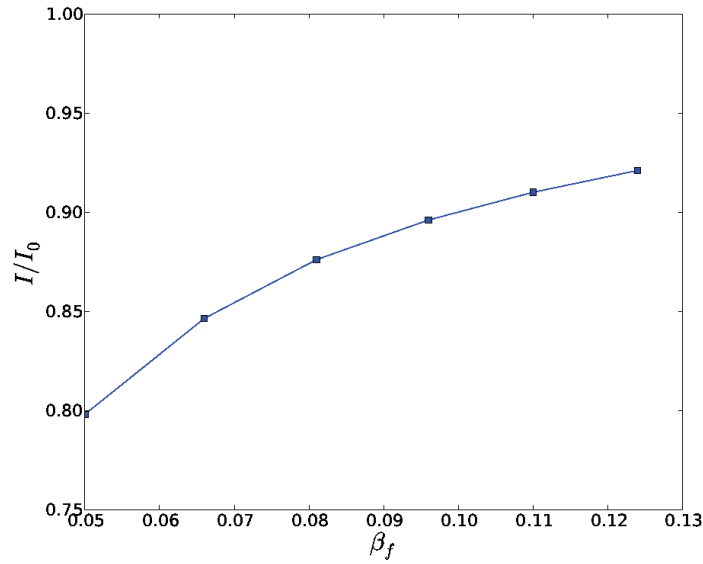


Figure 2.4: Dimensionless incident laser amplitudes required for different  $\beta_f$  for the case of left and right circularly polarized light and  $B_s = 0$ . The initial plasma density  $n_0/n_c = 10$  and  $\Omega_c = 0.5$ .

Poisson's equation is,

$$\frac{d^2\gamma_i}{dz^2} = \frac{2\omega_{pi}^2\gamma_f\beta_f}{c^2\beta_{iz}} \quad (2.21)$$

where  $\omega_{pi} = (4\pi n_0 Z^2 e^2 / m_i)^{1/2}$  is the ion plasma frequency. The first integral of Eq.2.21 reads as,

$$\frac{d\gamma_i}{dz} = \frac{2\omega_{pi}}{c} \sqrt{\gamma_f\beta_f} (\gamma_i^2 - 1)^{1/4} \quad (2.22)$$

The longitudinal electric field  $E_z = (m_i c^2 / e) d\gamma_i / dz$  can be determined from Eq.(18). The local ion velocity in lab frame  $v_{iL}$  can be obtained by relativistic velocity transformation as  $v_{iL} = (v_i + v_f) / (1 + v_i v_f / c^2)$ . Upon integration of Eq.2.22 the thickness of the ion space charge is found to be  $v_f / 3\omega_{pi}$  extending from say  $z = -\delta$  to  $z = 0$  moving together with the electron sheath with constant velocity  $v_f$  with the ion density going to infinity at  $z = -\delta$  and the longitudinal electric field to zero. In this treatment they have ignored the ion region of constant density that extends beyond the ion sheath towards the incoming laser. This ion region undergoes coulomb explosion and its density continues to decrease uniformly with time with its origin fixed at the initial position of the plasma (say  $-z_i$ ). To analyze the coulomb explosion of ion space charge region we transform from Eulerian variables  $(z, t)$  to Lagrangian variables  $(z_0, \tau)$ , where

$$\tau = t, \quad z_0 \equiv z - \int_0^\tau d\tau' v(z_0, \tau') \quad (2.23)$$

The space and time derivatives transform according to,

$$\frac{\partial}{\partial z} \equiv \left[ 1 + \int_0^\tau d\tau' \frac{\partial}{\partial z_0} v(z_0, \tau') \right]^{-1} \frac{\partial}{\partial z_0} \quad (2.24)$$

and,

$$\frac{\partial}{\partial t} = \frac{\partial}{\partial \tau} - v(z_0, \tau) \left[ 1 + \int_0^\tau d\tau' \frac{\partial}{\partial z_0} v(z_0, \tau') \right]^{-1} \frac{\partial}{\partial z_0} \quad (2.25)$$

In terms of the Lagrangian variables  $(z_0, \tau)$ , the force equation for ions become,

$$\frac{\partial}{\partial \tau} v(z_0, \tau) = \frac{Ze}{m_i} E(z_0, \tau) = \omega_{pi}^2 z_0 \quad (2.26)$$

The initial condition for the electric field in this region has been taken to be linearly increasing with distance. The equation of continuity can be expressed as,

$$\frac{\partial}{\partial \tau} \left( n_i(z_0, \tau) \left[ 1 + \int_0^\tau d\tau' \frac{\partial}{\partial z_0} v(z_0, \tau') \right] \right) = 0 \quad (2.27)$$

The solution of equations 2.26 and 2.27 are,

$$v = \omega_{pi}^2 z_0 \tau = \frac{\omega_{pi}^2 z t}{\left[ 1 + \frac{\omega_{pi}^2 t^2}{2} \right]} \quad (2.28)$$

and,

$$n_i(z, t) = \frac{n_0}{\left[ 1 + \frac{\omega_{pi}^2 t^2}{2} \right]} \quad (2.29)$$

where  $n_0$  is the equilibrium ion density. From Eqs. 2.28 and 2.29 we see that the velocity of ions increases linearly with distance, with ion velocity zero at  $z = -z_i$  and the ion density decreasing with time. Before the start of acceleration process the ion space charge region extends upto the distance  $z_d$  (say) to balance the ponderomotive force to electrostatic force, which is given by,

$$z_d = \frac{E_{max}}{4\pi e n_0} \quad (2.30)$$

Where  $E_{max}$  is computed numerically from Eq.(14). In an overdense plasma the response time of plasma electrons to the laser fields is less than one laser period. In case of linear polarization with normal incidence, the electrons attain a drift velocity caused by  $\mathbf{v} \times \mathbf{B}_{laser}$  which eludes steady state solution. For ion acceleration, the choice of circular polarization rests on its advantage that the oscillatory part of  $\mathbf{v} \times \mathbf{B}_{laser}$  force is zero. The plasma electrons respond to the laser field in the order of few plasma periods. For concreteness we can assume that in overdense plasmas the electron sheath is pushed upto a steady state velocity  $v_f$  in one laser time period  $t_L$  as the results are insensitive to this choice. Beyond this the laser piston starts to move with a constant velocity  $v_f$ . Due to coulomb explosion the ions reaching  $z = -\delta$  from the side of incident laser attain very high velocities. As the ion density rapidly increases at this point they tend to loose their velocity till it becomes equal to  $v_f$ . The complete induced electrostatic field profile can be

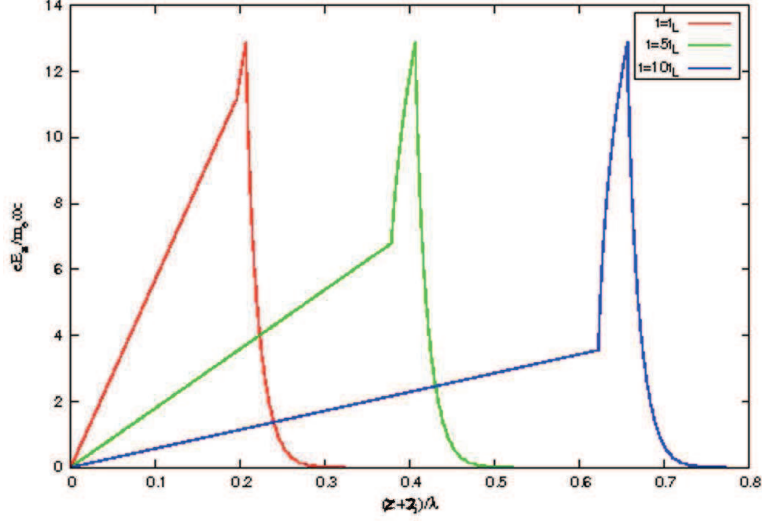


Figure 2.5: Induced longitudinal electric field at different times for  $n_0/n_c = 10$ ,  $\beta_f = 0.05$ ,  $\Omega_c = 0.5$  and  $\alpha = +1$ .  $\lambda$  is the laser wavelength.

obtained by adding the fields with in the electron sheath and the part derived from coulomb explosion of ions in the region  $[-z_i, -\delta]$  and the ion sheath  $[-\delta, 0]$ . We see that this electric field first linearly increases in the region  $[-z_i, -\delta]$ , then takes a jump in  $[-\delta, 0]$ . The jump becomes more prominent at the point of reflection with time as the coulomb exploding ions and the reflected ions tend to get deposited at this point from opposite sides leading to increase in ion density. Finally the electric field decays down to zero in  $[0, z_{es}]$ . The complete electrostatic field profile is shown at different times in Fig. 2.5. Direct ion acceleration via laser piston has been described using the concept of reflection of incoming ions from the ion sheath. In the piston frame the plasma ions approach the ion sheath with velocity  $-v_f$  and decelerates as it progresses upstream before getting reflected at  $z = -\delta$ . These ions never overshoot the ion sheath. However, if we have an incoming test ion towards the laser pulse, it will overshoot the ion sheath and move into the region  $z < -\delta$ , further experiencing the decelerating field. The initial velocity of the test ion determines whether it will be reflected from somewhere in the region  $[-z_i, -\delta]$  or will be lost in the region  $[z < -z_i]$ . The equation of motion of ions entering the region  $[-z_i, -\delta]$  can be described by the force equation,

$$\frac{dp_i}{dt} = eE(z) \quad (2.31)$$

where  $E(z) = 4\pi en_i(t)z$  with  $n_i(t)$  given by Eq. 2.29. Substituting for  $p_i$  Eq. 2.31 takes the form,

$$\frac{d^2z}{dt^2} = \frac{4\pi^2\mu n_0 z}{(1 + 2\pi^2\mu n_0 t^2)} \left[ 1 - \left( \frac{dz}{dt} \right)^2 \right]^{3/2} \quad (2.32)$$

Solution of Eq. 2.32 gives the trajectory of incoming test ion. The initial position at which the test ion enters the region undergoing coulomb explosion is  $z = -\delta'$  (say) which moves ahead with time with velocity  $v_f$  such that at any time  $t$ ,  $\delta' = \delta + v_f(t - t_L)$ . At  $t = t_L$ ,  $\delta' = \delta$ . When the test ion enters this region at time  $t_L$  it had already lost kinetic energy equal to  $m_i c^2 / e(\gamma_f - 1)$ . With the remaining velocity it continues to experience further deceleration till it comes to rest. If the ion continues to have some residual velocity at  $z = -z_i$  it will be lost, otherwise will be reflected and chase  $\delta'$ . Upon reflection the ion has to travel a longer distance as the laser piston moves ahead with velocity  $v_f$ . The velocity of the reflected ion at the time at which the two trajectories coincide is the velocity with which it re-enters the laser piston. Upon entering the laser piston its further gains energy equal to  $m_i c^2 / e(\gamma'_f - 1)$ , where  $\gamma'_f$  is the ion relativistic factor in the lab frame. Fig. 2.6 shows the trajectories of test ion with velocities  $-0.25c$ ,  $-0.20c$  and  $-0.15c$  together with that of the laser piston for  $n_0/n_c = 10$ ,  $\mu = 1/2000$ ,  $\Omega_c = 0.5$ ,  $Z = 1$  and  $\beta_f = 0.05$ . At  $t = t_L$ , the point at which the test ion overshoot the plasma ion sheath is given by  $\delta' = z_d - v_f/3\omega_{pi}$ , where  $z_d$  is given by Eq. 2.30. The point of intersection of the ion beam and laser piston trajectories determines the time at which the test ion re-enters the piston. Fig. 2.7 shows the velocities of this ion with time. It can be seen that at the time of intersection the magnitude of velocities of the test ion has increased than what it was initially. Upon moving through the piston this ion further gain energy equal to the energy achieved by plasma ions undergoing direct acceleration. We find that the kinetic energy of this incoming test ion gets enhanced by this process or in other words the ion space charge region behind the ion sheath acts as an amplifier to an incoming ion. The kinetic energy of test ion of velocities  $-0.25c$ ,  $-0.20c$  and  $-0.15c$  are 33.52, 21.07 and 11.7 MeV respectively corresponding to which the reflected ion energies are 87.82, 64.46 and 44.50 MeV. For given plasma parameters and piston velocity there is a maximum velocity  $v_{bmax}$  that an incoming test ion can have to get reflected

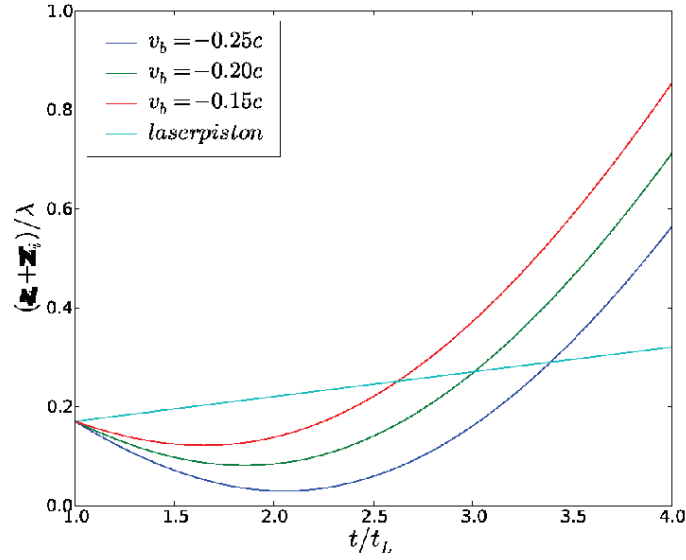


Figure 2.6: Trajectories of incoming test ion with different velocities within the ion space charge region undergoing coulomb explosion together with that of the laser piston. The laser piston moves ahead with a constant velocity because of which the test ion has to traverse a longer distance to enter the piston region upon reflection.

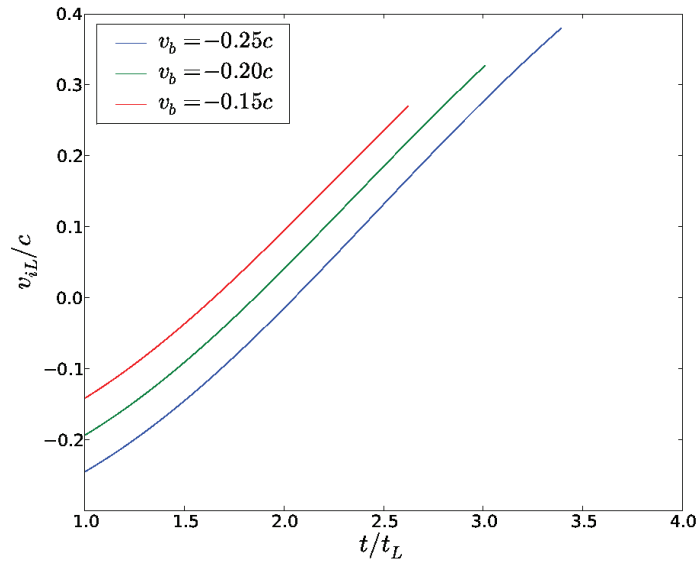


Figure 2.7: Velocity profile of test ion incident with different initial velocities within the ion space charge region with time. The graphs are plotted upto the time at which the reflected ion re-enter the laser piston.

from the coulomb exploding space charge region. This maximum ion velocity is determined numerically from Eq.2.32. The ion with velocity  $v_{bmax}$  are reflected from  $z = -z_i$ . In order to derive a relationship between the incident and reflected velocity of incoming test ion, we first note the relative velocity of the incoming ion and the double layer. The relative velocity  $V$  can be obtained by relativistic velocity addition as,

$$V = \frac{v_b + v_f}{1 + v_b v_f} \quad (2.33)$$

where  $v_b$  is the incoming test ion velocity in the lab frame. If  $v_{iL}$  is the velocity of reflected test ion in lab frame, then, in the frame of the double layer, conservation of momentum gives,

$$\gamma_f m_i V = \gamma_f m_i \frac{v_{iL} - v_f}{1 - v_{iL} v_f} \quad (2.34)$$

which gives,

$$v_{iL} = \frac{V + v_f}{1 + V v_f} \quad (2.35)$$

In the non-relativistic limit  $v_{iL} = v_b + 2v_f$ . Fig. 2.8 shows maximum velocity magnitude  $|v_{bmax}|$  that an incoming test ion can have for different  $\beta_f$  keeping initial ion density constant. Higher  $\beta_f$ 's represent higher incident laser intensity. We observe that for higher laser intensities  $|v_{bmax}|$  increases. Fig. 2.9 shows reflected ion velocities for different  $|v_{bmax}|$ .

## 2.3 Conclusions

In this chapter we have presented a theory for laser induced ion acceleration in the presence of a longitudinal static magnetic field and have explored the property of ion space charge region to amplify the velocity of incoming ion beams. The region of ion space charge undergoing coulomb explosion has been discussed. It has been found that the density of this region decreases uniformly with time.

Under the influence of a static longitudinal magnetic field, the electron sheath gets significantly influenced. The observations for RCP and LCP light are completely opposite. While LCP light penetrates to a larger distance inside the sheath, RCP light goes to a relatively smaller distance. The rate at which the field of RCP light falls inside the electron sheath is faster than that of LCP, throwing light on the fact that ponderomotive force is enhanced due to cyclotron effects in the former case.

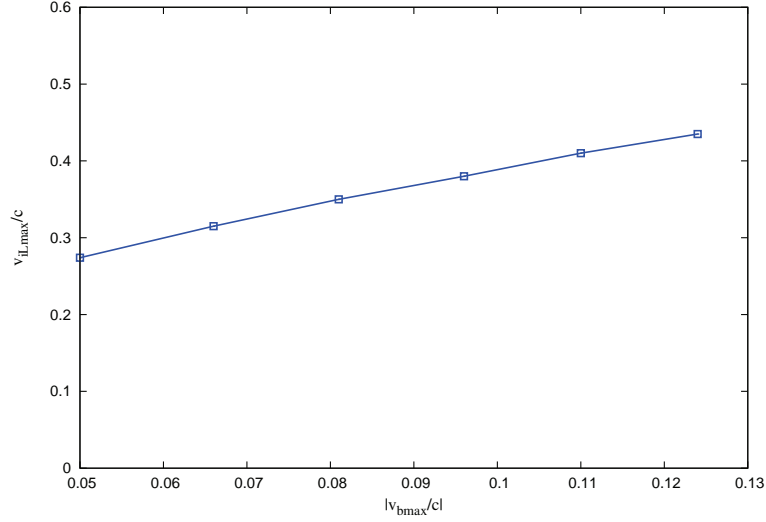


Figure 2.8: Maximum velocity magnitude the incoming test ion can have for different  $\beta_f$  keeping initial ion density constant.  $n_0/n_c = 10, \mu = 1/2000, \Omega_c = 0.5$  and  $Z = 1$ .

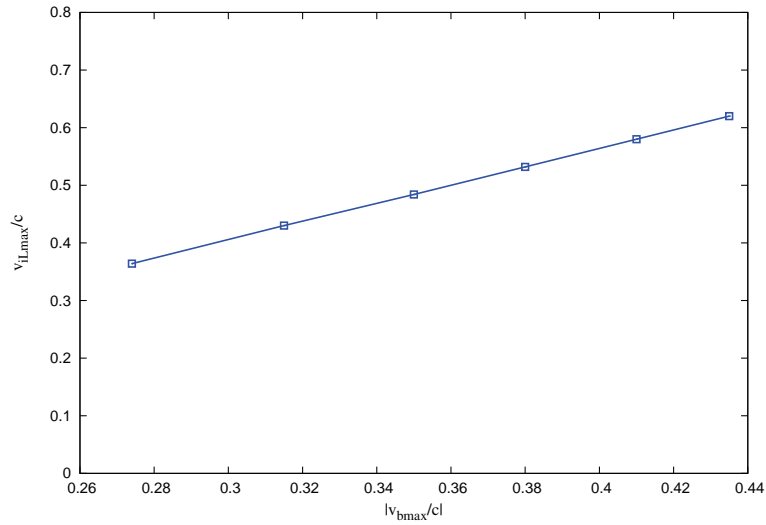


Figure 2.9: Reflected ion velocities for different  $|v_{bmax}|$ .  $n_0/n_c = 10, \mu = 1/2000, \Omega_c = 0.5$  and  $Z = 1$ .

Because of this effect the required laser intensity to achieve a given ion velocity via direct laser acceleration goes down. However, the advantage of this property remains limited only till small ion velocities. With aiming to achieve higher ion velocities the required intensities approach closer to that required without magnetic fields. Also it has been observed that for a given ion velocity, there is an upper limit for the magnetic field in case of RCP light. As we go beyond this limit, the electron sheath breaks before the radiation pressure is balanced by the electrostatic field. Under such circumstances there will not be any stable double layer, which is essential for this type of acceleration.

The longitudinal magnetic field discussed in this paper can either be externally applied or self generated. Circularly polarized light induces electron gyrations in the plane perpendicular to the direction of propagation. If there is inhomogeneity in laser intensity along transverse direction, the radial ponderomotive force will generate radial density gradient. The electron gyration and radial density gradient will together produce azimuthal current which will induce strong axial magnetic field. By this method, at ultra-relativistic intensities  $\omega_e \approx \omega$  or  $\Omega_e \rightarrow 1$  can be achieved, which will suffice our requirement to observe the phenomena described in this paper. A similar description is also given in [46].

Direct ion acceleration has been attributed only to the laser piston comprising of ion and electron sheath. The ions accelerated in this case are the ones reflected from the other end of the ion sheath. Beyond this ion sheath there is an ion region which undergoes coulomb explosion, but it does not play any role in direct acceleration process. However, with introduction of incoming test ion, this region displays its amplification properties. Incoming ion significantly amplifies their energy by passing through this region. If we have two plasma targets, on which laser pulse falls in opposite directions, then by appropriately timing the interaction of lasers with the target plasma, we can make ion beams obtained from direct RPA from one of the targets as an incoming ion beam source for the other. This ion beam will undergo velocity amplification by the coulomb exploding part of the other target. Such multi-target multistage processes can significantly enhance ion energies. In [37], multistage ion acceleration was described, which to be realized required longer laser pulse length. Here we have presented a different method of multistage ion acceleration involving more than one target.

The most likely multi-dimensional effect that will be of interest in this area is the

Chapter 2. Ponderomotive Ion Acceleration in dense magnetized laser-irradiated  
thick target plasmas

Rayleigh-Taylor instability. In the presence of a magnetic field, the RT instability may be subject to some stabilizing effects. Detailed analysis has been presented in later chapter.

# Bibliography

- [1] J. Denavit, Phys Rev. Lett. **69**, 3052 (1992).
- [2] S. C. Wilks, W. L. Kruer, M. Tabak and A. B. Langdon, Phys. Rev. Lett. **69**, 1383 (1992).
- [3] Esirkepov, T. and Borghesi, M. and Bulanov, S. V. and Mourou, G. and Tajima, T., Phys. Rev. Lett. **92**, 17500 3 (2004).
- [4] Dan Haberberger, Sergei Tochitsky, Frederico Fiuza, Chao Gong, Ricardo A. Fonseca, Luis O. Silva, Warren B. Mori and Chan Joshi, Nature Phys. **8**, 95 (2012).
- [5] G. Mourou and D. Umstadter, Phys. Fluids B **4**, 2315 (1992).
- [6] G. Mourou, C.P.J. Barty and M.D. Perry, Phys. Today **51**, 22 (1998).
- [7] V. Yanovsky, V. Chvykov, G. Kalinchenko, P. Rousseau, T. Planchon, T. Matsuoka, A. Maksimchuk, J. Nees, G. Cheriaux, G. Mourou and K. Krushelnick, Opt. Express **16**, 2109 (2008).
- [8] Hegelich B. M., Albright B. J., Cobble J., Flippo K., Letzring S., Paffett M., Ruhl H., Schreiber J., Schulze R. K. and Fernandez J. C., Nature **439**, 441 (2006).
- [9] Ledingham K. J., Phys. D **37**, 2341 (2004).
- [10] Kodama R., Nature **412**, 2341 (2004).
- [11] Roth M., Phys. Rev. Lett. **86**, 436 (2001).
- [12] Temporal M., Honrubia J. J. and Atzeni S., Phys. Plasmas **9**, 3098 (2002).
- [13] N. Naumova, T. Schlegel, V. T. Tikhonchuk, C. Labaune, I. V. Sokolov and G. Mourou, Phys. Rev. Lett. **102**, 025002 (2009).
- [14] Yin L., Albright B. J., Hegelich B. M. and Fernandez J. C., Laser and Particle Beams **24**, 291 (2006).

- [15] Xiaomei Zhang, Baifei Shen, Xuemei Li, Zhangying Jin, Fengchao Wang and Meng Wen, *Phys. Plasmas* 14, 123108 (2007).
- [16] P. Mora, *Phys. Rev. Lett.* 90,185002 (2003).
- [17] V. Yu. Bychenkov, V. N. Novikov, D. Batani, V. T. Tikhonchuk, and S. G. Bochkarev, *Phys. Plasmas* 11, 3242 (2004), DOI:10.1063/1.1738649.
- [18] S. C. Wilks, A. B. Langdon, T. E. Cowan, M. Roth, M. Singh, S. Hatchett, M. H. Key, D. Pennington, A. MacKinnon, and R. A. Snavely, *Phys. Plasmas* 8, 542 (2001), DOI:10.1063/1.1333697.
- [19] Y. Sentoku, T. E. Cowan, A. Kemp, and H. Ruhl, *Phys. Plasmas* 10, 2009 (2003), DOI:10.1063/1.1556298.
- [20] A. J. Kemp and H. Ruhl, *Phys. Plasmas* 12, 033105 (2005), DOI:10.1063/1.1856933.
- [21] Gibbon Paul, *Phys. Rev. E* 72, 026411 (2005).
- [22] Macchi Andrea, Cattani Federica, Liseykina, Tatiana V. and Cornolti Fulvio *Phys. Rev. Lett.* 94, 165003 (2005).
- [23] Silva Luís O., Marti Michael, Davies Jonathan R., Fonseca Ricardo A., Ren Chuang, Tsung Frank S. and Mori Warren B. *Phys. Rev. Lett.* 92, 015002 (2004).
- [24] Amol R. Holkundkar and N. K. Gupta, *Phys. Plasmas* 15, 123104 (2008).
- [25] A P L Robinson, P Gibbon, M Zepf, S Kar, R G Evans and C Bellei *Plasma Physics and Controlled Fusion* 51, 024004 (2009).
- [26] T. Schlegel, N. Naumova, V. T. Tikhonchuck, C. Labaune, I. V. Sokolov and G. Mourou, *Phys. Plasmas* 16, 083103 (2009).
- [27] Yan X. Q., Lin C., Sheng Z. M., Guo Z. Y., Liu B. C., Lu Y. R., Fang J. X. and Chen J. E., *Phys. Rev. Lett.* 100, 135003 (2008).
- [28] V K Tripathi, C S Liu, X Shao, B Eliasson and R Z Sagdeev, *Plasma Physics and Controlled Fusion* 51, 024014 (2009).

- [29] Macchi, Andrea, Veghini, Silvia and Pegoraro, Francesco, *Phys. Rev. Lett.* **103**, 085003 (2009).
- [30] Nishihara K, Amitani H, Murakami M, Bulanov S V and Esirkepov T Z (2001), High energy ions generated by laser driven Coulomb explosion of cluster, *Nucl. Instrum. Methods Phys. Res. A* **464**, 98-102.
- [31] Bychenkov V Yu and Kovalev V F (2005), Coulomb explosion in a cluster plasma, *Fiz. Plazmy* **31**, 203-8.
- [32] Kovalev V F, Bychenkov V Y and Mima K (2007), Quasimonoenergetic ion bunches from exploding microstructured targets, *Phys. Plasmas* **14**, 103110.
- [33] Kovalev V F, Popov K I, Bychenkov V Y and Rozmus W (2007), Laser triggered Coulomb explosion of nanoscale symmetric targets, *Phys. Plasmas* **14**, 053103.
- [34] Esirkepov T Zh, Bingham R, Bulanov S V, Honda T, Nishihara K and Pegoraro F (2000), Coulomb explosion of a cluster irradiated by a high intensity laser pulse, *Laser Part. Beams* **18**, 503-6.
- [35] Xiaomei Zhang, Baifei Shen, M. Y. Yu, Xuemei Li, Zhangying Jin, Fengchao Wang and Meng Wen, *Phys. Plasmas* **14**, 113108 (2007).
- [36] T. V. Liseikina and A. Macchi, *Applied Physics Lett.* **91**, 171502 (2007).
- [37] Xiaomei Zhang, Baifei Shen, Xuemei Li, Zhangying Jin, and Fengchao Wang, *Phys. Plasmas* **14**, 073101 (2007) ; doi:10.1063/1.2746810.
- [38] Predhiman Kaw and John Dawson, *Physics of Fluids* **13**, 472 (1970).
- [39] Lai C. S., *Phys. Rev. Lett.* **36**, 966 (1976)
- [40] Cattani F., Kim A., Anderson D. and Lisak M., *Phys. Rev. E* **62**, 1234 (2000).
- [41] Shen Baifei and Xu Zhizhan, *Phys. Rev. E* **64**, 056406 (2001).
- [42] Sheng, Z. M., and J. Meyer-ter-Vehn. "Inverse Faraday effect and propagation of circularly polarized intense laser beams in plasmas." *Physical Review E* **54**, no. 2 (1996): 1833.

- [43] Karpman, V. I., and A. G. Shagalov. "The ponderomotive force of a high-frequency electromagnetic field in a cold magnetized plasma." *Journal of Plasma Physics* **27** (1982): 215-224.
- [44] Hertel, Riccardo. "Theory of the inverse Faraday effect in metals." *Journal of magnetism and magnetic materials* **303**, no. 1 (2006): L1-L4.
- [45] H. Cai, W. Yu, S. Zhu, and C. Zhou, *Phys. Rev. E* **76**, 036403 (2007).
- [46] Anamika Sharma, C. S. Liu and V. K. Tripathi, *Phys. Plasmas* 17, 013101 (2010) ; doi:10.1063/1.3278600.
- [47] R. C. Jensen and A. W. Fairhall, *Phys. Rev.* 109, 942(1958).
- [48] D. B. Duncan and J. E. Perry, *Phys. Rev.* 82, 809(1951).

# 3

## Self consistent model for ponderomotive ion acceleration of laser irradiated two species dense target plasmas

### 3.1 Introduction

The ability of high intensity lasers to produce energetic ions have been of enormous interest as they can generate nearly monoenergetic ion beams at very short distance [1, 2] and its applications ranging cancer research to inertial fusion [3, 4, 5, 6, 7, 8]. Chapters 1 and 2 introduced ion acceleration mechanisms like TNSA [9, 10, 11, 12, 13], “Light Sail” radiation pressure acceleration (LS-RPA) [14, 15, 16, 17, 18, 19] and Hole Boring radiation pressure acceleration (HB-RPA) [8, 2, 20, 21, 22, 23, 24, 25, 26, 27]. Rayleigh Taylor (RT) instability in the process of LS-RPA has been studied in [18, 19]. The central motivation to study this area is to develop high energy ion beam sources with available lasers. A lot of effort is being given to develop techniques to increase ion kinetic energies keeping the incident laser intensity as constant. Previous chapter discussed the effect of a static longitudinal magnetic field on this process. It was found that ponderomotive force was enhanced for a right circularly polarized (RCP) light as the direction of rotation of electrons in the electron sheath of the laser piston under the influence of laser fields and the externally applied magnetic field are the same. This leads to increase in kinetic energies of obtained ion beams. On the other hand, left circularly polarized (LCP) light had the opposite effect because the electron

quiver motion and cyclotron motion are in opposite directions. Thus by coupling magnetic field to the laser field can generate higher energy ions. Recently there has been an increasing interest in laser ion acceleration with mixed target plasmas. In this case the target plasma is composed of more than one ion species with different masses. In [28, 29, 30] a plasma target composed of two ion species was analyzed. It was found that the velocity of the heavy ion obtained in this case was higher than what would have been achieved with a target composed of only the heavy ions with laser of the same intensity and plasma with same number density. Hence, mixing the target plasma with lighter ions prove to be advantageous. In [29], the study was performed using different number densities of the two species. It was found that the acceleration was more efficient when the number density of the heavier species was less. In [30], the treatment of this process was performed taking the mass density of the composite target instead of number density. They concluded that the piston velocity was inversely proportional to the square root of the mass density of the composite target. So far the treatment for laser ion acceleration for mixed target plasma has been limited to conservation laws, i.e. conservation of energy and momentum. In [26, 27] a complete analytical treatment of the laser piston was given for a single species target. In this chapter, we present a detailed analytical treatment of the steady state regime of ion acceleration in the laser piston composed of two ion species. In the analytical model we describe the internal structure of the laser piston as well as the coulomb exploding ion region lying behind the piston using a two fluid model. The entire accelerating electrostatic field has been described. We emphasize the need for such investigation by performing the stability analysis of the accelerating structure using the information obtained from this treatment. Further the evolution of coulomb exploding part of ion space charge region with different charge states of the plasma ion species has been described. The dependence of reflection of incoming ion beam from the coulomb exploding part on the charge state of the beam species has also been explored.

## 3.2 Acceleration process with two ion species

Here we first recollect the expression for the steady state velocity attained by the charge separation layer or the laser piston for a two ion species. In the reference frame of the piston moving with velocity  $v_f = \beta_f c$ , i.e. the instantaneous rest frame (IRF), the laser intensity turns out to be  $I = I_0(1 - \beta_f)/(1 + \beta_f)$  where  $I_0$  is the incident laser intensity in the lab frame. In the IRF, all the plasma ions appear to approach the piston with velocity  $v_f$ . Making the assumption that in the steady state all the ions are reflected from the laser piston, the conservation of momentum gives,

$$\frac{I_0}{c} \frac{1 - \beta_f}{1 + \beta_f} = \gamma_f^2 \beta_f^2 \sum_i m_i n_i \quad (3.1)$$

where the subscript “i” refers to the number of ion species,  $m$  and  $n$  are the ion mass and number density. The piston velocity thus obtained from Eq. 3.1 is,

$$\beta_f = \frac{\sqrt{\Xi}}{1 + \sqrt{\Xi}} \quad (3.2)$$

with  $\Xi = I_0/c^3 \sum_i m_i n_i$ . The piston velocity thus can be seen as a function of the incident laser intensity and the total mass density of the target plasma. The velocity of the reflected ion can be obtained in the lab frame by relativistic velocity transformation as  $v_{iL} = 2v_f/(1 + \beta_f^2)$  and the corresponding kinetic energy is given as,

$$\Gamma = m_i c^2 \left[ \frac{2\Xi}{1 + \sqrt{\Xi}} \right] \quad (3.3)$$

The calculations discussed so far had not analyzed the basic mechanism of acceleration of these ions. Also it has not provided the details of the structure of the laser piston. The structure of the laser piston for single ion species has been discussed in detail in [26] and with a longitudinal magnetic field in [27]. In the following work, we present a detailed description of the ion space charge and electron sheath for a two ion species target. Studying the ion acceleration phenomena keeping the total ion number density constant and changing the number density ratio of the two species is found to yield interesting results.

### 3.3 Ion space charge for a two species target

We have seen in [26, 27] that because of different response times of ions and electrons, the ion sheath lags behind the electron sheath. In case of two species plasma, both the ion species because of their different masses will respond to the induced electric field at different time scales. So, instead of a double layer, the laser piston will comprise of a triple layer in this case. A schematic diagram of the acceleration process for two species target has been presented in Fig.3.1. It emphasizes on the different regions with in the target during the interaction of laser with the target plasma. In case of a two species target, the ion separation layer can be studied by dividing it into three parts. First, the region  $[-\delta_l, 0]$ , which comprises of both the ion species. Second, is the region  $[-\delta_h, -\delta_l]$  where primarily the heavier species are present and third, the region undergoing coulomb explosion comprising of both the ion species extending from  $z = -z_i$  to  $z = -\delta_h$ .

#### 3.3.1 Mixed species ion sheath

We first investigate the ion sheath comprising of both the species in the region  $[-\delta_l, 0]$ . As the ion species are massive as compared to the electrons, we neglect their quiver motion due to the laser fields. The longitudinal electric field, induced due to charge separation are the ones that accelerate the ions. In the frame moving with the laser piston, the ion species in the undisturbed plasma appear to come towards the sheath and the ones accelerated by the electrostatic field appear to move outward towards the undisturbed plasma gaining velocity. The conservation of ion particle flux and the continuity equation yields a relation between ion density and velocity for both the species. For incoming ions, we have  $n_l^-(z)v_{lz}^- = -n_{l0}\gamma_f v_f$  and  $n_h^-(z)v_{hz}^- = -n_{h0}\gamma_f v_f$  where  $n$  and  $v$  represents ion density and velocity respectively and the subscript  $l$  and  $h$  corresponds to the lighter and heavier species.  $n_{l0}$  and  $n_{h0}$  are the initial ion number density of both the species.  $v_f$  is the velocity of the charge separation layer and  $\gamma_f$  is the relativistic factor corresponding to  $v_f$ . For the ions moving towards the undisturbed plasma a similar relation gives  $n_l^+(z)v_{lz}^+ = n_{l0}\gamma_f v_f$  and  $n_h^+(z)v_{hz}^+ = n_{h0}\gamma_f v_f$ . Taking consideration for incoming and outgoing ions of both species, their density with in the sheath can be written

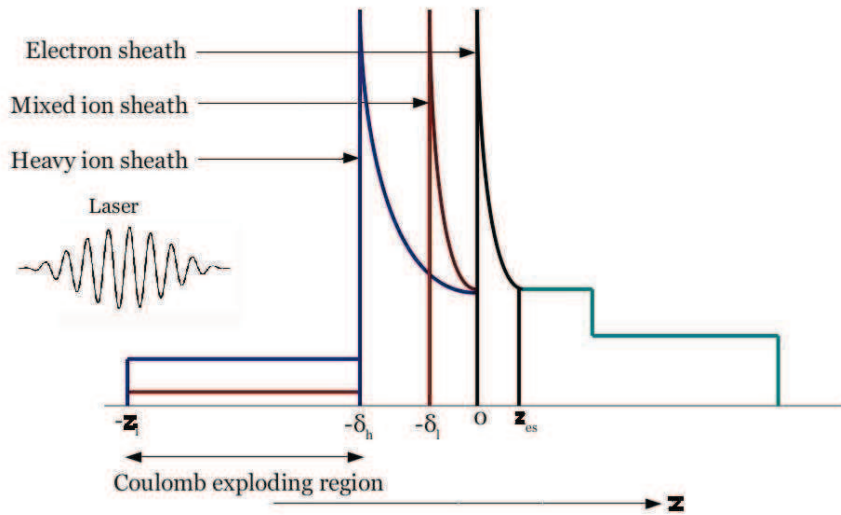


Figure 3.1: Charge separation layer maintained by the radiation pressure of the incident laser. The blue curve represent heavy ions, red represent light ions and black curve refers to electrons. The region  $[0, z_{es}]$  represents the electron sheath. The region  $[-\delta_l, 0]$  is an ion sheath comprising of both the light and heavy ion species.  $[-\delta_h, -\delta_l]$  comprises primarily of the heavy ion species and in the region  $[-z_i, -\delta_h]$  the ions are undergoing coulomb explosion.  $z > z_{es}$  is the region of undisturbed plasma.

as,

$$n_l(z) = 2n_{l0}\gamma_f \frac{\beta_f}{\beta_{lz}}; \quad n_h(z) = 2n_{h0}\gamma_f \frac{\beta_f}{\beta_{hz}} \quad (3.4)$$

As both the ion species are moving in the same potential, ion energy conservation gives,

$$\frac{KE_l + Z_l e \phi(z)}{m_l c^2} = \frac{KE_h + Z_h e \phi(z)}{m_h c^2} = \gamma_f - 1 \quad (3.5)$$

where  $KE_l$  and  $KE_h$  are the local kinetic energies of lighter and heavier ion species respectively.  $m_l$ ,  $m_h$ ,  $Z_l$  and  $Z_h$  are the mass and charge of the ions and  $\phi(z)$  is the local electrostatic potential within the sheath. Under this consideration, the relation between the  $\gamma$ factors of both the ion species can be derived as,

$$\frac{m_l c^2}{Z_l e} (\gamma_f - \gamma_l(z)) = \frac{m_h c^2}{Z_h e} (\gamma_f - \gamma_h(z)) \quad (3.6)$$

To determine the electrostatic field  $E_z$ , the Poisson's equation gives,

$$\frac{dE_z}{dz} = 4\pi Z_l e n_l(z) + 4\pi Z_h e n_h(z) \quad (3.7)$$

The electrostatic potential  $\phi(z)$  follows the relation  $Z_l e \phi(z) = m_l c^2 (\gamma_f - \gamma_l(z))$ . Hence substituting for  $E_z = -d\phi/dz$  gives,

$$Z_l e E_z = m_l c^2 \frac{d\gamma_l}{dz} \quad (3.8)$$

Substituting Eq.3.8 in Eq.3.7 and using Eq.3.4, we arrive at,

$$\frac{d^2 \gamma_l}{dz^2} = 2 \frac{\omega_{pl}^2}{c^2} \gamma_f \beta_f \left( \frac{1}{\beta_{lz}} + \frac{Z_h n_{h0}}{Z_l n_{l0}} \frac{1}{\beta_{hz}} \right) \quad (3.9)$$

where  $\beta_{lz} = (1 - 1/\gamma_l^2)^{1/2}$  and  $\omega_{pl} = (4\pi n_{l0} Z_l^2 e^2 / m_l)^{1/2}$ . To solve this equation, we require  $\gamma_l$  and its first derivative at the point of reflection of the lighter ions i.e. at  $z = -\delta_l$ . At this point  $\gamma_l = 1$ . For the first derivative we integrate the above equation by first multiplying it with  $d\gamma_l/dz$ . The first integral obtained is,

$$\frac{d\gamma_l}{dz} = \left[ 4 \frac{\omega_{pl}^2}{c^2} \gamma_f \beta_f \left[ \sqrt{\gamma_l^2 - 1} + \frac{n_{h0} m_h}{n_{l0} m_l} \sqrt{\gamma_h^2 - 1} \right] \right]^{1/2} \quad (3.10)$$

From this relation we can obtain the profile of  $E_z$  within the sheath in the region  $[-\delta_l, 0]$  composed of both species of ions. At the boundary of reflection of lighter ions ( $z = -\delta_l$ ), the electric field can be obtained by putting  $\gamma_l = 1$  which turns out to be,

$$E_z(-\delta_l) = \frac{m_l c^2}{Z_l e^2} \left[ 4 \frac{\omega_{pl}^2}{c^2} \gamma_f \beta_f \frac{n_{h0} m_h}{n_{l0} m_l} \sqrt{\gamma_h^2 - 1} \right]^{1/2} \quad (3.11)$$

At  $z = -\delta_l$  the heavier ions still has got residual velocity in the negative direction. As a result of this, these heavier species overshoot the mixed ion sheath and undergo further deceleration forming another sheath behind  $z = -\delta_l$  comprising of only the heavier species. The velocity with which these ions enter the heavy ion sheath is given by,

$$\beta_{hz}(-\delta_l) = \left( 1 - \frac{1}{\gamma_h^2(-\delta_l)} \right)^{1/2} \quad (3.12)$$

where,

$$\gamma_h(-\delta_l) = \gamma_f - \frac{Z_h m_l}{Z_l m_h} (\gamma_f - 1) \quad (3.13)$$

### 3.3.2 Heavier species ion sheath

The heavier species enter into this region further experiencing deceleration before getting reflected at  $z = -\delta_h$ . The heavier ion density goes to infinity at the point of reflection. The longitudinal electric field in this region is given by  $E_z = -d\phi/dz$  where  $\phi = m_h c^2 / Z_h e (\gamma_f - \gamma_h(z))$ . Here, Poisson's equation together with the longitudinal electric field can be written as,

$$\frac{d^2 \gamma_h}{dz^2} = 2 \frac{\omega_{ph}^2}{c^2} \gamma_f \frac{\beta_f}{\beta_{hz}} \quad (3.14)$$

where  $\beta_{hz} = (1 - 1/\gamma_h^2)^{1/2}$  and  $\omega_{ph} = (4\pi n_{h0} Z_h^2 e^2 / m_h)^{1/2}$ . The first integral of Eq.3.14 read as,

$$\frac{d\gamma_h}{dz} = \frac{2\omega_{ph}}{c} \sqrt{\gamma_f \beta_f (\gamma_h^2 - 1)^{1/4}} \quad (3.15)$$

The boundary condition at  $z = -\delta_h$  required to solve Eq. 3.14 is  $\gamma_h(-\delta_h) = 1$  and  $d\gamma_h/dz|_{z=-\delta_h} = 0$ . Solving Eq. 3.14 will give the density and velocity profile of the heavier species together with the longitudinal electric field. The longitudinal

electric field in this region is given by,

$$E_z[-\delta_h, -\delta_l] = \frac{m_h c^2}{Z_h e} \frac{d\gamma_h}{dz} \quad (3.16)$$

The boundary  $-\delta_l$  can be determined by equating the heavier ion velocity obtained from Eq. 3.14 to Eq. 3.12. Using this we can also numerically compute the thickness of the heavier ion sheath. Fig.3.2 shows the ion density profiles in the sheath for three different initial number density ratios ( $n_{h0}/n_{l0}$ ) of the ions viz. 1/9, 3/7 and 1 with  $\beta_f = 0.2$  and  $n_0/n_c = 10$ , where  $n_0$  is the total initial ion number density and  $n_c = m_e \omega^2 / 4\pi e^2$  is the critical density. We must note that the ion sheath thickness for heavier species is greater than that for the lighter ones and the separation between the two ion sheaths decreases with increasing ratio. Fig.3.3 shows the velocity profile of the accelerated  $C^{6+}$  and  $H^+$  ions in the frame of the laser piston with  $\beta_f = 0.2$  and different  $n_{h0}/n_{l0}$ . As the zone responsible for acceleration of ions comprises of two distinct sheath, we can say that there is a jump in electrostatic potential at  $z = -\delta_l$ . Fig.3.4 shows the electrostatic potential in the sheath. The jump at  $z = -\delta_l$  was also observed in the PIC simulations of [28]. Thus, this treatment gives an understanding for such occurrence in the electrostatic field profile.

### 3.3.3 Coulomb exploding ion space charge region

In order to obtain analytical estimates of the physical processes that are involved in the ion space charge region behind the sheaths, i.e.  $[-z_i, \delta_h]$ , we adopt a two-fluid, cold ion model. Instead of Eulerian coordinates  $z, t$  we use Lagrangian coordinates  $z_{0\alpha}, \tau$ , where,

$$\tau \equiv t; \quad z_{0\alpha} \equiv z_\alpha - \int_0^\tau d\tau' v_\alpha(z_{0\alpha}, \tau') \quad (3.17)$$

and  $\alpha$  refers to the type of ion species under consideration (light and heavy in this case). The space and time derivatives transform according to,

$$\frac{\partial}{\partial z_\alpha} \equiv \left[ 1 + \int_0^\tau d\tau' \frac{\partial}{\partial z_{0\alpha}} v_\alpha(z_{0\alpha}, \tau') \right]^{-1} \frac{\partial}{\partial z_{0\alpha}} \quad (3.18)$$

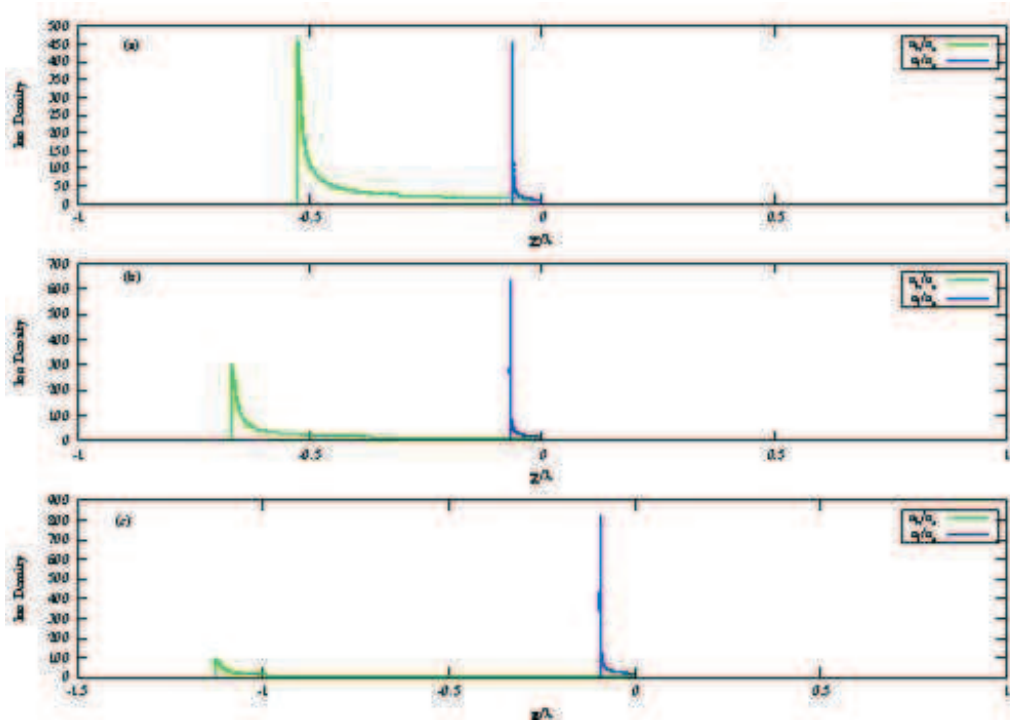


Figure 3.2: Density profiles of the ion species in the laser piston for  $n_0/n_c = 10$  and  $\beta_f = 0.2$ . The green curves represent heavier ions ( $C^{6+}$ ) and blue curves represent lighter ions ( $H^+$ ). (a) shows the ion sheaths for density ratio  $n_{h0}/n_{l0} = 1$ , (b) is for  $n_{h0}/n_{l0} = 3/7$  and (c) for  $n_{h0}/n_{l0} = 1/9$ .  $\lambda$  here is the laser wavelength.

and,

$$\frac{\partial}{\partial t} = \frac{\partial}{\partial \tau} - v_\alpha(z_{0\alpha}, \tau) \left[ 1 + \int_0^\tau d\tau' \frac{\partial}{\partial z_{0\alpha}} v_\alpha(z_{0\alpha}, \tau') \right]^{-1} \frac{\partial}{\partial z_{0\alpha}} \quad (3.19)$$

The force and continuity equation for both the species can be written in Lagrange coordinates as,

$$\frac{\partial}{\partial \tau} v_\alpha(z_{0\alpha}, \tau) = \frac{Z_\alpha e}{m_\alpha} E(z_{0\alpha}, \tau) \quad (3.20)$$

$$\frac{\partial}{\partial \tau} \left( n_\alpha(z_{0\alpha}, \tau) \left[ 1 + \int_0^\tau d\tau' \frac{\partial}{\partial z_{0\alpha}} v_\alpha(z_{0\alpha}, \tau') \right] \right) = 0 \quad (3.21)$$

Solutions of the Eqs.[3.20-3.21] for the light and heavy ions come out to be,

$$v_l = \frac{\omega_{pl}^2 z t}{\left[ 1 + \frac{\omega_{pl}^2 t^2}{2} \left( 1 + \frac{Z_h n_{h0}}{Z_l n_{l0}} \right) \right]} \left[ 1 + \frac{Z_h n_{h0}}{Z_l n_{l0}} \right] \quad (3.22)$$

$$v_h = \frac{\omega_{ph}^2 z t}{\left[ 1 + \frac{\omega_{ph}^2 t^2}{2} \left( 1 + \frac{Z_l n_{l0}}{Z_h n_{h0}} \right) \right]} \left[ 1 + \frac{Z_l n_{l0}}{Z_h n_{h0}} \right] \quad (3.23)$$

$$n_l(z, t) = \frac{n_{l0}}{\left[ 1 + \frac{\omega_{pl}^2 t^2}{2} \left( 1 + \frac{Z_h n_{h0}}{Z_l n_{l0}} \right) \right]} \quad (3.24)$$

$$n_h(z, t) = \frac{n_{h0}}{\left[ 1 + \frac{\omega_{ph}^2 t^2}{2} \left( 1 + \frac{Z_l n_{l0}}{Z_h n_{h0}} \right) \right]} \quad (3.25)$$

In case of a single ion species we saw in [27] that the velocity was dependent on initial ion density,  $z$  and  $t$ , whereas here, in case of mixed target, we see that besides these quantities the ratio of the equilibrium densities as well as ratio of charges of both the species play a role in the evolution of this structure. The time evolution of the number density of both the species normalized to their equilibrium density is shown in Fig.5.5 for different ion charge ratio. It can be seen that the density of the heavier species (carbon in this case) goes down slowly in time than that of lighter ones (Hydrogen). Also with the increase in charge on carbon i.e.  $C^{6+}$ , the rate of decrease of its density also increases.

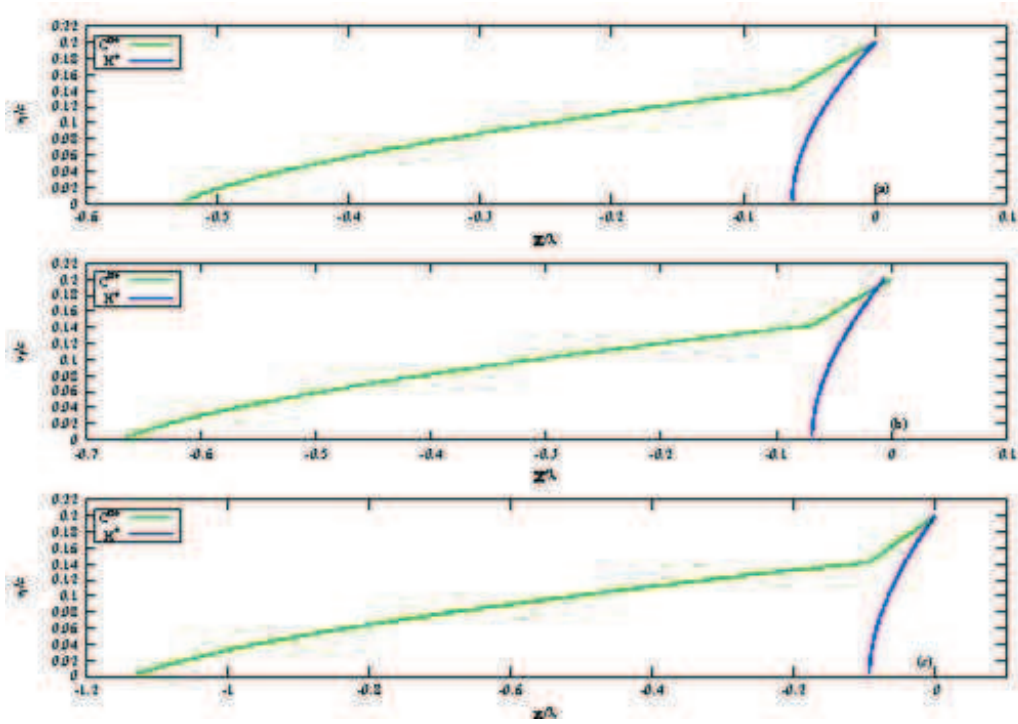


Figure 3.3: Velocity profiles of the ion species in the laser piston in the piston frame for  $n_0/n_c = 10$  and  $\beta_f = 0.2$ . The green curves represent heavier ions ( $C^{6+}$ ) and blue curves represent lighter ions ( $H^+$ ). (a) shows the local ion velocities within the piston for density ratio  $n_{h0}/n_{l0} = 1$ , (b) is for  $n_{h0}/n_{l0} = 3/7$  and (c) for  $n_{h0}/n_{l0} = 1/9$ .

Chapter 3. Self consistent model for ponderomotive ion acceleration of laser irradiated two species dense target plasmas

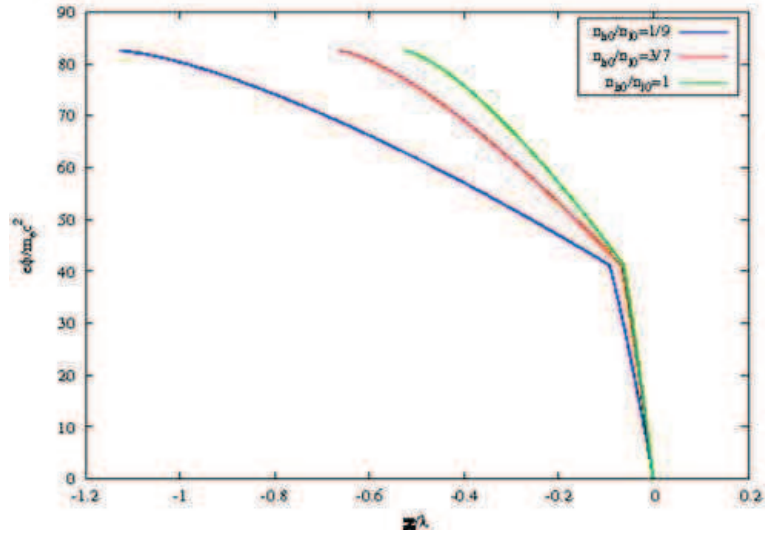


Figure 3.4: Electrostatic potential within the laser piston for  $n_0/n_c = 10$  and  $\beta_f = 0.2$  for different ratios of ion species.

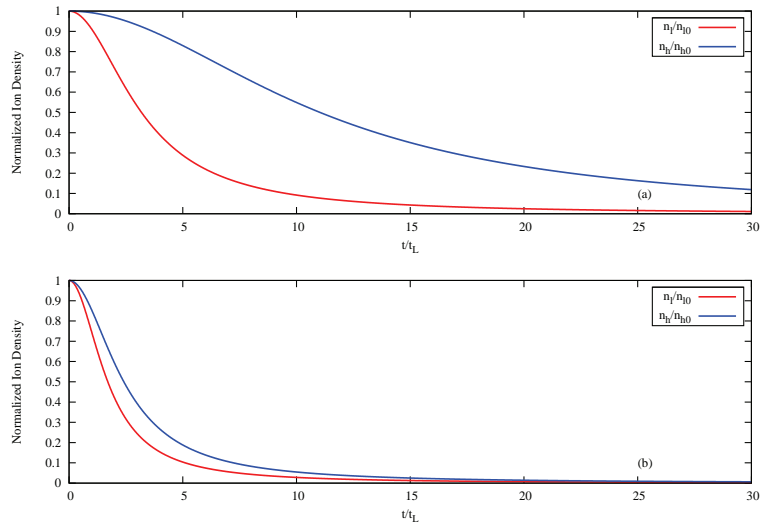


Figure 3.5: Time evolution of the number density of both the ion species normalized to their equilibrium densities. Blue curves represent carbon ions and green curves represent hydrogen. (a) shows the time evolution for  $C^+$  and  $H^+$ , whereas (b) is for  $C^{6+}$  and  $H^+$ .

### 3.4 Electron sheath for a two ion species target

To study the electron sheath in steady state, we consider the evanescent laser fields within the sheath. The evanescent electric and magnetic fields are given by,

$$\vec{E}_T = (\hat{x} + i\hat{y})E_T(z)\exp[-i\omega t]; \quad \vec{B}_T = \frac{c}{i\omega} \nabla \times \vec{E}_T \quad (3.26)$$

The electron sheath comprises of all the three species, i.e. electrons and the two ion species. As the mass of the ion species are very high as compared to that of electrons, their transverse motion due to the evanescent laser fields can be neglected. It is only the longitudinal electrostatic field that acts upon these ions. The momentum equation describing the electrons under the influence of evanescent laser fields can be written as,

$$\frac{d\vec{p}}{dt} = -e\vec{E}_T - \frac{e}{c}\vec{v}_e \times \vec{B}_T \quad (3.27)$$

where  $\vec{p}$  is the electron momentum and  $\vec{v}_e$  is the electron velocity. To determine the electron quiver velocity, the transverse component of the electron momentum equation gives,

$$\vec{v}_{e\perp} = (\hat{x} + i\hat{y})\frac{a_T c}{i\gamma_e} \exp[-i\omega t] \quad (3.28)$$

where  $a_T = eE_T/m_e\omega c$  is the dimensionless evanescent field amplitude,  $\gamma_e = (1 + p_{\perp}^2/m_e^2c^2 + p_{\parallel}^2/m_e^2c^2)^{1/2}$  is the electron relativistic factor and  $p_{\parallel} = \gamma_e m_e v_{ez}$  and  $p_{\perp} = \gamma_e m_e v_{e\perp}$  are the longitudinal and transverse components of the electron momentum with  $v_{ez}$  as the longitudinal electron velocity due to the induced electrostatic field. The ion relativistic factors are given by  $\gamma_l = (1 + p_l^2/m_l^2c^2)^{1/2}$  and  $\gamma_h = (1 + p_h^2/m_h^2c^2)^{1/2}$  for light and heavy species respectively.  $m_l$  and  $m_h$  are the masses of heavy and light species and  $p_l = \gamma_l m_l v_{lz}$  and  $p_h = \gamma_h m_h v_{hz}$  are the longitudinal momentum of the ion species with  $v_{lz}$  and  $v_{hz}$  as their respective velocities. The longitudinal electron velocity  $v_{ez}$  can be obtained from  $\gamma_e$  and Eq.3.28 as,

$$v_{ez} = \pm c \sqrt{(\gamma_e^2 - (1 + a_T^2))/\gamma_e} \quad (3.29)$$

In the frame of the charge separation layer moving with velocity  $v_f$  the electrons comprise of two streams. The ones undisturbed by the laser field appear to move

towards the charge separation layer. For these incoming electrons, from the equation of continuity we have  $n_e^- v_{ez}^- = -(Z_l n_{l0} + Z_h n_{h0}) \gamma_f v_f$  with  $n_e$  as the local electron density. For the electrons which are pushed by the laser towards the undisturbed plasma, the equation of continuity gives  $n_e^+ v_{ez}^+ = (Z_l n_{l0} + Z_h n_{h0}) \gamma_f v_f$ . By taking together the incoming and outgoing electrons, the total electron density with in the sheath comes as,

$$n_e(z) = 2(Z_l n_{l0} + Z_h n_{h0}) \frac{\gamma_f \beta_f}{\beta_e} \quad (3.30)$$

The densities of the ion species are given as  $n_l(z) = 2n_{l0} \gamma_f \beta_f / \beta_{lz}$  and  $n_h(z) = 2n_{h0} \gamma_f \beta_f / \beta_{hz}$ . As both the ion species and the electrons are moving in the same electrostatic potential, we can derive the relation between their respective  $\gamma$  factors as,

$$\gamma_l = \gamma_f - \frac{Z_l m_e}{m_l} (\gamma_e - \gamma_f); \quad \gamma_h = \gamma_f - \frac{Z_h m_e}{m_h} (\gamma_e - \gamma_f) \quad (3.31)$$

Incorporating the electron and ion densities described above with in the electron sheath the Poisson's equation takes the form,

$$\frac{d^2 \phi}{dz^2} = 8\pi e \gamma_f \beta_f \left( \frac{(Z_l n_{l0} + Z_h n_{h0})}{\beta_{ez}} - \frac{Z_l n_{l0}}{\beta_{lz}} - \frac{Z_h n_{h0}}{\beta_{hz}} \right) \quad (3.32)$$

where  $\phi = m_e c^2 / e (\gamma_e - 1)$  is the ponderomotive potential. Substituting for  $\phi$  in the Poisson's equation, it takes the form,

$$\frac{d^2 \gamma_e}{dz^2} = 2 \frac{\omega_{pe0}^2}{c^2} \gamma_f \beta_f \left( \frac{\gamma_e}{\sqrt{\gamma_e^2 - 1 - a_T^2}} - \frac{Z_l n_{l0}}{n_{e0}} \frac{\gamma_l}{\sqrt{\gamma_l^2 - 1}} - \frac{Z_h n_{h0}}{n_{e0}} \frac{\gamma_h}{\sqrt{\gamma_h^2 - 1}} \right) \quad (3.33)$$

where  $\omega_{pe0} = (4\pi n_{e0} e^2 / m_e)^{1/2}$  with  $n_{e0} = Z_l n_{l0} + Z_h n_{h0}$ . The presence of  $a_T$  in the above equation indicates that to determine  $\gamma_e$  we must also solve for  $a_T$ . As the longitudinal electric field is continuous,  $E_z$  at the interface of the mixed ion sheath and electron sheath (at  $z = 0$ ) is given by Eq.3.10 which can be written in terms of the electron relativistic factor  $\gamma_e$  as,

$$\left. \frac{d\gamma_e}{dz} \right|_{z=0} = -\frac{m_l}{Z_l m_e} \left[ 4 \frac{\omega_{pl}^2}{c^2} \gamma_f \beta_f \left[ \sqrt{\gamma_l^2 - 1} + \frac{n_{h0} m_h}{n_{l0} m_l} \sqrt{\gamma_h^2 - 1} \right] \right]^{1/2} \quad (3.34)$$

As has been described above that the ions do not exhibit quiver motion due to the evanescent laser fields, its only electrons which contribute to the refractive index of the plasma. Hence the wave equation for the fields with in the sheath can be described in the same way as in [26, 27],

$$\frac{d^2 a_T}{dz^2} = \frac{\omega^2}{c^2} \left( \frac{\omega_{pe}^2/\omega^2}{\gamma_e} - \frac{1 - \beta_f}{1 + \beta_f} \right) a_T \quad (3.35)$$

where  $\omega_{pe}$  corresponds to the local electron plasma frequency with in the sheath. Substituting for the local electron density from Eq.3.30, the field equation takes the form,

$$\frac{d^2 a_T}{dz^2} = 2 \frac{\omega_{pe0}^2}{c^2} \gamma_f \beta_f \frac{a_T}{\sqrt{\gamma_e^2 - 1 - a_T^2}} - \frac{\omega_0^2}{c^2} \frac{1 - \beta_f}{1 + \beta_f} a_T \quad (3.36)$$

The boundary condition to determine the incident laser intensity for total reflection in piston frame is given as [26],

$$\left( \frac{da_T}{dz} \right)^2 \Big|_{z=0} + \frac{\omega^2}{c^2} \frac{1 - \beta_f}{1 + \beta_f} a_T^2(0) = 4 \frac{\omega^2}{c^2} \frac{1 - \beta_f}{1 + \beta_f} a_0^2 \quad (3.37)$$

The coupled Eqs. 3.33 and 3.36 when integrated once by multiplying with their first derivatives and compared together with the boundary condition of Eqs.3.34 and 3.37 we obtain the analytical expression for the ion velocity in the moving frame which is the same as Eq.3.1 where the velocity was obtained using momentum conservation arguments. To integrate the coupled system of Eqs. 3.33 and 3.36 numerically, we determine the asymptotic solution by solving them backwards from  $z \gg c/\omega_{pe0}$ , and taking  $\gamma_e = \gamma_f + \delta\gamma$  and  $\delta\gamma, a_T(z) \ll 1$ . At  $z \gg c/\omega_{pe0}$  the first derivatives of  $\gamma_e$  and  $a_T$  read as,

$$\frac{d\delta\gamma}{dz} \Big|_{z \gg c/\omega_{pe0}} = - \left[ \frac{2\omega_{pe0}^2}{c^2} \frac{1}{\gamma_f \beta_f^2} \left[ a_T^2 \delta\gamma - 2\delta\gamma^2 \right] \right]^{1/2} \quad (3.38)$$

$$\frac{da_T}{dz} \Big|_{z \gg c/\omega_{pe0}} = - \left[ \frac{2\omega_{pe0}^2}{c^2} - \frac{\omega^2}{c^2} \frac{1 - \beta_f}{1 + \beta_f} \right]^{1/2} a_T \quad (3.39)$$

Here  $\delta\gamma$  can be taken to be of the same order as  $a_T^2$ . For a given  $\beta_f$  we obtain the initial value of the first derivative of the evanescent field from the above equations. Using these initial conditions, we can numerically integrate the coupled set of

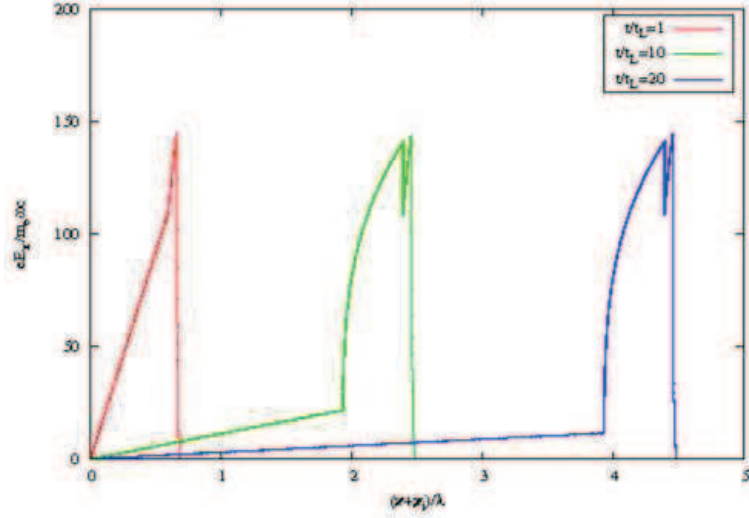


Figure 3.6: Spatial profile of longitudinal electric field  $E_z$  for  $n_0/n_c = 10$  and  $n_{h0}/n_{l0} = 1$  with  $\beta_f = 0.2$  at different times.

Eqs. 3.33 and 3.36 for a chosen  $\beta_f$ . The equations have to be terminated at the point when the longitudinal electric fields match the condition of Eq. 3.34. The longitudinal electric field in the electron sheath together with that of the ion space charge region described in three separate segments give the entire profile of  $E_z$ . Fig.3.6 shows the complete profile of  $E_z$  at different times. We must note the jump falling between the two ion sheaths. This occurs due to the mass difference in the ion species because of which the heavier ones lag behind the lighter ones. Such jump was also observed in the simulations of [28]. Thus the model successfully explain this observation. The initial charge separation occurring to balance the ponderomotive force and electrostatic force can be given by,

$$z_d = \frac{E_{max}}{4\pi(Z_l n_{l0} + Z_h n_{h0})e} \quad (3.40)$$

where  $E_{max}$  is computed from Eq. 3.34. The initial thickness of the coulomb exploding part can be taken o be  $z_c = z_d - \delta_h$ . We assume here that this separation is attained in one laser period as in overdense plasma the electron plasma frequency exceeds the laser frequency. This assumption is reasonable as the results are not

much influenced by this choice. Also, once the force balance is obtained, it is assumed that the laser piston moves with velocity  $v_f$ .

### 3.5 Stability analysis of Laser Piston

In this section, we explore the vulnerability of the accelerating structure to Rayleigh Taylor instability (RTI). As both the ion species achieve almost all of their kinetic energy within the ion sheath, we would limit our analysis to this structure. Also as the thickness of the ion sheath is of the order of a fraction of the laser wavelength, it would be reasonable to assume it as a thin sheet. In the steady state, the charge separation layer moves through the undisturbed plasma at constant velocity trapping and accelerating the ions that are at rest. Determining the onset of RTI in this layer and the factors on which it depends can help us in figuring out the time upto which the acceleration process can continue, or in other words, the maximum pulse length we can have as well as ways to suppress RTI.

We propose a fluid treatment of RTI for the accelerating layer by considering the ion sheath, in equilibrium, is supported against the laser ponderomotive force (radiation pressure) by the restoring electrostatic force generated due to charge separation. In the steady state, the radiation pressure “ $P_{rad}$ ” exerted on the charge separation layer is constant. In the instantaneous rest frame (IRF) i.e. the frame moving with the charge separation layer “ $P_{rad}$ ” is given as,

$$P_{rad} = \frac{2I_0}{c} \frac{1 - \beta_f}{1 + \beta_f} \quad (3.41)$$

where  $I_0$  is the incident laser intensity in the lab frame. For the present analysis, we consider the laser intensity to be uniform in the transverse direction. The validity of such analysis will hold closely for laser pulses that have a super-gaussian intensity profile along the transverse direction.

Let us consider two points  $(y_0, z_0)$  and  $(y_0 + \Delta y_0, z_0)$  on the ion sheath at the stage when the system is perturbed (say at  $t = 0$ ). These two points will evolve at some time (say  $t$ ) to the points  $(y, z)$  and  $(z + \partial z / \partial y_0 \Delta y_0, y + \partial y / \partial y_0 \Delta y_0)$ . The entire sheath can be divided into these small segments, and by analyzing the time evolution of this segment and integrating over the whole sheath along the transverse direction (i.e. y-direction), we can arrive at the evolution of the entire

ion sheath (i.e. accelerating structure). The mass of this small element can be given by,

$$dm = \sigma dy_0 = \left( \sum_i m_i \int n_i(z) dz \right) dy_0 \quad (3.42)$$

where  $\sigma$  is the surface mass density of the layer,  $m_i$  is the mass of the  $i^{th}$  species and  $n_i(z)$  is the local ion density within the sheath which can be determined numerically from Eqs. 3.4, 3.9 and 3.14. If “g” is the acceleration, then from the force balance we obtain,

$$P_{rad} dy_0 = g dm \quad (3.43)$$

or,

$$g = \frac{1}{\sum_i m_i \int n_i(z) dz} \frac{2I_0}{c} \frac{1 - \beta_f}{1 + \beta_f} \quad (3.44)$$

The  $y$  and  $z$  components of the force equation of the sheath element can be written as,

$$\begin{aligned} \frac{\partial p_z}{\partial t} &= -g dm + P_{rad} dy_0 \frac{\partial y}{\partial y_0} \\ \frac{\partial p_y}{\partial t} &= -P_{rad} dy_0 \frac{\partial z}{\partial y_0} \end{aligned} \quad (3.45)$$

where  $p_z = \gamma_f dm dz/dt$  and  $p_y = \gamma_f dm dy/dt$ . Hence, the equations take the form,

$$\begin{aligned} \frac{\partial^2 z}{\partial t^2} &= -\frac{g}{\gamma_f} + \frac{g}{\gamma_f} \frac{\partial y}{\partial y_0} \\ \frac{\partial^2 y}{\partial t^2} &= -\frac{g}{\gamma_f} \frac{\partial z}{\partial y_0} \end{aligned} \quad (3.46)$$

The above coupled set of equations give the time evolution of the segment of our consideration. In the non-relativistic case, the above equation turn out to be the same as that of [31]. When summed upon entire transverse direction (i.e. the complete ion sheath as a sum of these small segments), we get the time evolution of the entire ion sheath. It would be reasonable to expect the solution of the above equations as non-linear as a given perturbation need not be sinusoidal in the  $y, z$  plane. Hence, the solutions turn out to be,

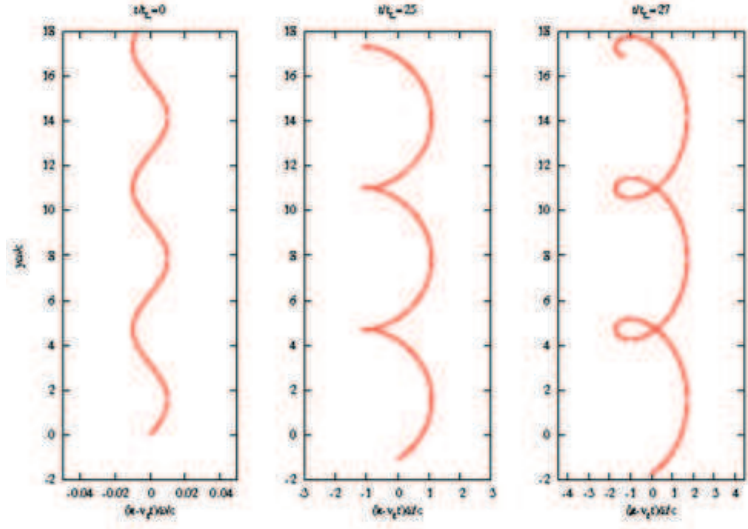


Figure 3.7: Time evolution of the laser piston of a composite target with  $n_0/n_c = 10$  and  $n_{h0}/n_{l0} = 1$  with the incident laser amplitude  $a_0 = 50$ .

$$\begin{aligned}
 z &= \Delta_0 \exp[t(kg/\gamma_f)^{1/2}] \cos(ky_0) \\
 y &= y_0 - \Delta_0 \exp[t(kg/\gamma_f)^{1/2}] \sin(ky_0)
 \end{aligned}
 \tag{3.47}$$

where  $\Delta_0$  is the perturbation amplitude and  $k$ , its corresponding wave number. Our aim would now be to analyze the time evolution of the ion sheath in the steady state as a function of incident laser intensity and target composition in terms of the number densities of two ion species. In this paper, we consider a target composed of hydrogen ( $H^+$ ) and carbon ( $C^{6+}$ ) ions whose masses normalized to electron mass are taken to be  $\tilde{m}_l = 2000$  and  $\tilde{m}_h = 24000$  respectively. We study the evolution of ion sheath for targets with total number density  $n_0/n_c = 10$  with the composition ratio  $n_{h0}/n_{l0} = 1/9, 3/7, 1$ . Fig. 3.7 shows the time evolution of a composite target with  $a_0 = 50$  and  $n_{h0}/n_{l0} = 1$ .  $a_0$  is the dimensionless laser amplitude incident on the plasma. We have taken  $\Delta_0 = 0.01\omega/c$  and  $k = \omega/c$ . We observe that a small perturbation induced at  $t = 0$  grows with time and at  $t = 25t_L$  (where  $t_L = 2\pi/\omega$ ) the cusps begin to form. At this time the ion sheath tends to become porous and eventually get torn apart. The time at which the cusps begin to form is the time after which we cease to get monoenergetic ions. Thus RTI prevents or

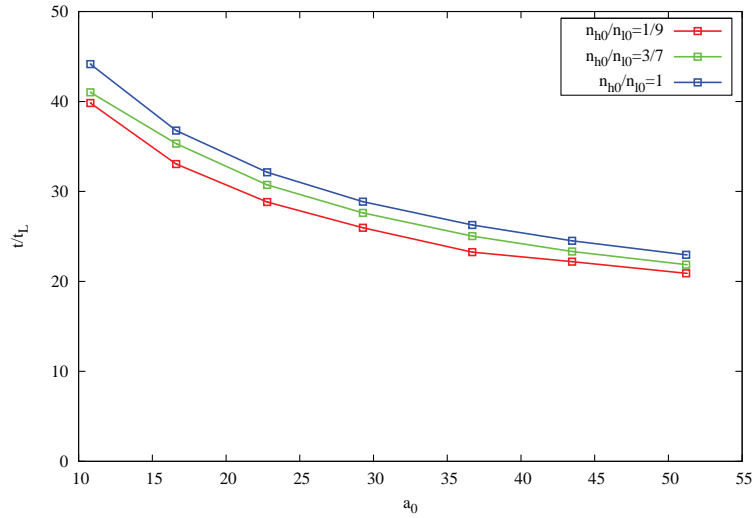


Figure 3.8: Cusp formation time with incident laser intensity for different target compositions keeping  $n_0/n_c = 10$ .

acts as a limiting factor on the time upto which we can accelerate the ions. Fig. 3.8 shows the cusp formation time with incident laser intensity for different target compositions. We can see that with increasing laser intensity the cusp formation time decreases, but the rate of decrease also goes down approaching an asymptotic behavior at the tail. Also with increasing ratio of  $n_{h0}/n_{l0}$  we see that this time goes up or RTI gets a little suppressed with increase in proportion of heavier ion species in the target.

### 3.6 Velocity amplification of an incoming test ion

We now focus our attention to the coulomb exploding ion space charge region. For the ion species at rest, the lighter ions are reflected from  $z = -\delta_l$  and the heavier ions are reflected from  $z = -\delta_h$ . If a test ion approaches this charge separation layer with some velocity, it will over shoot these ion sheath regions and move to the coulomb exploding part. This phenomena was explored for a single species plasma target in [27]. There, the momentum conservation lead to an additional velocity equal to nearly twice the double layer velocity to the test ion upon reflection.

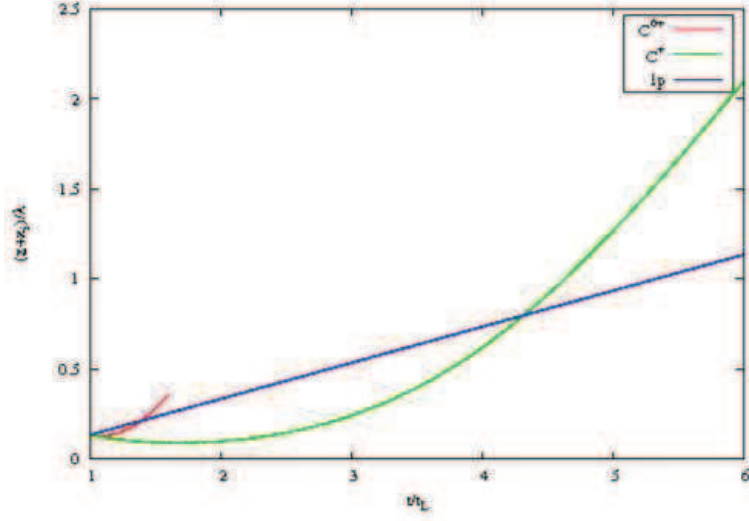


Figure 3.9: Trajectories of test ions comprising of  $C^+$  and  $C^{6+}$  with incident velocity  $v_b = -0.15c$ .  $n_0/n_c = 10$  and  $n_{h0}/n_{l0} = 1$ . Red curve is for  $C^{6+}$  and green for  $C^+$ . The blue line represent the laser piston moving with velocity  $v_f = 0.2c$ .

Thus, enhancing its kinetic energy. The double layer velocity was dependent on incident laser intensity, mass of the ion and its density. However, in case of a mixed target, i.e. a target where less massive ions are added to heavier ones, the charge separation layer moves with a higher velocity than what it would have been in case of a single species. The expression for the reflected ion velocity in the lab frame “ $v_{iL}$ ” remains the same as in [27], i.e.,

$$v_{iL} = \frac{V + v_f}{1 + Vv_f} \quad (3.48)$$

where  $V$  is the relative velocity of approach of the test ion towards the charge separation layer. But in this case as  $v_f$  is higher than that of single species for a given laser intensity and plasma density, the reflected velocity of the test ion is more as compared to what it would have been in case of single species target with same laser intensity. For a given incident laser intensity and density ratio of the ion species, there is a maximum permissible velocity of approach of the incoming test ion. This maximum velocity corresponds to the ion that gets reflected from

$z = -z_i$ . In order to determine this, we need to solve the equation of motion of the test ion inside the coulomb exploding region. The equation of motion is given by,

$$\frac{dp}{dt} = Z_b e E(z); \quad E(z) = 4\pi e (Z_l n_l(z, t) + Z_h n_h(z, t)) \quad (3.49)$$

where  $p = \gamma m_b v$  is the beam momentum with  $m_b$  as the mass of the beam species,  $v$  its velocity and  $\gamma$  its relativistic factor.  $Z_b$  is the charge on the test ion. Substituting for the densities from we obtain the equation of the trajectory of the incoming test ion as,

$$\frac{d^2 z}{dt^2} = \frac{m_l}{m_b} \frac{\omega_{pl}^2 z}{\left[1 + \frac{\omega_{pl}^2 t^2}{2} \left(1 + \frac{Z_h n_{h0}}{Z_l n_{l0}}\right)\right]} \frac{Z_b}{Z_l} \left[1 + \frac{Z_h n_h(z, t)}{Z_l n_l(z, t)}\right] \left[1 - \left(\frac{dz}{dt}\right)^2\right]^{3/2} \quad (3.50)$$

The incoming ion approaching the charge separation layer loses kinetic energy equal to  $m_b c^2 (\gamma_f - 1)$  while overshooting this layer and reaching  $z = -\delta_h$ . At this point the kinetic energy of the beam is  $m_b c^2 (\gamma - 1) = m_b c^2 (\gamma_b - \gamma_f)$ , where  $\gamma_b$  is the relativistic factor corresponding to  $v_b$ , the initial ion velocity. Hence,

$$\gamma = \gamma_b - \gamma_f + 1 \quad (3.51)$$

and,

$$v = \frac{dz}{dt} = -c \left(1 - \frac{1}{\gamma^2}\right)^{1/2} \quad (3.52)$$

This is taken to be the initial condition for solving the test ion trajectory using Eq.3.50. Fig.3.9 shows the trajectory of two test ions  $C^+$  and  $C^{6+}$  coming in with initial velocity  $v_b = -0.15$ . The straight line represents the laser piston moving with velocity  $0.2c$ ,  $n_0/n_c = 10$  and  $n_{h0}/n_{l0} = 1$ . We observe that  $C^{6+}$  is reflected before  $C^+$ . This is because the repulsive force exerted on  $C^{6+}$  is more than  $C^+$  due to excess charge present on it. Hence the maximum permissible incoming velocity is more for  $C^{6+}$  than  $C^+$ . The time of intersection of ion trajectories with that of laser piston is the time at which the test ion re-enter the ion sheath. Fig.3.10 shows the maximum permissible velocities for both  $C^{6+}$  and  $C^+$ . It can be seen that ions with greater charge can have higher incident velocities to get completely reflected. As the mass of both  $C^{6+}$  and  $C^+$  is the same, it is possible to obtain higher energy ions with increased charge states. Fig.3.11 shows the reflected ion

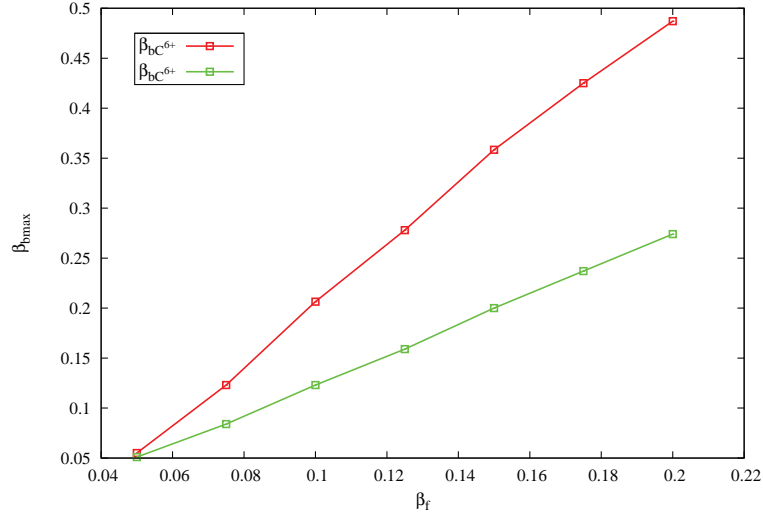


Figure 3.10: Maximum permissible incident velocities for test ion comprising of  $C^+$  and  $C^{6+}$ .  $n_{h0}/n_{l0} = 1$  and  $n_0/n_c = 10$ .

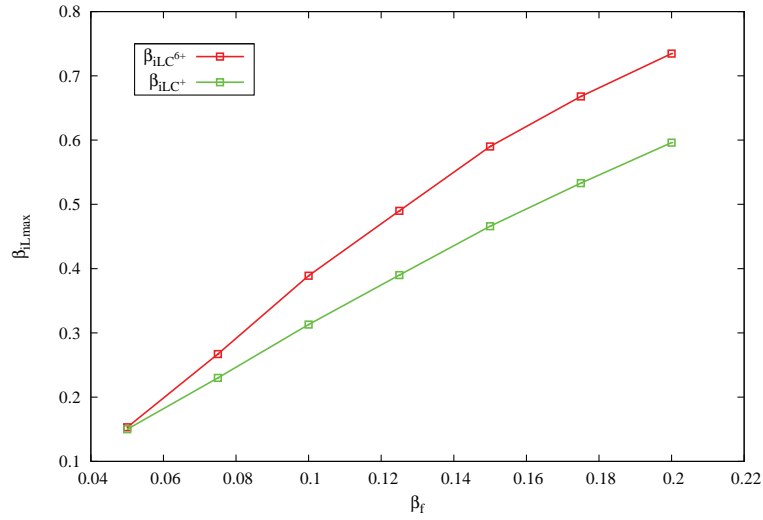


Figure 3.11: Reflected ion velocities corresponding to maximum permissible incident velocity for  $C^+$  and  $C^{6+}$ .  $n_{h0}/n_{l0} = 1$  and  $n_0/n_c = 10$ .

velocities corresponding to their maximum permissible velocity.

### 3.7 Conclusions

In this chapter, we have presented a complete analytical model for the ion charge separation region and the electron sheath created due to the ponderomotive force of the incident laser for a two ion species target. It was found that the lighter and heavier ions got reflected from different positions. From this, we discover that the laser piston in case of two ion species comprises of an electron sheath and two ion sheaths separated by a distance. The ion sheath close to the electron sheath comprises of both the ion species, the lighter ones are reflected from the other boundary of this sheath and the heavier ones overshooting this region. The heavier ions move further forming another sheath of primarily the heavier ion species before getting reflected at the point where the density blows up. The separation between the density peaks of these two sheaths decreases with increased proportion of number of heavy ions. Also, as there is ion density jump at two points, we observe a kink in the electrostatic field profile responsible for ion acceleration. In the coulomb exploding ion region, though the density goes down uniformly in time, it has been observed that the heavy ion species depletes slowly than the lighter ions. Also, the rate of depletion of ion density in this region increases with higher ion charge.

The description of the laser piston throws light on the thickness and mass of the ion sheath responsible for acceleration. As the acceleration gradient is determined by the radiation pressure exerted by the laser, the information for the ion sheath thickness and mass proves helpful in the stability analysis of the laser piston. Rayleigh Taylor instability plays an important role here. With time this instability grows making the laser piston porous to the incident light. At this point the ions ceases to accelerate. Analysis of the piston shows that RTI gets suppressed for targets where the proportion of heavy species is more. Also, with increase in incident laser intensity the cusp formation time goes down but at a slower rate showing nearly an asymptotic behavior at higher intensities.

The coulomb exploding ion charge region serves as a velocity amplifier for incoming ions. The maximum permissible velocity for these ions for a given laser and plasma

Chapter 3. Self consistent model for ponderomotive ion acceleration of laser  
irradiated two species dense target plasmas

parameters have been found to depend on the charge state of the beam species.  
Higher the charge on the ions, higher is the maximum permissible velocity.

# Bibliography

- [1] Yin L., Albright B. J., Hegelich B. M. and Fernandez J. C., *Laser and Particle Beams* 24, 291 (2006).
- [2] Xiaomei Zhang, Baifei Shen, Xuemei Li, Zhangying Jin, Fengchao Wang and Meng Wen, *Phys. Plasmas* 14, 123108 (2007)
- [3] Hegelich B. M., Albright B. J., Cobble J., Flippo K., Letzring S., Paffett M., Ruhl H., Schreiber J., Schulze R. K. and Fernández J. C., *Nature* 439, 441 (2006).
- [4] Ledingham K. J., *Phys. D* 37, 2341 (2004).
- [5] Kodama R., *Nature* 412, 2341 (2004).
- [6] Roth M., *Phys. Rev. Lett.* 86, 436 (2001).
- [7] Temporal M., Honrubia J. J. and Atzeni S., *Phys. Plasmas* 9, 3098 (2002).
- [8] N. Naumova, T. Schlegel, V. T. Tikhonchuk, C. Labaune, I. V. Sokolov and G. Mourou, *Phys. Rev. Lett.* 102,025002(2009).
- [9] P. Mora, *Phys. Rev. Lett.* 90,185002 (2003).
- [10] V. Yu. Bychenkov, V. N. Novikov, D. Batani, V. T. Tikhonchuk, and S. G. Bochkarev, *Phys. Plasmas* 11, 3242 (2004), DOI:10.1063/1.1738649.
- [11] S. C. Wilks, A. B. Langdon, T. E. Cowan, M. Roth, M. Singh, S. Hatchett, M. H. Key, D. Pennington, A. MacKinnon, and R. A. Snavely, *Phys. Plasmas* 8, 542 (2001), DOI:10.1063/1.1333697.
- [12] Y. Sentoku, T. E. Cowan, A. Kemp, and H. Ruhl, *Phys. Plasmas* 10, 2009 (2003), DOI:10.1063/1.1556298.
- [13] A. J. Kemp and H. Ruhl, *Phys. Plasmas* 12, 033105 (2005), DOI:10.1063/1.1856933.
- [14] Yan X. Q., Lin C., Sheng Z. M., Guo Z. Y., Liu B. C., Lu Y. R., Fang J. X. and Chen J. E., *Phys. Rev. Lett.* 100, 135003 (2008).

- [15] V K Tripathi, C S Liu, X Shao, B Eliasson and R Z Sagdeev, *Plasma Physics and Controlled Fusion* 51, 024014 (2009).
- [16] Macchi, Andrea, Veghini, Silvia and Pegoraro, Francesco, *Phys. Rev. Lett.* 103, 085003 (2009).
- [17] Esirkepov T., Borghesi M., Bulanov S. V., Mourou G. and Tajima T., *Phys. Rev. Lett.* 92, 175003 (2004).
- [18] F. Pegoraro and S. V. Bulanov, *Phys. Rev. Lett.*, 99, 065002 (2007).
- [19] K. Adusumilli, D. Goyal, and V. K. Tripathi, *Phys. Plasmas* 19, 013102 (2012), DOI:10.1063/1.3671957.
- [20] Wilks S. C., Kruer W. L., Tabak M. and Langdon A. B. *Phys. Rev. Lett.* 69, 1383 (1992).
- [21] Gibbon Paul, *Phys. Rev. E* 72, 026411 (2005).
- [22] Macchi Andrea, Cattani Federica, Liseykina, Tatiana V. and Cornolti Fulvio *Phys. Rev. Lett.* 94, 165003 (2005).
- [23] Silva Luís O., Marti Michael, Davies Jonathan R., Fonseca Ricardo A., Ren Chuang, Tsung Frank S. and Mori Warren B. *Phys. Rev. Lett.* 92, 015002 (2004).
- [24] Amol R. Holkundkar and N. K. Gupta, *Phys. Plasmas* 15, 123104 (2008).
- [25] A P L Robinson, P Gibbon, M Zepf, S Kar, R G Evans and C Bellei *Plasma Physics and Controlled Fusion* 51, 024004 (2009).
- [26] T. Schlegel, N. Naumova, V. T. Tikhonchuck, C. Labaune, I. V. Sokolov and G. Mourou, *Phys. Plasmas* 16, 083103 (2009).
- [27] Ujjwal Sinha and Predhiman K Kaw, *Phys. Plasmas*, (Accepted for publication)
- [28] Ji, Liangliang and Shen, Baifei and Zhang, Xiaomei and Wang, Fengchao and Jin, Zhangyin and Li, Xuemei and Wen, Meng and Cary, John R., *Phys. Rev. Lett.*, 101, 164802 (2008).

- [29] Zhang, Xiaomei and Shen, Baifei and Ji, Liangliang and Wang, Fengchao and Jin, Zhangying and Li, Xuemei and Wen, Meng and Cary, John R., Phys. Rev. ST Accel. Beams, 12, 021301 (2009).
- [30] A P L Robinson, D-H Kwon and K Lancaster, Plasma Physics and Controlled Fusion, 51, 095006 (2009).
- [31] Edward Ott, Phys. Rev. Lett., 29, 1429 (1972).

# 4

## Analytical model for axial magnetic field generation by interaction of radially inhomogeneous laser pulse with solid target

### 4.1 Introduction

Relativistic interaction of laser pulses with plasma has long been studied where it has been shown that there is non linear coupling between plasma and electromagnetic waves [1, 2]. Arrival of laser systems capable of producing intensities higher than  $10^{20}W/cm^2$  and pulse length in the sub picosecond regime has made them an attractive choice for development of compact particle accelerators [3, 4, 5, 6]. Further studies have shown a variety of effects, one of which is generation of quasistatic magnetic (QSM) fields in plasma by laser pulses [7, 8, 9, 10, 11, 12, 13, 14, 15, 16]. This problem is of both fundamental and applied interest like particle acceleration, inertial confinement fusion, X-ray generation and radiation of pulsars [17, 18, 19]. Spontaneous magnetic fields can be generated by several mechanisms, including non-parallel density and temperature gradients [20], the ponderomotive force associated by incident laser [7, 8] and the currents of fast electrons generated during the interaction [10]. It was discussed in [21, 22] that application of a static axial magnetic field had a significant impact on the process of ion acceleration using ultra-intense lasers incident on solid targets. In these studies the source of axial

magnetic field was not discussed and it was assumed that the magnetic fields required were either self generated or externally applied. The magnetic fields required for such studies were of the order of 100MG. It was shown in [7, 8] that linearly polarized ultra-intense lasers can drive axial currents that can generate azimuthal magnetic field close to 1 Gegagauss. In studies by [13, 14, 15, 16] it was shown that circularly polarized lasers can drive azimuthal currents that in turn generates an axial magnetic field. Further, it has been seen that circularly polarized light inherently induce a magnetization in the plasma via inverse Faraday effect (IFE) when transverse effects are taken into account [13, 23, 24]. This magnetization leads to an additional axial magnetic field. Together adding for both the effects i.e. azimuthal current and magnetization current gives a net axial magnetic field [13].

The studies of laser matter interaction in previous chapters have considered evolution in one spatial dimension, which inherently assumed uniform transverse distribution of laser intensity and ponderomotive force exerted by them. However, in real scenario the laser pulse has a finite cross section and transverse intensity profile. We have seen in earlier studies [22, 25, 26] that the laser ponderomotive force stuffed plasma electrons in front of it leading to an electron density spike and formation of an electron sheath in which electron density decreased axially. However because of one-dimensional treatment it was assumed that this density was uniform along transverse direction. When an azimuthally symmetric circularly polarized laser beam of finite cross section is normally incident on an overdense plasma, it exerts a non uniform ponderomotive force radially. As a result different segments of the electron sheath are pushed inside the plasma upto varying distances. Also the peak of the electron density spike in front of the laser pulse varies as we move out radially. This induces radial inhomogeneity in electron density. For a laser pulse with radially decreasing intensity, the extent upto which electron sheath is pushed inside the plasma reduces as we move radially outwards. This leads to formation of a cavity region behind the electron sheath [16].

In the study by Sheng and Meyer-ter-Vehn [13], the laser intensity and plasma electron density profile was chosen arbitrarily. Besides this only the radial profile of the magnetic field was described. In another study by Cai et. al [16] the contribution due to magnetization current was not taken into account as well as there was no algebraic expression given for the magnetic field generated. Further,

ion acceleration due to induced charge separation field was neglected in both the studies. In this chapter, we present a self-consistent analytical model for generation of axial magnetic field by interaction of a radially inhomogeneous circularly polarized laser pulse with a solid target. In our model, the laser fields and electron density in the electron sheath are determined self consistently using the incident laser pulse profile and initial plasma density. The motion of plasma ions under the influence of charge separation field has also been taken into account. Because of a radial dependence of laser intensity the ponderomotive force varies radially because of which the electron density with in the sheath becomes radially inhomogeneous as opposed to one-dimensional studies described in previous chapters. This radial inhomogeneity introduces an azimuthal current in the sheath, which in turn produces an axial magnetic field. Further, because of circular polarization the plasma electrons produce circular motion under the influence of laser field. This circular motion mimics a current loop and hence induces a magnetic moment. Adding up the magnetic moments of all the electrons in the sheath gives rise to a net magnetization in the plasma which in turn gives a magnetization current. The magnetization and azimuthal currents are roughly of the same order of magnitude and hence to provide an accurate description both of them should to be taken into account. Also the axial profile of the magnetic field that exists with in the electron sheath has been described.

This chapter is organized as follows. In the next section we present the basic equations governing the plasma dynamics and the laser fields inside the plasma. Using them the electron density and laser field profiles in the sheath is determined. Next we analyze the extent upto which the electrons are ponderomotively pushed inside and hence analyze the formation of density cavitation. In the fourth section we understand the axial magnetic field generation and derive a complete analytical expression for axial magnetic field for a transverse gaussian incident laser field. Finally the conclusions of the study is presented.

## 4.2 Laser fields in the electron sheath

We consider a cylindrical plasma column in the region  $0 < z < L$ . A radially inhomogeneous circularly polarized ultra-intense laser is incident on the plasma

Chapter 4. Analytical model for axial magnetic field generation by interaction of radially inhomogeneous laser pulse with solid target

from  $0 > z$  side. The incident and reflected electric field vectors of the laser pulse can be written as,

$$\vec{E}_i = (\hat{e}_r + i\alpha\hat{e}_\theta)E_0(r)\exp[-i(\omega t - kz)] \quad (4.1)$$

$$\vec{E}_r = (\hat{e}_r + i\alpha\hat{e}_\theta)RE_0(r)\exp[-i(\omega t + kz)] \quad (4.2)$$

where  $E_0(r)$  is the electric field amplitude which varies radially,  $R$  is the reflection coefficient and  $\alpha = 1$  for circular and 0 for linear polarization. The plasma electrons are pushed inside via ponderomotive force to form an electron sheath leaving behind an ion space charge such that the electron plasma boundary shifts from  $z = 0$  to  $z = \Delta(r)$ . For a laser pulse with radially decreasing intensity, the radiation pressure also decreases as  $r$  increases. Because of this the electron plasma boundary is pushed to varying distances inside the plasma as we move along  $r$ . As the ions do not respond to the laser fields, the ion space charge region can be treated as vacuum. Thus  $z = \Delta(r)$  is the vacuum plasma interface at a given  $r$ . Inside the electron sheath, the laser fields are evanescent and can be written as,

$$\vec{E}_T = (\hat{e}_r + i\alpha\hat{e}_\theta)E_T(r, z)\exp[-i(\omega t)], \quad \vec{B}_T = \frac{c}{i\omega}\nabla \times \vec{E}_T \quad (4.3)$$

The momentum equation of the plasma electrons in the sheath under the influence evanescent laser fields can be written as,

$$\frac{d\vec{p}}{dt} = -e\vec{E}_T - \frac{e}{c}(\vec{v} \times \vec{B}_T) \quad (4.4)$$

where  $\vec{p}$  is the electron momentum. Taking transverse component of the above equation, the quiver velocity of the electrons can be written as,

$$\vec{v}_\perp = (\hat{e}_r + i\alpha\hat{e}_\theta)\frac{a_T(r, z)c}{i\gamma_e}\exp[-i\omega t] \quad (4.5)$$

where  $a_T = eE_T(r, z)/m_e\omega c$  is the dimensionless evanescent laser amplitude and  $\gamma_e = (1 + p_\parallel^2/m_e^2c^2 + p_\perp^2/m_e^2c^2)^{1/2}$  is the electron relativistic factor. Usually  $p_\perp \gg p_\parallel$  where  $p_\perp = \gamma_e m_e v_\perp$ . Substituting for  $v_\perp$  from Eq. 4.5, the electron relativistic factor  $\gamma_e = (1 + a_T(r, z)^2)^{1/2}$ . The charge separation induces a longitudinal electric field which in turn induces a longitudinal velocity to the ions. To maintain the

Chapter 4. Analytical model for axial magnetic field generation by interaction of radially inhomogeneous laser pulse with solid target

charge separation, the electron sheath moves with a constant velocity. As discussed earlier, because of radially decreasing ponderomotive force the charge separation distance decreases with  $r$ . As a result, the induced longitudinal electric field also decreases radially. Hence, the ions at different radial locations are accelerated to different velocities. Because if this different surface elements of the electron sheath move through the plasma with different velocities. To analyze this the sheath can be divided into different segments radially. Each segment moves with constant velocity  $v_f(r)$ . In the frame moving with a segment of electron sheath, the ions within the sheath consists of two opposite directed streams. Thus, from the conservation of particle flux, the ion density in the sheath can be written as,

$$n_i(r) = 2n_0\gamma_f(r) \frac{\beta_f(r)}{\beta_{iz}(r)} \quad (4.6)$$

with  $\beta_f(r) = v_f(r)/c$  and  $\beta_{iz} = v_{iz}(r)/c$  where  $v_{iz}(r)$  is the longitudinal ion velocity at a given  $r$ . To calculate  $\beta_f$ , we recollect the momentum conservation equation in the frame of the moving electron sheath given by,

$$\frac{2I_0(r)}{c^3} \frac{1 - \beta_f}{1 + \beta_f} = 2\gamma_f^2 m_i n_0 \beta_f^2(r) \quad (4.7)$$

Algebraically solving this equation, we arrive at the expression for  $\beta_f(r)$  as,

$$\beta_f(r) = \frac{\sqrt{a_0^2(r)\mu/n_0}}{1 + \sqrt{a_0^2(r)\mu/n_0}} \quad (4.8)$$

where  $a_0(r) = eE_0(r)/m_e\omega c$  with  $m_e$  as the electron mass and  $\omega$  is the incident laser frequency.  $\mu = m_e/m_i$  i.e. the electron to ion mass ratio and  $n_0$  is the initial plasma density normalized to the critical density  $n_c = m_e\omega^2/4\pi e^2$ . Thus, for a given plasma target the velocity of the electron sheath in the lab frame can be determined by the incident laser amplitude. Assuming azimuthal symmetry and taking ion density in the sheath as given by Eq. 4.6, the Poisson's equation takes the form,

$$\frac{1}{r} \frac{\partial}{\partial r} \left( r \frac{\partial \gamma_e}{\partial r} \right) + \frac{\partial^2 \gamma_e}{\partial z^2} = \frac{\omega_{p0}^2}{c^2} \left[ \frac{n_e(r, z)}{n_0} - 2\gamma_f \beta_f \frac{\gamma_i}{\sqrt{\gamma_i^2 - 1}} \right] \quad (4.9)$$

Chapter 4. Analytical model for axial magnetic field generation by interaction of radially inhomogeneous laser pulse with solid target

Now, for the laser fields inside the sheath, the evanescent amplitude can be written as  $a_T(r, z) = a_T(r, z)\theta(r)$ , where  $\Theta(r)$  is the function determining the radial field profile.  $\Theta(r) = \exp[-r^2/\sigma^2]$  for Gaussian laser intensity with spot size  $\sigma$ . Here  $a_T(r, z)$  is a slowly varying function of  $r$  as compared to  $\Theta(r)$ . Hence  $\partial(a_T\Theta)/\partial r \approx a_T\partial(\Theta)/\partial r$ . A similar approximation has been made in [16, 27, 28]. Therefore the electron relativistic factor  $\gamma_e = \sqrt{1 + a_T^2(z)\Theta^2(r)}$ . In the sheath region, as the ions and electrons are moving under the same electrostatic field, the relationship between their relativistic factors can be written as,

$$\gamma_i(r, z) = \gamma_f(r) - \mu(\gamma_e(r, z) - \gamma_f(r, z)) \quad (4.10)$$

This equation gives the dependence of  $\gamma_i$  on evanescent laser field via  $\gamma_e$ . To account for the evanescent laser field inside the electron sheath, we need to take into account the wave equation governing  $a'_T$  given by,

$$\nabla^2 a'_T(r, z) = \frac{\omega^2}{c^2} \left( \frac{\omega_{pe}^2/\omega^2}{\gamma_e} - \frac{1 - \beta_f(r)}{1 + \beta_f(r)} \right) a'_T \quad (4.11)$$

where  $\omega_{pe}$  is the local electron plasma frequency at a given  $r$  and  $z$ . For a laser with Gaussian radial profile, i.e.  $\Theta(r) = \exp[-r^2/\sigma^2]$ , combining Eqs. 4.9 and 4.11 gives the local electron density with in the sheath as,

$$\begin{aligned} \frac{n_e(r, z)}{n_c} = & 2\gamma_f\beta_f \frac{\gamma_i^2\gamma_e}{\sqrt{\gamma_i^2-1}} \frac{n_0}{n_c} - \gamma_e a_0^2 \Theta^2 \left[ \frac{4}{\sigma^2} \left[ \frac{r^2}{\sigma^2} - 1 \right] - \delta \right] \\ & + \frac{\Theta^2}{\gamma_e} \left( \frac{\partial a_T}{\partial z} \right)^2 + \frac{2\gamma_e a_T^2 \Theta^2}{\sigma^2} \left[ \frac{r}{\sigma^2} \left( \frac{1+\gamma_e^2}{\gamma_e^2} \right) - 1 \right] \end{aligned} \quad (4.12)$$

where  $\delta = 1 - \beta_f(r)/1 + \beta_f(r)$ . It can be noted that for a chosen axial position  $z$ , the electron density  $n_e$  varies along  $r$ . As the electron density in the sheath is a steady function of radial position under high ponderomotive pressure, substituting for electron density in Eq. 4.11, the wave equation will have different solutions at different radial positions [16, 27, 28]. To solve this case, we divide the cross section of the laser pulse into small parts and consider the propagation of each part as a plane wave inside the sheath similar to [16, 27, 28]. The wave equation is solved backwards from the a distance  $z \gg \Delta(r)$  where the laser fields nearly vanish and by choosing a  $\beta_f$  obtained from 4.8 for a given laser pulse amplitude,

plasma density and ion mass. Upon solving Eq. 4.11, we can obtain the entire evanescent laser field profile inside the electron sheath as well as density profile can be calculated at a given  $r$ . At the boundary, i.e. at the interface of charge separation the tangential components of electric and magnetic fields should be continuous at a given  $r$  say  $r_0$ . This gives the condition,

$$\left(\frac{da_T}{dz}\right)^2 \Big|_{r_0, z=0} + \frac{\omega^2}{c^2} \frac{1 - \beta_f(r)}{1 + \beta_f(r)} a_T^2(r_0, 0) = 4 \frac{\omega^2}{c^2} \frac{1 - \beta_f(r)}{1 + \beta_f(r)} a_0^2(r_0) \quad (4.13)$$

The solutions of Eq.4.11 has to be terminated at the position where the boundary condition given by Eq. 4.13 is satisfied. The electrostatic potential  $\phi(r, z)$  inside the electron sheath is given by,

$$\phi(r, z) = \frac{m_e c^2}{e} (\gamma_e(r, z) - 1) \quad (4.14)$$

The electrostatic field  $E_{es}(r, z)$  can be determined as  $E_{es}(r, z) = -d\phi(r, z)/dz$ . At a given radial position  $r_0$ , the longitudinal electrostatic field profile in the sheath can be computed using the following expression,

$$E_{es}(r_0, z) = -\frac{m_e c^2}{e} \Theta^2(r_0) a_T(z) \frac{da_T}{dz} \quad (4.15)$$

The initial distance  $\Delta(r_0)$  upto which the electron sheath is pushed can be calculated using the expression,

$$\Delta(r_0) = \frac{E_{es}(r_0, \Delta(r_0))}{4\pi n_0 e} \quad (4.16)$$

The segment of electron sheath at the radial location  $r_0$  moves with velocity  $v_f(r_0)$ . Hence, its axial position after time  $t$  will be  $z = \Delta(r_0) + v_f(r_0)t$ . Fig. 4.1 shows the electron density profile in the sheath at radial locations  $r/\sigma = 0, 0.25, 0.5$  at times  $\omega t = 0, 10, 20$ . We can see that the peak density of the electron sheath decreases as we move radially outwards. Also, the longitudinal velocity of the segment at  $r = 0$  is maximum and decreases radially. Because of this the curvature of the electron sheath increases with time. Fig. 4.2 shows the evanescent laser fields inside the sheath at various radial locations at  $t = 0$ .

Chapter 4. Analytical model for axial magnetic field generation by interaction of radially inhomogeneous laser pulse with solid target

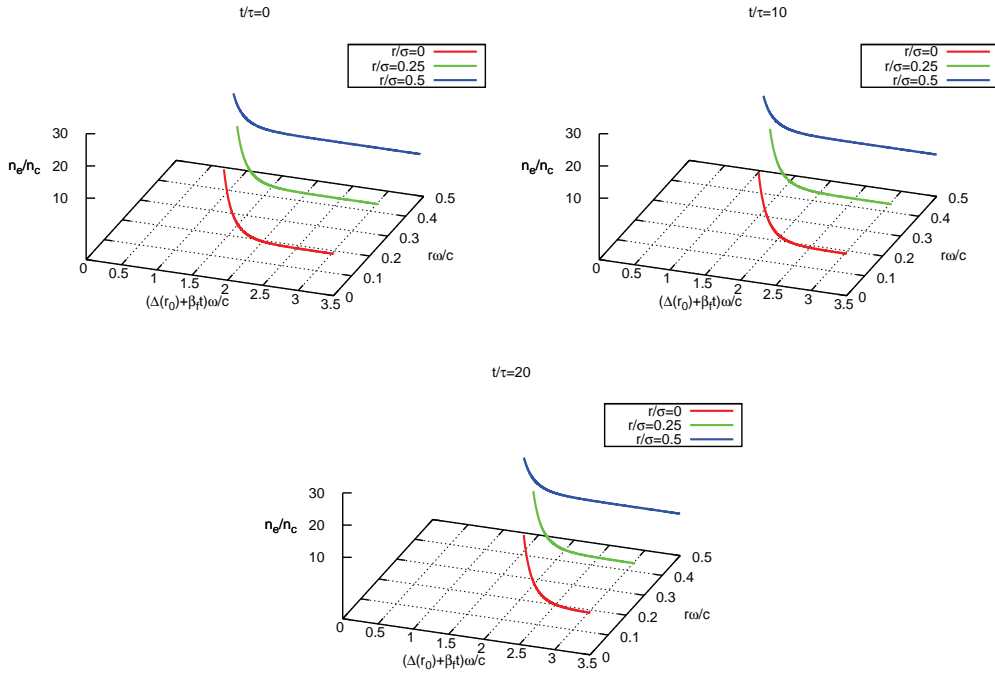


Figure 4.1: Density profiles of the electrons in the sheath at different times for  $n_0/n_c = 2$  and  $a_0 = 2$  for a gaussian laser pulse and homogeneous overdense plasma at different radial locations. The red curves represent electron density at  $r/\sigma = 0$ , green curves represent electron density at  $r/\sigma = 0.25$  and blue curves represent electron density at  $r/\sigma = 0.5$ .  $\Delta(r_0)$  is the electron displacement at  $t/\tau = 0$  at a given  $r$ .

Chapter 4. Analytical model for axial magnetic field generation by interaction of radially inhomogeneous laser pulse with solid target

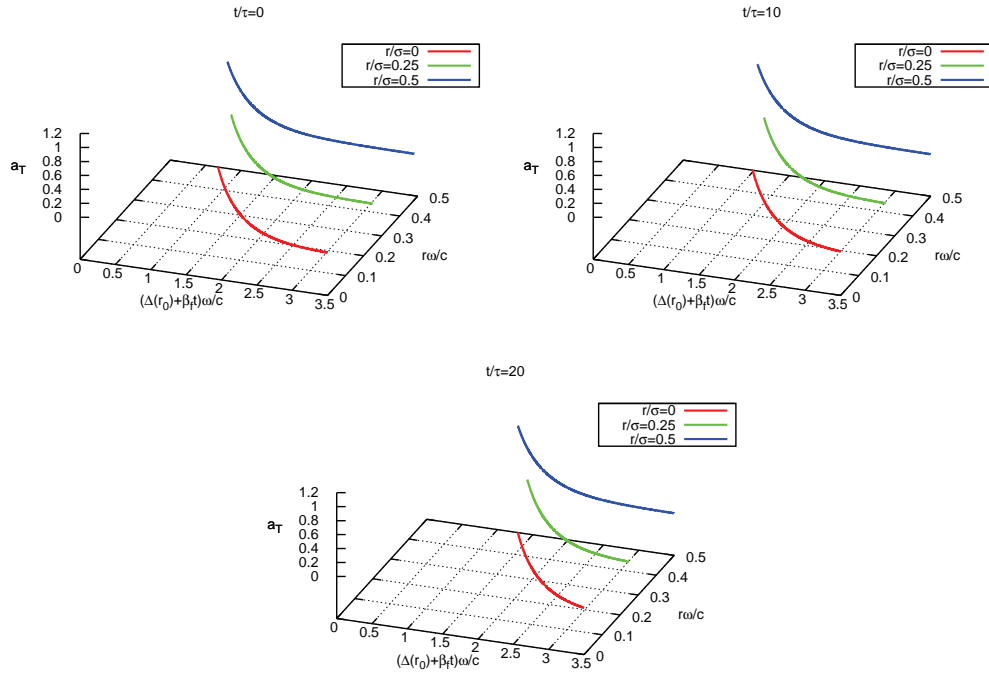


Figure 4.2: Evanescent laser field profiles in the electron sheath at different times for  $n_0/n_c = 2$  and  $a_0 = 2$  for a gaussian laser pulse and homogeneous overdense plasma at different radial locations. The red curves represent evanescent field at  $r/\sigma = 0$ , green curves represent the field at  $r/\sigma = 0.25$  and blue curves at  $r/\sigma = 0.5$ .  $\Delta(r_0)$  is the electron displacement at  $t/\tau = 0$  at a given  $r$ .

### 4.3 Magnetic field generation

Using the fluid treatment for electrons in the sheath, we introduce a small density perturbation such that  $n_e(r, z) = n_{e0}(r, z) + n$ , where  $n_{e0}(r, z)$  is the equilibrium electron density in the steady state and  $n$  is the density perturbation at fundamental frequency. From the equation of continuity, we find the density perturbation of electrons to be,

$$n = -\frac{i}{\omega} \nabla \cdot (n_e \mathbf{v}_\perp) \quad (4.17)$$

Substituting for  $v_\perp$  from Eq. 4.5 in Eq. 4.17, we can obtain the perturbed density. We notice from the previous section that electron cavitation is formed when a relativistic laser pulse irradiates a plasma. Therefore the electron density in the sheath have gradients both in the axial and radial directions to the laser propagation. The laser field oscillates in the transverse direction, which for circular polarization makes is plasma electrons trace helical path. Thus, a slowly varying current  $\mathbf{J}_\theta$  is generated which can be calculated using the expression  $\mathbf{J}_\theta = -\langle en\mathbf{v} \rangle$ , where  $\langle \rangle$  denotes the average over one laser cycle ( $\omega^{-1}$ ). For a cylindrically symmetric incident laser beam, this current can be expressed as,

$$\mathbf{J}_\theta = \frac{\alpha e a_T^2 \Theta c^2}{\gamma_e \omega} \frac{\partial}{\partial r} \left( \frac{n_e}{\gamma_e} \right) \hat{e}_\theta \quad (4.18)$$

From Eq. 4.18 it is clear that inhomogeneity in electron density drives an azimuthal current in the plasma. From Eq. 4.13 it is clear that when a radially inhomogeneous laser pulse is normally incident on a homogeneous plasma it induces a radial inhomogeneity in electron density. Thus, such laser pulses can drive azimuthal currents which can act as source for axial magnetic field.

Next we look into the motion of plasma electrons under the influence of laser fields. In the field of a circularly polarized laser these electrons produce circular motion. Thus, each electron mimics a current loop and hence with each electron is associated a magnetic dipole moment  $\mathbf{m} = -e/2c \langle \mathbf{r}_0 \times \mathbf{v}_\perp \rangle$  where  $\mathbf{r}_0$  is the orbit radius. This when summed over entire electron sheath generates a plasma magnetization  $\mathbf{M}$ .

$$\mathbf{M} = -\frac{\alpha n_e a_T^2 \theta^2 c}{\gamma_e^2 \omega} \hat{e}_z \quad (4.19)$$

Chapter 4. Analytical model for axial magnetic field generation by interaction of radially inhomogeneous laser pulse with solid target

Hence in the steady state, the total magnetic field  $\mathbf{B}_s$  can be calculated from,

$$\nabla \times \mathbf{B}_s = \frac{4\pi}{c} \mathbf{J}_\theta + 4\pi \nabla \times \mathbf{M} \quad (4.20)$$

In cylindrical geometry with no externally applied magnetic field and under the assumption that axial magnetic field vanishes at infinite radius, Stokes theorem gives,

$$\frac{\omega_c}{\omega} = -\alpha \left[ \frac{a_T^2 \Theta^2 n_e}{\gamma_e} - \int_r^\infty \frac{a_T^2 \Theta^2}{\gamma_e} \frac{d}{dr} \left( \frac{n_e}{\gamma_e} \right) dr \right] \quad (4.21)$$

where  $\omega_c = eB_s/m_e c$ . From Eq. 4.21 it is clear that axial magnetic field generation is attributed to circular polarization of incident laser as  $\alpha = 0$  for linearly polarized laser light and hence there is no azimuthal and magnetization current in this case. An algebraic expression for the magnetic field can be calculated directly from Eq. 4.21 by choosing a radial intensity profile  $\Theta$  for the incident laser. For  $\Theta = \exp(-r^2/\sigma)$  the integral in Eq. 4.21 can be solved. This region covers for most of the spot size. Substituting for electron density from Eq. 4.13 in Eq. 4.21, we get the expression for magnetic field as,

$$\begin{aligned} \frac{\omega_c}{\omega} = & \alpha \left( -4\gamma_f n_0 [2\ln\gamma_e - a_T^2 \Theta^2] + \frac{8a_T^2}{\sigma^2} [\gamma_e(\sigma^2 + r^2) - 1] - \right. \\ & \frac{\sigma^2 \gamma_e \ln[\gamma_e - 1]}{\Theta^2} - 4 \frac{a_T^2}{\sqrt{1 + a_T^2}} \left[ \frac{2}{\sigma^4} + \delta \right] \left[ \psi_1 + \frac{a_T^2 \psi_2}{\sigma^2(1 + a_T^2)} + \frac{a_T^2}{\sigma^4} \frac{a_T^2 - 2}{(1 + a_T^2)^2} \psi_3 \right. \\ & 2 \left( \frac{\partial a_T}{\partial z} \right)^2 \left[ a_T^2 \left[ \frac{1}{\gamma_e^3} - 1 \right] - \left[ \frac{1}{\gamma_e} - 1 \right] \right] + \frac{2}{\sigma^2} (\gamma_e - 1) \left[ 1 - \frac{2a_T^2}{\sigma^2} \right] \\ & \left. + \frac{4a_T^2}{(1 + a_T^2)^{5/2}} \left[ \xi_1 + \frac{5a_T^2}{\sigma^2(1 + a_T^2)} \xi_2 + \frac{5a_T^2(5a_T^2 - 2)}{2\sigma^4(1 + a_T^2)^2} \xi_3 \right] - \frac{a_T^2 \Theta^2 n_e}{\gamma_e^2} \right) \end{aligned} \quad (4.22)$$

where,

$$\begin{aligned} \psi_1 &= \frac{\sigma^2}{2^4} [\sigma \sqrt{2\pi} [1 - \text{Erf}(\sqrt{2}r/\sigma)] + 4r\Theta^2] \\ \psi_2 &= \frac{\sigma^2}{2^6} [3\sigma^3 \sigma \sqrt{2\pi} [1 - \text{Erf}(\sqrt{2}r/\sigma)] + 4r\Theta^2 (3\sigma^2 + 4r^2)] \\ \psi_3 &= \frac{\sigma^2}{2^8} [15\sigma^5 \sigma \sqrt{2\pi} [1 - \text{Erf}(\sqrt{2}r/\sigma)] + 4r\Theta^2 (15\sigma^2 + 20\sigma^2 r^2 + 16r^4)] \end{aligned} \quad (4.23)$$

Chapter 4. Analytical model for axial magnetic field generation by interaction of radially inhomogeneous laser pulse with solid target

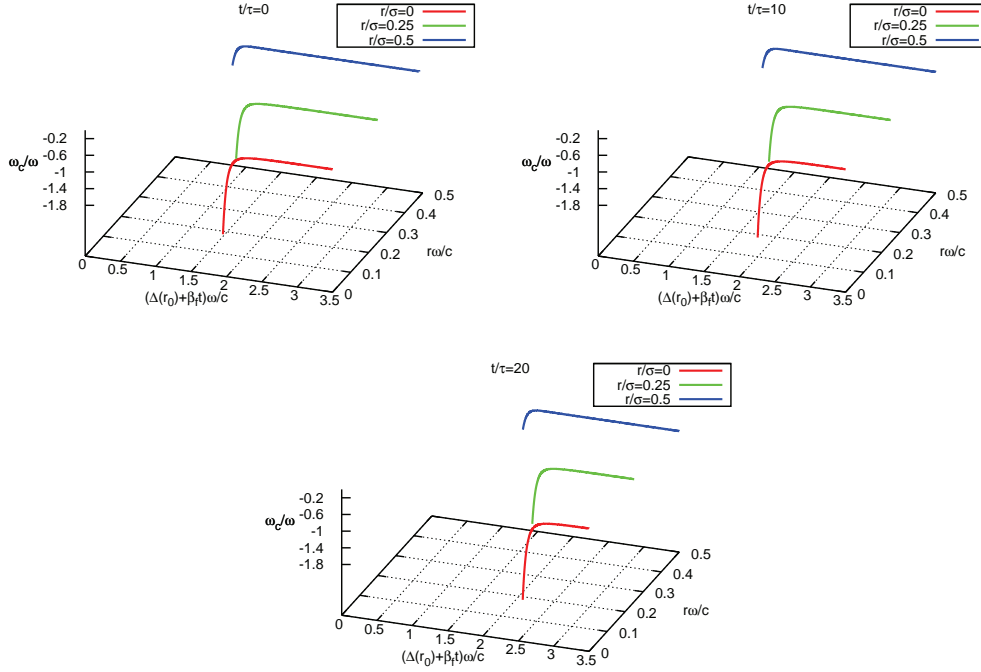


Figure 4.3: Normalized axial magnetic field profiles in the electron sheath at different times for  $n_0/n_c = 2$  and  $a_0 = 2$  for a gaussian laser pulse and homogeneous overdense plasma at different radial locations. The red curves represent axial magnetic field at  $r/\sigma = 0$ , green curves the field at  $r/\sigma = 0.25$  and blue curves at  $r/\sigma = 0.5$ .  $\Delta(r_0)$  is the electron displacement at  $t/\tau = 0$  at a given  $r$ .

and,

$$\begin{aligned}
 \xi_1 &= \frac{\sigma^2}{2^5} [\sigma\sqrt{2\pi}[1 - \text{Erf}(\sqrt{2}r/\sigma)] + 4r\theta^4] \\
 \xi_2 &= \frac{\sigma^2}{2^8} [3\sigma^3\sqrt{\pi}[1 - \text{Erf}(2r/\sigma)]] \\
 \xi_3 &= \frac{\sigma^2}{2^{11}} [15\sigma^5\sqrt{\pi}[1 - \text{Erf}(2r/\sigma)] + 4r\theta^2[15\sigma^4 + 40\sigma^2r^2 + 64r^4]]
 \end{aligned} \tag{4.24}$$

We observe that the magnetic field generated is dependent on the evanescent laser field profile. Self consistently the axial profile of the induced magnetic field can be calculated at a given radial location by simultaneously solving Eqs. 4.11 and 4.23. Solving for the magnetic field at different radial position gives entire

to dimensional picture. Fig. 4.3 shows the axial profile of normalized magnetic field at radial position  $r/\sigma = 0, 0.25, 0.5$  for  $a_0 = 2$  and  $n_0 = 2n_c$ . We observe that the peak value of magnetic field is at the interface and decreases with  $z$ . The magnetic field is present only in the electron sheath and goes to zero towards the region of undisturbed plasma. Also the peak value diminishes as we move radially outwards. We see that with self consistent electron density modification by a radially inhomogeneous laser pulse, magnetic fields close to 100 MG can be generated for  $a_0 = 2$  and laser wavelength  $\lambda = 1\mu m$ . These values are comparable to that mentioned in [7, 8, 9, 13].

## 4.4 Conclusions

In this chapter, we have presented a theory for axial magnetic field generation via interaction of radially inhomogeneous laser field with overdense plasma targets. The interaction of a radially inhomogeneous circularly polarized laser pulse on an overdense plasma produces an electron sheath on the target surface. The electron density in the sheath varies along  $r$ . This electron density and the evanescent laser fields is determined self consistently from the incident laser and initial plasma parameters. This allows us to calculate the magnetic field in plasma for a given laser and plasma parameters. It is seen that ultra-intense quasi static axial magnetic fields are produced during this process. It is found that the magnetic field persists only in the electron sheath and peaks at the interface of charge separation and falls to zero towards the undisturbed plasma region. Also for a laser pulse with radially decreasing intensity the magnetic field is maximum at the center and decreases as we move radially outwards. The effect of charge separation field has also been taken into account, which accelerates the plasma ions. Because of this the electron sheath moves through the undisturbed plasma. As the radiation pressure varies along  $r$ , the propagation velocity of different radial elements of the electron sheath varies along the radius. The central sheath element moves at the maximum velocity and this velocity decreases as we move along  $r$ . Because of this there is a formation of an electron cavity region.

We observe that the axial magnetic field is attributed to azimuthal plasma currents generated due to electron density inhomogeneity as well as magnetization

current due to induced magnetic dipole moment of the plasma electrons. Both these components are comparable in magnitude and hence should be taken into account. In earlier studies by Sheng and Meyer-ter-Vehn [13] the axial magnetic field was calculated with predetermined electron density profile. In our study, the electron density is determined by the plasma parameters and incident laser pulse. In the study by Cai. et. al. [16] they had neglected the magnetization current. Also they did not give any expression for  $B_z$ . In this work we have successfully derived an expression for  $B_z$ . The calculations yield good results for low intensity lasers. For high intensity we will have to include electron cyclotron frequency in the relativistic factor which is beyond the scope of present analysis.

# Bibliography

- [1] A. I. Akhiezer and R. V. Polovin, *Sov. Phys. JETP* **3**, 696 (1956).
- [2] John Dawson, *Phys. Rev. Lett.* **113**, 383 (1959).
- [3] T. Tajima, J. Dawson, *Phys. Rev. Lett.* **43**, 267 (1979).
- [4] S. P. D. Mangles, C. D. Murphy, Z. Najmudin et al., *Nature (London)* **431**, 535 (2004).
- [5] C. G. R. Geddes, Cs. Toth, J. van Tilborg et al., *Nature (London)* **431**, 538 (2004).
- [6] J. Faure, Y. Glinec, A. Pukhov et al., *Nature (London)* **431**, 541 (2004).
- [7] S. C. Wilks, W. L. Kruer, M. Tabak, and A. B. Langdon, *Phys. Rev. Lett.* **69**, 1383 (1992).
- [8] R. N. Sudan, *Phys. Rev. Lett.* **70**, 3075 (1993).
- [9] A. Pukhov and J. Meyer-ter-Vehn, *Phys. Rev. Lett.* **76**, 3975 (1996)
- [10] M. Tatarakis, I. Watts, F. N. Beg, E. L. Clark, A. E. Dangor, A. Gopal, M. G. Haines, P. A. Norreys, U. Wagner, M.-S. Wei, M. Zepf, and K. Krushelnick, *Nature (London)* **415**, 280 (2002)
- [11] V. I. Berezhiani, S. M. Mahajan, and N. L. Shatashvili, *Phys. Rev. E* **55**, 995 (1997).
- [12] M. Borghesi, A. J. MacKinnon, A. R. Bell, R. Gaillard, and O. Willi, *Phys. Rev. Lett.* **81**, 112 (1998).
- [13] Z. M. Sheng and J. Meyer-ter-Vehn, *Phys. Rev. E* **54**, 1833 (1996).
- [14] C. Y. Zheng, X. T. He, and S. P. Zhu, *Phys. Plasmas* **12**, 044505 (2005).
- [15] B. Qiao, S. P. Zhu, C. Y. Zheng, and X. T. He, *Phys. Plasmas* **12**, 053104 (2005).
- [16] H. Cai, W. Yu, S. Zhu, and C. Zhou, *Phys. Rev. E* **76**, 036403 (2007).

- [17] M. Tabak, J. Hammer, M. E. Glinsky, W. L. Kruer, S. C. Wilks, J. Woodworth, E. M. Campbell, and M. D. Perry, *Phys. Plasmas* **1**, 1626 (1994).
- [18] R. Kodama et al., *Nature (London)* **412**, 798 (2001).
- [19] P. Goldreich and W. H. Julian, *Astrophys. J.* **157**, 869 (1969).
- [20] J. A. Stamper, J. M. Dawson, K. Papadopoulos, R. N. Sudan, S. O. Dean, and E. A. Mclean, *Phys. Rev. Lett.* **26**, 1012 (1971)
- [21] Anamika Sharma, C. S. Liu, and V. K. Tripathi, *Physics of Plasmas* **17**, 013101 (2010).
- [22] Ujjwal Sinha and Predhiman Kaw, *Phys. Plasmas* **19**, 033102 (2012)
- [23] Karpman, V. I., and A. G. Shagalov. "The ponderomotive force of a high-frequency electromagnetic field in a cold magnetized plasma." *Journal of Plasma Physics* **27** (1982): 215-224.
- [24] Hertel, Riccardo. "Theory of the inverse Faraday effect in metals." *Journal of magnetism and magnetic materials* **303**, no. 1 (2006): L1-L4.
- [25] Ujjwal Sinha, *Physics of Plasmas* **19**, 043104 (2012)
- [26] T. Schlegel, N. Naumova, V. T. Tikhonchuck, C. Lobaune, I. V. Sokolov, and G. Mourou, *Phys. Plasmas* **16**, 083103 (2009).
- [27] S. X. Luan, Wei Yu, M. Y. Yu, G. J. Ma, Q. J. Zhang, Z. M. Sheng, and M. Murakami, *Physics of Plasmas* **18**, 042701 (2011).
- [28] Binod Kumar Pandey and V. K. Tripathi, *Phys. Scr.* **79**, 025101 (2009).

# 5

## Relativistic Theory for Multistage Ion Acceleration

### 5.1 Introduction

We have seen so far that pondermotive force of circularly polarized laser gives rise to a stable double layer on the surface of a semi-infinite overdense plasma. This double layer acts as a laser piston that moves through the plasma with constant velocity reflecting the plasma ions at rest giving rise to a nearly monoenergetic ion beam. This mode of ion acceleration is referred to as hole boring radiation pressure acceleration (HB-RPA) [1, 9, 3, 4, 5, 6, 7, 8, 9, 10]. On the other hand, there is another regime of radiation pressure acceleration called the "Light Sail" (LS) mode of acceleration [11, 12, 13, 14] which differs from HB-RPA in such a way that the thickness of the plasma target is almost of that of the laser piston. Both the acceleration process continues till the laser pulse persists. The difference between them being that HB-RPA is a steady state process, meaning that as the laser piston moves with constant velocity through the plasma it reflects the plasma ions with the same velocity, thus increasing the number of ions in the beam obtained with time. So as long as the laser pushes the piston, the ions keep getting added to the beam. On the other hand LS-RPA is not a steady state process where the target is pushed as a whole. Here the laser acts as a propeller accelerating the target whose velocity increases with time. So in this case longer the pulse we have, higher is the energy of the obtained ions.

In case of HB-RPA we see that if the laser piston has travelled across the entire

plasma target, the entire target starts to move with velocity nearly twice that of the piston velocity. In the frame of this moving target, the plasma closely resembles its initial state. When laser falls on this moving target, the situation in the moving frame becomes similar to the initial stage as the velocity of light in vacuum is same in all reference frames. Thus the entire process can be repeated again. One such study has been presented in [15]. However, this study was limited to non-relativistic ion velocities. At high velocities, it is essential to incorporate the relativistic effects. In this chapter we recollect the analytical description of the HB-RPA process in both relativistic and non-relativistic limits. Next we give an analytical description of the second stage of ion velocity and finally verify it with 1D3V particle in cell (PIC) simulations. Also we compare the relativistic results with the non-relativistic ones described in [15] and emphasize on the importance of this analysis.

## 5.2 Non Relativistic theory of HB-RPA

### 5.2.1 First acceleration process

When a laser pulse of intensity  $I$  is normally incident on a collisionless plasma of single ion species then because of radiation pressure its surface is pushed inside the plasma. This surface moves with a constant velocity  $v_f$  (say). If we shift to the frame of this moving surface called the instantaneous rest frame (IRF) we observe the plasma ions which were at rest in the lab frame approaching the plasma surface with velocity  $-v_f$ . In a steady state situation the total number of ions at the surface must not change. Hence, for the conservation of particle number we must have an ion beam moving out of the surface with velocity  $v_f$ . Thus momentum balance in the IRF gives the relation,

$$\frac{2I}{c} = 2m_i n_i v_f^2 \quad (5.1)$$

where  $m_i$  is the ion mass and  $n_i$  is the initial plasma ion density. Rearranging Eq. 5.1 we can determine the surface velocity as,

$$v_f = \sqrt{\frac{I}{m_i n_i c}} \quad (5.2)$$

In the IRF, it is this velocity with which the ions move. To obtain the velocity in lab frame, we make a Galilean transformation which gives the ion velocity  $v_i = 2v_f$ . The kinetic energy of the ions can therefore be written as,

$$E = 2m_i \frac{I}{m_i n_i c} \quad (5.3)$$

It is convenient to relate the laser intensity to the dimensionless field amplitude  $a_0$  as  $I = \alpha a_0^2 n_c m_e c^3$ . Here  $\alpha = 1$  in case of circular polarization and  $\alpha = 1/2$  for linear polarization,  $m_e$  is the electron mass,  $n_c = m_e \omega^2 / 4\pi e^2$  is the critical density. For a plasma with ion species of atomic number  $Z$ , atomic mass  $A$  and ion mass  $m_p$ , the ion velocity turns out to be as in [3, 5, 8]

$$\frac{v_i}{c} = 2 \sqrt{\frac{Z m_e n_c}{A m_p n_e} a_0} \quad (5.4)$$

where  $n_e$  is the initial electron density. All the initially undisturbed ions are reflected by the large electric potential at the surface arising due to local charge separation induced by the laser pulse. The surface is steady as there is no  $\mathbf{J} \times \mathbf{B}$  heating mechanism to interact with the ions. In the present situation the light pressure overwhelms the electron thermal pressure.

### 5.2.2 Second acceleration process

After the first acceleration stage we end up with the generation of a quasi-monoenergetic ion beam. The entire plasma target becomes a slab moving with velocity  $v_i = 2v_f$ . From relativity we know that the velocity of light in vacuum is the same in all frames of reference. Hence, if the laser pulse is long enough such that even after the entire plasma slab is accelerated it continues to push it, then it is possible to begin a second stage of acceleration. As the entire slab is moving with a constant velocity, we can move into its reference frame where we again have a stationary target with a laser pulse incident on it. In this reference frame, the ions will acquire the same velocity  $v_i = 2v_f$ . Upon Galilean transformation back to the lab frame, the ion velocity turns out to be twice that of the first stage of acceleration i.e  $v_i = 4v_f$  or the kinetic energy gets enhanced by a factor of four. These results were shown by zhang et. al [3] using 1D3V particle in cell simulations. But the laser

intensities used could generate non relativistic ion velocities. If higher intensities are used such that the ions become relativistic, a fully relativistic formulation of this problem is necessary. We present such an analysis in the coming sections.

## 5.3 Relativistic theory of HB-RPA

### 5.3.1 First Acceleration Process

In order to incorporate relativistic effects in the theory presented above, two things are to be considered. First, the light intensity in the IRF is not equal to that in the lab frame. From the analysis presented in [16], we see that light reflected from a surface moving with velocity  $v_f$  is Doppler shifted. Considering this effect together with the conservation of photon number, the light intensity in the IRF can be shown as,

$$\frac{I_{IRF}}{I} = \frac{1 - v_f/c}{1 + v_f/c} \quad (5.5)$$

Second thing that we need to consider is the relativistic density modification as in the IRF the entire plasma appears to drift with velocity  $v_f$ . For a plasma of initial ion density  $n_i$  in the lab frame, the density in the IRF will be  $\gamma_f n_i$  where  $\gamma_f = 1/\sqrt{1 - v_f^2/c^2}$ . After recognizing these modifications we can proceed to write down the relativistic momentum balance equation in the IRF as,

$$\frac{2I}{c} \left( \frac{1 - v_f/c}{1 + v_f/c} \right) = 2\gamma_f^2 m_i n_i v_f^2 \quad (5.6)$$

Eq. 5.6 can be rearranged to a quadratic equation in  $v_f$ . Choosing a dimensionless variable  $\beta_f = v_f/c$  and  $\Xi = I/m_i n_i c^3$ , the dimensionless quadratic equation in  $\beta_f$  is,

$$(\Xi - 1)\beta_f^2 - 2\Xi\beta_f + \Xi = 0 \quad (5.7)$$

Solving for the root of Eq. 5.7, the plasma surface velocity turns out to be,

$$\beta_f = \frac{\sqrt{\Xi}}{1 + \sqrt{\Xi}} \quad (5.8)$$

Recalling the condition of conservation of particle flux, Eq. 5.8 also represents the ion beam velocity in the IRF. To obtain the ion velocity  $v_i$  in the lab frame we make a Lorentz transformation which gives,

$$\frac{v_i}{c} = \frac{2\beta_f}{1 + \beta_f^2} \quad (5.9)$$

Consequently the ion kinetic energy  $\epsilon$  can be calculated using the formula  $\epsilon = m_i c^2 (1/\sqrt{1 - v_i^2/c^2} - 1)$ , where  $v_i$  can be substituted from Eq. 5.9 to give,

$$\epsilon = m_i c^2 \left[ \frac{1 + \beta_f^2}{1 - \beta_f^2} - 1 \right] \quad (5.10)$$

### 5.3.2 Second Acceleration Process

In section 5.2.2 we saw that long laser pulses can initiate a second stage of acceleration. In the non relativistic limit the calculations were simple. The second stage ion velocity and the required time period to initiate a second stage could be calculated just by linear addition. However, as we have seen in section 5.3.1, the scenario changes when relativistic effects become important. The non relativistic results will not hold here and hence a fully relativistic formulation of the process must be done. To analyze this, we assume that the entire plasma slab has undergone acceleration and is moving with uniform velocity  $v_i$ . The time required to attain this is,

$$t = \frac{L}{v_f} \quad (5.11)$$

We define the lab frame as  $K$  and the frame moving with velocity  $v_i$  as  $K'$ . As seen in [16], the light intensity perceived by a moving body differs from that emitted by the source. Hence laser intensity  $I$  in frame  $K$  will become  $I' = I(1 - v_i/c)/(1 + v_i/c)$  in frame  $K'$ . With this new intensity  $I'$  the surface velocity  $v'_f$  can be calculated similarly as Eq. 5.6 which comes out to be,

$$\beta'_f = \frac{v'_f}{c} = \frac{\sqrt{\Xi'}}{1 + \sqrt{\Xi'}} \quad (5.12)$$

where  $\Xi' = I'/m_i n_i c^3$ . The ion velocity in the frame  $K'$  turns out to be,

$$\frac{v'_i}{c} = \frac{2\beta'_f}{1 + \beta'^2_f} \quad (5.13)$$

Hence the ion velocity in the lab frame after the second stage  $\beta_{i2} = v_{i2}/c$  can be obtained by relativistic velocity addition as,

$$\beta_{i2} = \frac{\beta_i + \beta'_i}{1 + \beta_i \beta'_i} \quad (5.14)$$

The total time  $t_{total}$  and number of laser wavelengths  $N$  required to push the entire plasma target to velocity  $v_{i2}$  can be given as,

$$t_{total} = t + t' \quad (5.15)$$

$$N = \frac{t_{total}}{\tau} \quad (5.16)$$

where  $t' = L/v'_f$  and  $\tau$  is the time period for one laser wavelength.

## 5.4 Comparison with PIC simulations

A set of 1D3V particle in cell (PIC) simulations were carried out using the code LPIC++ [17] to compare with the theory proposed above. In our simulation, the space and time are denoted by dimensionless quantities  $x/\lambda$  and  $t/\tau$ , respectively. Here  $\lambda$  is the laser wavelength and  $\tau$  is the time of one laser cycle ( $\tau = \lambda/c$ ). Through out the simulations we have used circular polarization of the incident laser pulse. The pulse duration is taken to be  $100\tau$  and it is assumed to have a flat top profile. The amplitude of the laser pulse is given by a dimensionless parameter  $a = eE_0/m_e\omega c$  where  $E_0$  is the laser electric field amplitude,  $e$  and  $m_e$  are the charge and mass of electron respectively and  $\omega$  is the laser frequency. Laser amplitude  $a$  is related to laser intensity as  $I = 1.37 \times 10^{18}[a^2/\lambda(\mu m)^2]W/cm^2$ . In our simulations we have used  $a = 20, 30$  for different plasma densities. The laser pulse is incident normally on the plasma surface and the direction of its propagation is taken to be the  $+vex$  axis and opposite as  $-vex$ . The ion density is always written in units of critical density  $n_c = m_e\omega^2/4\pi e^2$ . The mass of the electron  $m_e = 1$  and the ions considered here are hydrogen ions with  $m_i = 1836$ .

We use 200 cells per wavelength to model the plasma and each cell contains 100 macroparticles. If the number of macroparticles per cell will be small then the results obtained will depend on the number of macroparticles used. The stability of the results are assured by taking sufficient number of macroparticles. In our simulations we have seen that the results do not change after 70 particles per cell. So for our entire study we have chosen 100 macroparticles per cell. The number of ions corresponding to each macroparticle will depend on the chosen initial plasma density.

In this study, a circularly polarized flat laser pulse of amplitude  $a = 20$  and  $30$  is incident on a homogeneous plasma slab of thickness  $4\lambda$ . The simulation domain is of length  $35\lambda$  and the plasma is located between  $11\lambda$  and  $15\lambda$ . The origin  $x = 0$  is taken as the left boundary of the simulation domain. Once the laser enters the simulation domain, it takes  $11\tau$  to reach the plasma slab. For simplicity in comparison with analytical estimates, we take the time of interaction to be  $t = 0$ . Hence the laser pulse enters the simulation domain from the left boundary at  $t = -11\tau$ . We know that the velocity of the laser piston is given by  $\beta_f = \sqrt{\Xi}/(1 + \sqrt{\Xi})$  with  $\Xi = (Zm_en_c/Am_in_e)a^2$ . For  $a = 20$  and  $n_i = 10n_c$  the piston velocity  $\beta_f = 0.1286$ . Hence for this case the time required to accelerate all the ions of the plasma target comes out to  $t = 31\tau$ . Fig. 5.1 shows the ion density profile at at times  $t = -11\tau, 31\tau, 50\tau$  and  $70\tau$  for  $a = 20$  and  $n_i = 10n_c$ . We can see that at  $31\tau$  the tail of the ions is at  $15\lambda$  implying that the laser piston has traversed the entire plasma slab accelerating all the ions. Also the velocity of ions in the lab frame after the first stage can be calculated from Eq. 5.9 as  $\beta_i = 0.253$ . In the frame moving with velocity  $\beta_i$ , the incident intensity is given by  $I' = I(1 - v_i/c)/(1 + v_i/c)$ . Hence  $\beta'_f = 0.102$  and  $\beta'_i = 0.202$ . Upon relativistically adding  $\beta_i$  and  $\beta'_i$ , we derive the ion velocity in the lab frame after the second stage as  $\beta_{i2} = 0.43$ . The time period for the entire second stage of this process is  $t' = 39\tau$ . Hence the total time  $t_{total}$  required for all the ions to attain velocity  $\beta_{i2}$  is  $t_{total} = 70\tau$ . Fig. 5.2 shows the laser generated longitudinal electric field profile and velocity spectrum of ions at  $31\tau, 50\tau$  and  $70\tau$ . From the velocity spectrum we can see that at  $31\tau$  majority of ions attain a single velocity of  $0.248c$  resulting into a peak. Also at  $50\tau$  we can see a second peak emerging at  $0.41c$  into which all ions get dumped at  $70\tau$ . We see more and more ions are accelerated to higher velocity from  $0.248c$  to  $0.41c$ . At  $31\tau$  almost all the ions have the same velocity. By the

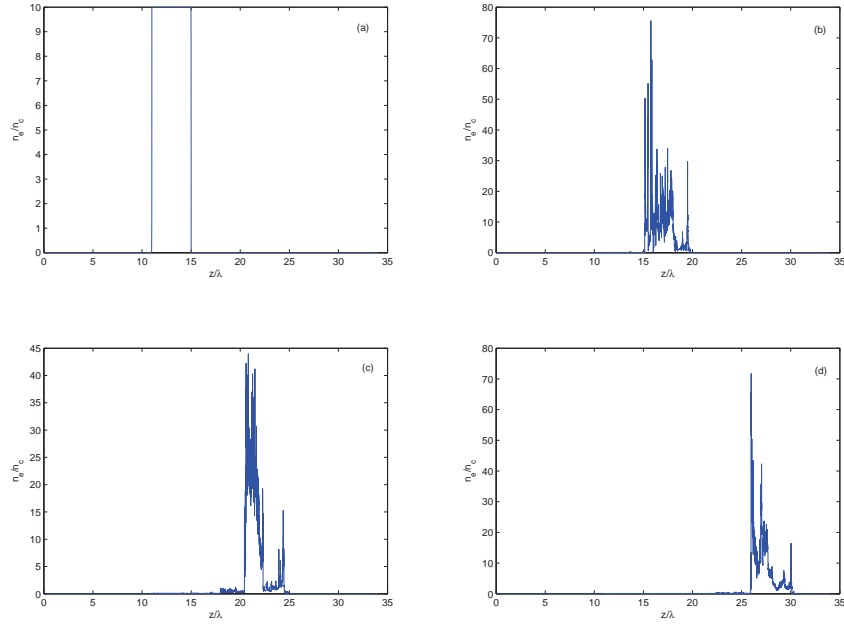


Figure 5.1: Spatial density profile of ions at different times for  $n_i = 10n_c$  and  $a_0 = 20$ . In (a) the ion density at time  $-11\tau$  is shown i.e. when the face of the laser pulse is at the extreme left of the simulation domain and the ions are undisturbed. (b) shows the ion density profile at  $31\tau$ . We can notice here that the tail of the plasma is at  $15\lambda$  hence indicating that all the ions have passed through the accelerating field generated by the double layer by this time. (c) and (d) shows ion densities at  $50\tau$  and  $70\tau$  respectively, from which we can see that the ions have been further displaced leading to a indication of multistage acceleration process.

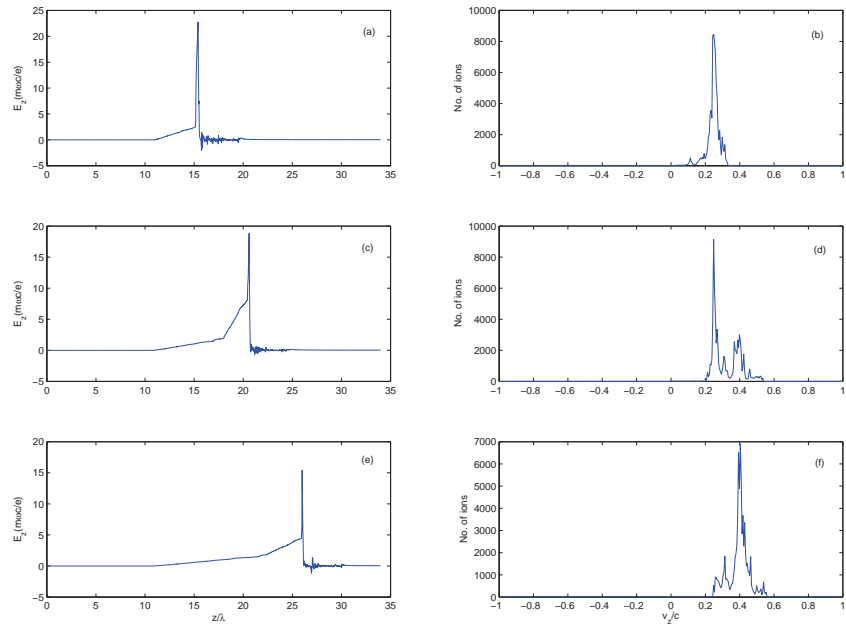


Figure 5.2: Figures (a), (c) and (e) shows the longitudinal electric field at times  $31\tau$ ,  $50\tau$  and  $70\tau$  respectively for  $n_i = 10n_c$  and  $a_0 = 20$ . (b), (d) and (f) shows the longitudinal velocity spectrum at similar times. We see that at  $31\tau$  the ions peak at a velocity  $0.248c$ . At  $47\tau$  we can see a second peak emerging at  $0.41c$  to which almost all the ions get dumped at  $70\tau$ .

time  $50\tau$  we see a second stage of ion velocities emerging and at  $70\tau$  almost all the ions have been dumped into the second stage. The time required by all ions to attain steady state velocity matches fine with our analytical calculations. Also the first and second stage ion velocities are the close to what has been predicted by the analytical model presented. Figs. 5.3 and 5.4 present similar studies for  $a = 30$  with all other parameters remaining the same.

In order to study velocity and energy scaling a series of simulations were carried out for initial plasma densities  $1n_c$  to  $15n_c$  with  $a_0 = 20$  and  $30$  separately. As predicted by the analytical theory for laser penetration [18, 19, 20, 21] it was found that the stable double layer formation and ion acceleration began from initial density  $6n_c$  for  $a_0 = 20$ , and for  $a_0 = 30$  this value was  $7n_c$ . A set of ion velocities and energies obtained via simulation results are plotted with their corresponding analytically predicted values and non-relativistic results given by Zhang *et al.*, are plotted in Figs. 5.5, 5.6, 5.7 and 5.8. From these figures it is clear that the ion velocities and energies are in good agreement with our fully relativistic calculations. Theory also predicts correct time required to attain steady state velocity. It can also be concluded that even if the ratio  $\frac{I}{\rho c^3}$ , which is nothing but the ratio of incident laser energy to the rest mass energy of the ions, is very small still the relativistic results hold.

## 5.5 Conclusions

In this chapter, the interaction of a normally incident circularly polarized laser pulse on a solid target is studied. We found that for a cold target, a flat top laser pulse acts as a steady piston and drives a flow of ions in front of the surface into the target. The electrostatic field induced by the charge separation at the front surface of the target is steady enough to accelerate ions in multiple stage i.e. after the whole plasma target is accelerated to a quasi-monoenergetic state, another acceleration process begins for the continuing steady state. We have presented the relativistic corrections to the theory of multistage ion acceleration presented in [15]. In the regime of large  $\Xi = (Zm_e n_c / Am_i n_e) a^2$ , the predictions of a pure non-relativistic model diverge significantly. The hole boring velocity for both the first and second stage has been determined, which in turn gave the correct estimate

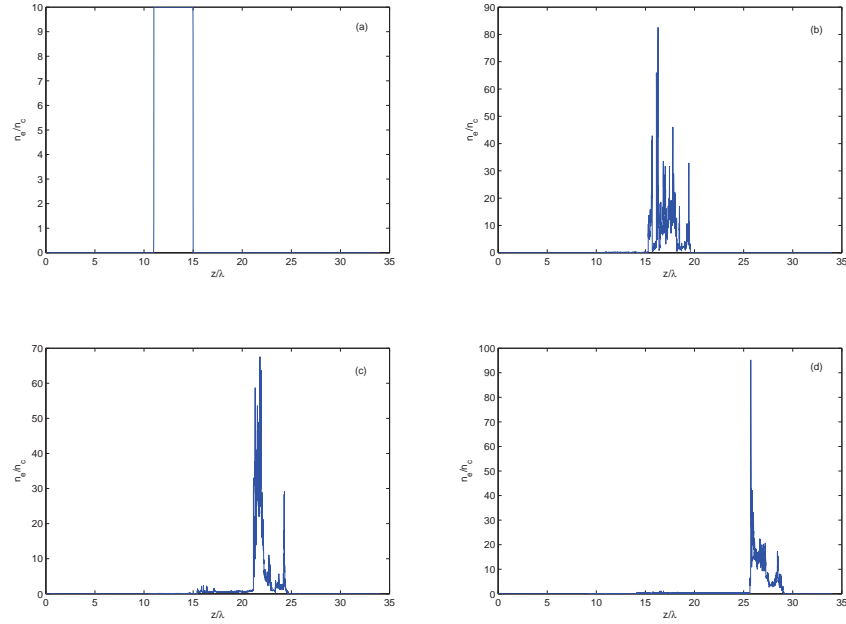


Figure 5.3: Spatial density profile of ions at different times for  $n_i = 10n_c$  and  $a_0 = 30$ . In (a) the ion density at time  $-11\tau$  is shown i.e. when the face of the laser pulse is at the extreme left of the simulation domain and the ions are undisturbed. (b) shows the ion density profile at  $23\tau$ . We can notice here that the tail of the plasma is at  $15\lambda$  hence indicating that all the ions have passed through the accelerating field generated by the double layer by this time. (c) and (d) shows ion densities at  $35\tau$  and  $45\tau$  respectively, from which we can see that the ions have been further displaced leading to a indication of multistage acceleration process.

## Chapter 5. Relativistic Theory for Multistage Ion Acceleration

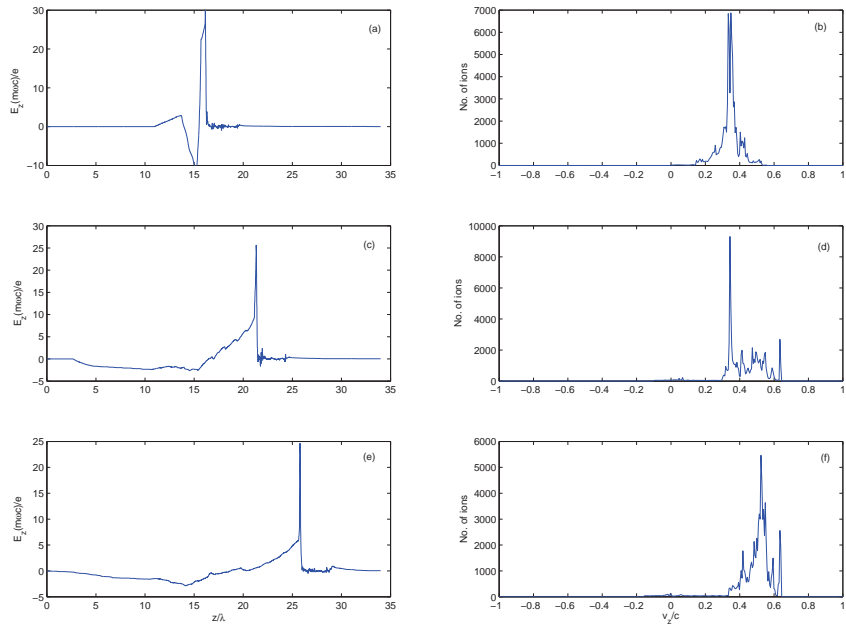


Figure 5.4: Figures (a), (c) and (e) shows the longitudinal electric field at times  $23\tau$ ,  $35\tau$  and  $45\tau$  respectively for  $n_i = 10n_c$  and  $a_0 = 30$ . (b), (d) and (f) shows the longitudinal velocity spectrum at similar times. We see that at  $23\tau$  the ions peak at a velocity  $0.348c$ . At  $45\tau$  we can see a second peak at a velocity of  $0.524c$ .

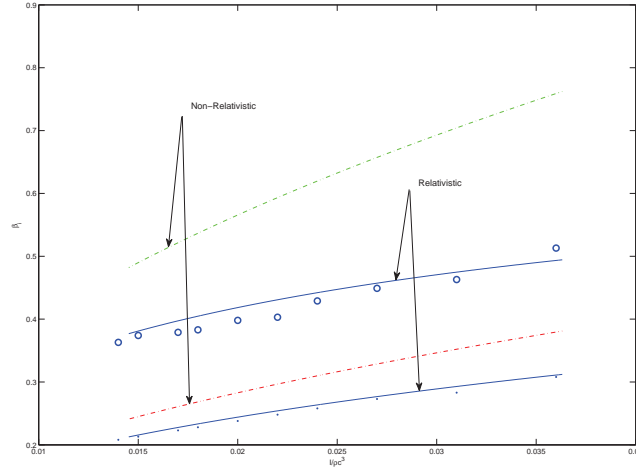


Figure 5.5: Plots of  $1^{st}$  and  $2^{ND}$  stage ion velocity of accelerated ions for  $a_0 = 20$ . The analytical results are represented by solid lines and the dots and circles represent first and second stage velocities respectively. The broken lines are the non-relativistic results.

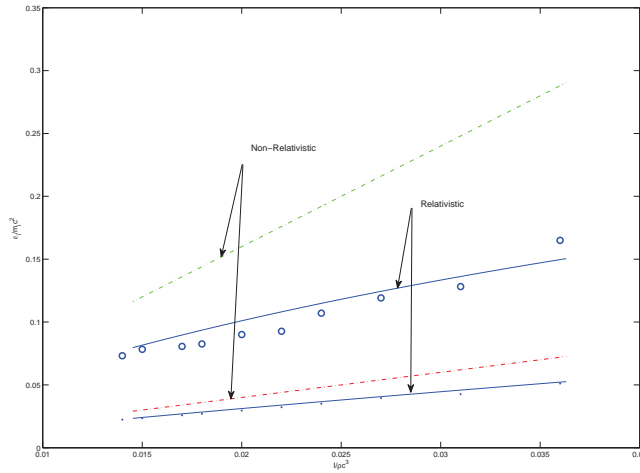


Figure 5.6: Plots of  $1^{st}$  and  $2^{ND}$  stage ion kinetic energy of accelerated ions for  $a_0 = 20$ . The analytical results are represented by solid lines and the dots and circles represent first and second stage velocities respectively. The broken lines are the non-relativistic results.

## Chapter 5. Relativistic Theory for Multistage Ion Acceleration

of the time required to accelerate all ions in both stages. The relativistic results are in excellent agreement with 1D3V PIC simulations.

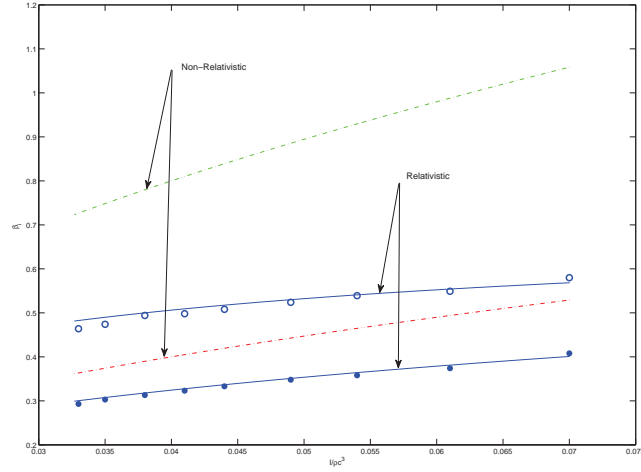


Figure 5.7: Plots of 1<sup>st</sup> and 2<sup>nd</sup> stage ion velocity of accelerated ions for  $a_0 = 30$ . The analytical results are represented by solid lines and the dots and circles represent first and second stage velocities respectively. The broken lines are the non-relativistic results.

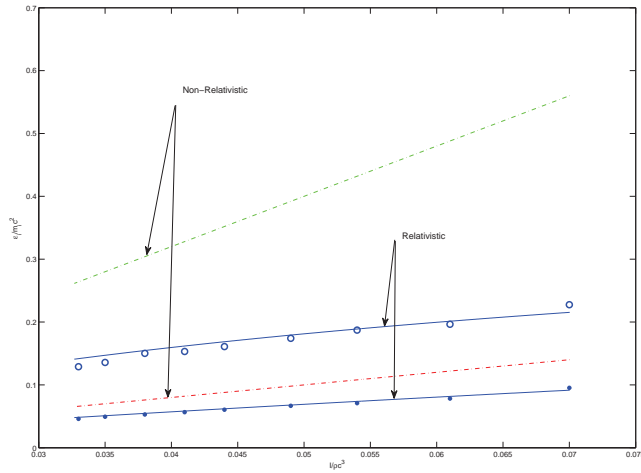


Figure 5.8: Plots of 1<sup>st</sup> and 2<sup>nd</sup> stage ion kinetic energy of accelerated ions for  $a_0 = 30$ . The analytical results are represented by solid lines and the dots and circles represent first and second stage velocities respectively. The broken lines are the non-relativistic results.

# Bibliography

- [1] N. Naumova, T. Schlegel, V. T. Tikhonchuck, C. Labaune, I. V. Sokolov and G. Mourou, Phys. Rev. Lett. 102,025002(2009).
- [2] T. Schlegel, N. Naumova, V. T. Tikhonchuck, C. Labaune, I. V. Sokolov and G. Mourou, Phys. Plasmas **16**, 083103 (2009).
- [3] Xiaomei Zhang, Baifei Shen, Xuemei Li, Zhangying Jin, Fengchao Wang and Meng Wen, Phys. Plasmas 14, 123108 (2007).
- [4] Gibbon Paul, Phys. Rev. E 72, 026411 (2005).
- [5] Macchi Andrea, Cattani Federica, Liseykina, Tatiana V. and Cornolti Fulvio Phys. Rev. Lett. 94, 165003 (2005).
- [6] Silva Luís O., Marti Michael, Davies Jonathan R., Fonseca Ricardo A., Ren Chuang, Tsung Frank S. and Mori Warren B. Phys. Rev. Lett. 92, 015002 (2004).
- [7] Amol R. Holkundkar and N. K. Gupta, Phys. Plasmas 15, 123104 (2008).
- [8] A P L Robinson, P Gibbon, M Zepf, S Kar, R G Evans and C Bellei Plasma Physics and Controlled Fusion 51, 024004 (2009).
- [9] T. Schlegel, N. Naumova, V. T. Tikhonchuck, C. Labaune, I. V. Sokolov and G. Mourou, Phys. Plasmas 16, 083103 (2009).
- [10] Ujjwal Sinha and Predhiman K Kaw, Phys. Plasmas **19**, 033102 (2012).
- [11] Yan X. Q., Lin C., Sheng Z. M., Guo Z. Y., Liu B. C., Lu Y. R., Fang J. X. and Chen J. E., Phys. Rev. Lett. 100, 135003 (2008).
- [12] V K Tripathi, C S Liu, X Shao, B Eliasson and R Z Sagdeev, Plasma Physics and Controlled Fusion 51, 024014 (2009).
- [13] Macchi, Andrea, Veghini, Silvia and Pegoraro, Francesco, Phys. Rev. Lett. 103, 085003 (2009).
- [14] Esirkepov, T. and Borghesi, M. and Bulanov, S. V. and Mourou, G. and Tajima, T., Phys. Rev. Lett. **92**, 17500 3 (2004).

- [15] Xiaomei Zhang, Baifei Shen, Xuemei Li, Zzhangying Jin and Fengchao Wang, *Phys. Plasmas* **14**, 073101 (2007).
- [16] A. Einstein, *Ann. Phys. (Leipzig)* **322**, 891 (1905).
- [17] R. Lichters, R. E. W. Pfund, and J. Meyer-Ter-Vehn, LPIC++: A parallel one-dimensional relativistic electromagnetic particle-in-cell-code for simulating laser-plasma-interactions, Report MPQ 225, Max-Planck-Institut for Quantenoptik, Garching, Germany, 1997, the code is available at <http://www.lichters.net/download.html>.
- [18] Predhiman Kaw and John Dawson, *Physics of Fluids* **13**, 472 (1970).
- [19] Lai C. S., *Phys. Rev. Lett.* **36**, 966 (1976)
- [20] Cattani F., Kim A., Anderson D. and Lisak M., *Phys. Rev. E* **62**, 1234 (2000).
- [21] Shen Baifei and Xu Zhizhan, *Phys. Rev. E* **64**, 056406 (2001).

# 6

## Conclusion and Future Direction

### 6.1 Conclusions

The acceleration of ions to high energies by interaction of circularly polarized lasers with overdense plasmas is a topic of immense interest and has been investigated both analytically and numerically. The analytical studies have been primarily concentrated to one dimension whereas higher dimensional studies have been performed using particle in cell codes. Higher dimensional simulations have tried to analyze the stability of the structures formed due to laser ponderomotive force and responsible for acceleration of ions. In the present thesis we have devised analytical models for the mechanism of ion acceleration in the presence of an externally applied magnetic field. Further we have extended the theory to incorporate the effect of multiple species in the plasma target and the effect of finite cross section of the incident laser beam. We have also performed 1D3V particle in cell simulations to study the effect of longer laser pulses, the results of which have been analytically explained. We provide a chapter wise summary of the thesis and draw important conclusions on the basis of that.

In chapter 2 the hole boring mode of ion acceleration has been analytically studied in the presence of a static axial magnetic field. As described earlier, in bulk targets the ponderomotive force exerted on the plasma electrons pushes them out upto an extent that the charge separation field is balanced. Ions being massive do not respond to the oscillating electric and magnetic fields of the laser. However, the light

momentum is transferred to them via an induced axial electrostatic field. Considering a fluid treatment of plasma species, increased response time and continuity of ions lead to an ion sheath behind the electron sheath giving rise to a double layer. It is the electrostatic field in this double layer that accelerates the plasma ions. The thickness of the ion sheath is very small as compared to the entire ion space charge lying behind the electron sheath. The residual ions lying behind this sheath do not contribute to the accelerated ion beam obtained from the process. As the acceleration takes place in the double layer, this structure is often referred as “laser piston”. With the acceleration of ions to higher velocities, they tend to move out of the laser piston creating a charge imbalance. To replenish the lost ions, the laser piston moves ahead towards the undisturbed plasma trapping plasma ions at rest. This process steadily continues till the laser pulse keeps pushing the electrons. The studies performed so far has considered plasma electrons responding to incident laser fields only. If we apply a static axial magnetic field  $\mathbf{B}_s$ , these electrons will produce additional cyclotron motion with frequency  $\omega_c = e\mathbf{B}_s/m_e c$ . For such a case the dielectric constant in the relativistic case takes the form  $\epsilon = (1 - \omega_{peff}^2/\omega^2)$ , where  $\omega_{peff} = \omega_{pe}/\sqrt{\gamma_e - \alpha\Omega_c}$ .  $\omega_{pe}$  is the local electron plasma frequency,  $\alpha = \pm 1$  for right and left circularly polarized light,  $\Omega_c = \omega_c/\omega$  and  $\gamma_e$  is the electron relativistic factor. For evanescent solutions of the laser field in the electron sheath  $\epsilon < 0$ . In case of left circularly polarized (LCP) light for an overdense plasma, we can choose any value of  $\Omega_c$  or  $B_s$  as  $\alpha = -1$ . However, the laser intensity required to achieve a given piston velocity in this case is higher than that without magnetic field. With increase in magnetic field, the required incident laser intensity also increases for LCP. For right circularly polarized (RCP) light there is a restriction on the choice of  $\Omega_c$  as  $\alpha = +1$  and  $\epsilon$  has to be kept negative. In this case, the required laser intensity to achieve a piston velocity is less than that for  $\Omega_c = 0$ . We observe that for RCP  $\omega_{peff}$  increases with application of magnetic field because the direction of electron gyration due to electric field of the laser is the same as that induced due to externally applied magnetic field. As a result, the skin depth  $c/\omega_{peff}$  decreases because of which the transmitted laser field in the electron sheath decreases for a fixed laser intensity. As the laser field falls to zero at a shorter distance in the electron sheath, the ponderomotive force increases with magnetic field for RCP. For LCP the effect is reversed as the electron gyrations induced by the laser and applied magnetic field are opposite, hence  $\omega_{peff}$  decreases

with magnetic field.

Looking further towards the ion space charge, we mentioned initially that behind the ion sheath of the laser piston lies residual plasma ions that do not take part in direct acceleration process. Under the influence of induced electrostatic field they undergo coulomb explosion. Analyzing the dynamics of this region shows that the density of ions here decrease uniformly in time. We have seen earlier that the plasma ions at rest in the undisturbed part get trapped and accelerated by the laser piston. If we have a test ion moving with some velocity towards the laser piston, then it would overshoot and enter the coulomb exploding part. Its interaction with this region will decelerate it further and reflect from some point within. Solving the equation of motion for such test ion in this region, it is found that upon reflection their energies get enhanced. Hence, the coulomb exploding part acts as an energy amplifier. For a given plasma parameters and piston velocity, there is a maximum velocity that an incoming test ion can have to get reflected from the coulomb exploding space charge region. This maximum beam velocity is determined numerically.

In chapter 3, a self consistent analytical model was developed to study HB-RPA in plasma targets composed of two ion species. It was clear from chapter 2 that in plasma targets composed of single ion species the plasma ions at rest got reflected from the laser piston and formed nearly a mono-energetic beam as a result of momentum transfer from laser to ions. From the conservation of momentum it is clear that for a given laser the velocity of lighter ions will be more than that of heavier ions. For a cold target of two ion species with different masses, there are two acceleration stages. One is for the light ions and the other for heavy ions. The response time of light ions is smaller than the heavy ones, as a result they tend to accelerate earlier. At a later time, when the interaction becomes stable, both the species are accelerated together by the induced electrostatic field and their velocities tend to be equal. The velocity of heavier ions is higher in mixed plasma than what would have been obtained in case of pure heavy ion target for the same incident laser intensity and plasma density.

Previous theories on this mechanism did not focus on the structure of the laser piston for such cases. They resorted to the law of conservation of momentum to arrive at the ion velocities. We have described a fully analytical model for the structure of the laser piston for two ion species. When the laser ponderomotive force pushes

the electrons outwards, the lighter ions respond to the induced field before the heavier ones. The ion sheath forming close to the electron sheath contains both species, with the light ion density blowing up. However, at this point the heavier ion density is finite hence another sheath of primarily heavy species forms behind this layer. Thus the accelerating region for the heavy species is composed of three stages, first the heavy ion sheath then the mixed ion sheath and finally in the electron sheath. The lighter ions undergo acceleration in the mixed ion sheath and electron sheath. Thus the laser piston in such case consists of a triple layer instead of a double layer as in the case of single species plasma. This structure has been presented in the model proposed in chapter 3. The model describes the thickness and potential structure of the laser piston. The presence of two ion sheaths as a result of difference in response time of the the two ion species leads to a jump in potential at the interface of these sheaths. It was previously observed in particle in cell (PIC) simulations but remained unexplained till now.

The structure of laser piston shows that its thickness is a fraction of incident laser wavelength, hence it can be looked upon as a thin fluid layer supported against induced electrostatic force analogous to gravity by the pressure of a massless fluid (the laser radiation pressure in this case). Rayleigh-Taylor (RT) instability, in this case can play a destructive role depending on the duration upto which the acceleration process continues and its evolution. The acceleration gradient is determined by the radiation pressure exerted by the laser, the information for the ion sheath thickness and mass is derived from the model described. The analysis was done by dividing the entire ion sheath into small segments and looking into their evolution in time and finally summing them up, thus arriving at the evolution of the entire sheath. The time evolution of the segments is given by the parametric equation,

$$\begin{aligned} z &= \Delta_0 \exp[t(kg)^{1/2}] \cos(ky_0) \\ y &= y_0 - \Delta_0 \exp[t(kg)^{1/2}] \sin(ky_0) \end{aligned} \quad (6.1)$$

where  $\Delta_0$  is the initial perturbation,  $t$  is the time,  $k$  the perturbation wavelength and  $g$  the acceleration. With time, this instability grows making the laser piston porous to the incident light. At this point the ions cease to accelerate. Analysis of the piston shows that RT instability gets suppressed for targets where the proportion of heavy species is more. Also, with increase in incident laser intensity, the

cusplike formation time goes down but at a slower rate showing nearly an asymptotic behavior at higher intensities.

The studies reported so far are one-dimensional and hence do not take into account the finite pulse width. To include the effect of finite pulse width and transverse intensity profile, an analytical two-dimensional fluid model has been proposed in chapter 4. The steepening of the electron density profile in the originally homogeneous overdense plasma and the formation of electron cavitation as the electrons are pushed inside the plasma is determined self consistently. With introduction of transverse inhomogeneity in laser pulse intensity, the ponderomotive force exerted also varies along this direction. Because of this, a transverse inhomogeneity in electron density is also introduced. This inhomogeneity in electron density and light intensity produces nonzero currents in the azimuthal direction for a circularly polarized laser. Besides this, the circular motion of single electron produces plasma magnetization. The azimuthal and magnetization current together generate an axial magnetic field. The generation of axial magnetic field is governed by the equation,

$$\nabla \times \mathbf{B}_s = \frac{4\pi}{c} \mathbf{J}_\theta + 4\pi \nabla \times \mathbf{M} \quad (6.2)$$

where  $\mathbf{B}_s$  is the induced axial magnetic field,  $\mathbf{J}_\theta$  is the azimuthal current and  $\mathbf{M}$  is the induced magnetization. In our study we have found that during the course of ion acceleration, the finite pulse width of the laser induces these currents. We have successfully derived an expression for axial magnetic field generated self consistently by a circularly polarized laser pulse. Previous studies had either neglected the magnetization current or had used a pre-determined electron density and laser intensity. In this study the electron density and evanescent laser fields inside the electron sheath are determined self consistently by the laser and plasma parameters. It has been found that the magnetic field generated extends upto the electron sheath only and decreases axially and radially. The mechanism predicts generation of magnetic field of hundreds of megagauss.

In chapter 5 we analyze the effect of a long relativistic circularly polarized laser pulse on a finite bulk target. In case of laser ion acceleration with bulk targets, it is the laser piston described in previous works that move through the undisturbed plasma and steadily accelerate ions at rest. In this process, the number of ions in the accelerated beam keeps increasing with time as the piston moves through the

plasma. For a target of finite thickness the distance upto which the laser piston traverses depends on the piston velocity and laser pulse duration. However, if the thickness of the target is such that the time required by the laser piston to cover entire plasma is less than the pulse duration, then the process gets repeated again. This process has been referred as “multistage acceleration”. For non-relativistic piston velocities this phenomenon has been described before. But, as we go to relativistic piston velocities, the non-relativistic results hold no more. We have presented a fully relativistic calculation for second stage ion velocities and energies. To verify our calculations, we performed a fully relativistic 1D3V particle in cell (PIC) simulations using the code LPIC++. It was found that the relativistic calculations matched very well with the simulation results. Also it was seen that at relativistic piston velocities, the non-relativistic results differed by a huge margin.

## 6.2 Future Directions

The results presented in this thesis illustrate several interesting physical phenomena and provide a basis for further investigations as direct extensions to this work. In this regard, we suggest below some open problems which can be addressed in the future.

- In the present work, it has been assumed that the plasma is weakly coupled. In studies related to laser fusion, the ions sometimes are strongly coupled. The coupling is given by

$$\Gamma = \frac{(Ze)^2}{aT} \quad (6.3)$$

where  $Ze$  is the charge on the plasma species,  $a$  is the interparticle distance and  $T$  is the temperature. When a laser pulse is incident on such a plasma, then the restoring force generated against the ponderomotive pressure included the viscoelastic force besides the regular induced charge separation field. It has been shown that high intensity lasers may penetrate efficiently in the plasma by accelerating ions in the forward direction. Further, the high directionality seems to be very useful in heating the core. However, plasma in such case is at times in a strongly coupled state and the studies so far have not taken this into account. An analytical model for ion acceleration in a

strongly coupled plasma can be developed which can give a better insight. Further, it appears that growth rate of Rayleigh Taylor (RT) instability is suppressed when the plasma ions are strongly coupled. We have seen in chapter 3 that RT instability plays spoil sport in the ion acceleration process by making the laser piston porous to the incident laser. By lowering the growth rate the acceleration process can continue for a longer time adding more charge to the accelerated beam.

- It has been shown by Schlegel et. al. (Phys. Plasmas **16**, 083103 (2009)) and Sinha and Kaw (Phys. Plasmas **19**, 033102 (2012)) that a circularly polarized laser normally incident of a homogeneous plasma induces a charge separation on the surface due to ponderomotive force. This charge separation leads to a longitudinal electric field which accelerates the plasma ions, thus acting as a laser piston. The velocity of this laser piston is dependent on the incident laser intensity and plasma density. For constant intensity and plasma density, the piston velocity is a constant. However, with the introduction of density inhomogeneity in the plasma, the piston velocity varies as it moves through the plasma. The acceleration of ions is due to the induced charge separation field directly depends on the ponderomotive force exerted by the laser. With increase in ponderomotive force, the accelerated ion velocity also increases. It was shown by Lindl and Kaw (Phys. Fluids **14**, 371 (1971)) that in case of oblique incidence of a laser on an inhomogeneous plasma the solution of exact wave equation leads to an interesting resonance effect which predicts that the magnitude of ponderomotive force exerted is greater than that obtained conventionally. As the ponderomotive force is enhanced or in other words swells in this region because of a resonance between laser and excited plasma wave, it can generate high charge separation electric field. If the pulse is long enough, this field can be maintained for a long time and plasma ions can be accelerated. The enhancement in ponderomotive force due to resonance effect can thus be exploited to obtain high ion energies.